Morten Bjerkås

Ice actions on offshore structures
with applications of continuous wavelet transforms on ice load
signals

NTNU
Innovation and Creativity

To my parents,
who gave me the possibilities

Abstract

Ice actions on offshore structures are one of the main concerns for engineering activities in cold areas with ice-infested waters. This thesis deals with three aspects of ice actions, namely design ice loads from level ice, dynamic ice actions of resonant character, and the actions caused by ridged ice.

Ice pressures on full-scale structures have been summarized in the present work. The scatter in reported values has been partly explained by categorization with respect to the applied measuring devices, structural characteristics and geographical locations. An existing design code was found to fit well for the widest structures and dramatically over-predict ice loads for structures of widths less than four metres. The present work was concerned with the analyses of full-scale data from the Norströmsgrund lighthouse conducted in the LOLEIF and STRICE projects (1999-2003). Analyses of time records from ice crushing indicate that the effective structural width should not be reduced from full width when predicting design ice loads.

New applications of continuous wavelet transforms have been presented using the Morlet wavelet for the detection of intervals with ice loads of resonant character. The typical length of intervals with ice-induced structural vibrations appeared to be from 1.9-8.6 seconds; however, one interval lasting for 80 seconds was also detected. Ice loads of resonant character were found to occur more frequently warmer the ice. A critical speed was also found. This critical speed seemed to be higher the thicker the ice. Studies of the initial phase of intervals with ice-induced vibrations also revealed two mechanisms that could cause steady-state vibrations, namely circumferential cracking and internal cracking.

Fourteen incidents of ice ridge actions on the Norströmsgrund lighthouse were selected to reveal more details about actions from ridged ice to a vertical structure. A keel-to-sail ratio of 8.2 was estimated with a keel depth evolution of -0.04 m/day during a period from 3 March to 4 April, 2002. Four different failure modes were detected together with an insignificant influence from the increasing keel depth on the highest measured loads.

In-situ and laboratory measurements were conducted on ridged and level ice from the Barents Sea and the Van Mijen fjord on Svalbard where the level ice generally was found to be stronger than consolidated ice in ridges. Vertical samples with ice columns in the loading direction were found to be stronger than horizontal samples. Consolidated ice from ridges had an equal hardness to level ice, but was harder than ice rubble.

Sammendrag

Iskrefter på konstruksjoner til havs er en av hovedutfordringene når infrastruktur skal etableres i kalde områder med is i sjøen. Denne avhandlingen behandler tre aspekter omkring iskrefter mot konstruksjoner, nemlig; beregning av de høyeste lastene som kan opptre fra flat is, dynamiske iskrefter av resonanskarakter og krefter fra skrugarder mot faste konstruksjoner.

En oppsummering som viser målte iskrefter på fullskala konstruksjoner indikerer stor spredning i rapporterte data. Denne spredningen kan delvis forklares ved hjelp av kategorisering av data med hensyn på anvendt måleutstyr, konstruksjonens karakteristiske data og geografisk plassering. En eksisterende designkurve er vist å passe bra til de bredeste konstruksjonene. For konstruksjoner som er smalere enn fire meter ser kurven ut til å overestimere islasten betydelig. Arbeidet som er presentert i denne avhandlingen presentere analyser av fullskala data fra Norströmsgrund fyrtårn målt i forbindelse med prosjektene LOLEIF og STRICE i perioden 1999 til 2003. Analyser av tidsserier fra isknusing viser at den effektive bredden av en konstruksjon ikke kan reduseres så mye som tidligere antatt hvis den største mulige islasten skal beregnes.

En ny anvendelse av en kjent metode med små skalerbare bølger begrenset i tid og frekvens tilpasset et målt tidssignal er vist for detektering av isknusing av resonanskarakter. Typiske lengder av intervaller med is-induserte vibrasjoner var på 1.9 – 8.6 sekunder. Det lengste intervallet som ble funnet var på omlag 80 sekunder. Islaster av resonanskarakter ble funnet oftest når isen var varm. Den kritiske drifthastigheten som kunne forårsake is-induserte vibrasjoner viste seg å være høyere når isen var tykk enn når den var tynn. Videre studier viste at to ulike mekanismer kunne sette i gang is-induserte vibrasjoner. Den første mekanismen var sirkulære sprekker i isen som forårsaket samtidig belastning av konstruksjonen i hele dens bredde. Den andre mekanismen var interne sprekker i isens kontaktsone med konstruksjonen.

For å gi bedre innblikk i detaljene omkring belastning fra skrugarder på vertikale konstruksjoner ble 14 skruisers interaksjon med Norströmsgrund fyrtårn valgt for videre

analyser. Forholdet mellom kjøldybde og seilhøyde ble beregnet til gjennomsnittlig 8.2, noe høyere enn tidligere rapportert. Den gjennomsnittlige kjøldybden viste seg å avta med 0.04 m/dag i gjennomsnitt fra 3 Mars til 4 April, 2002. Fire ulike bruddtyper av skrugarder ble observert. Økende kjøldybde så ikke ut til å påvirke nivået av målte belastninger betydelig. Felt og laboratorium undersøkelser av skrugarder i Barentshavet og i Van Mijen fjorden på Svalbard er rapportert, hvor den flate isen som omslutter skruisen viste seg å være noe sterkere enn den konsoliderte isen i en skrugard. Vertikale iskjerner ble observert å være sterkere enn horisontale iskjerner. Konsolidert is fra skrugarder hadde samme hardhet som flat is, men var generelt hardere enn ukonsolidert is i skrugarder.

Acknowledgements

Working on this thesis has been an exciting and interesting period of my life. I want to thank my supervisor Professor Sveinung Løset, Department of Civil and Transport Engineering, NTNU who gave me access to the most complete source of full-scale data on ice-structure interaction ever recorded. As well, he introduced me to his network that has some of the world's leading engineers and scientists who are engaged with arctic problems. Without his support during these years and the funding from the Faculty of Engineering Science and Technology, NTNU, there would obviously not have been any ice research for me.

Two great authorities among researchers working with arctic problems have been of exceptional support. Professor Mauri Määttänen, Helsinki University of Technology taught me about ice actions on structures through a course on the University Centre in Svalbard (UNIS) and in answers of numerous emails. During a two week stay at Norströmsgrund lighthouse, Dr Devinder S. Sodhi (retired from Cold Regions Research and Engineering Laboratory) introduced me to his explanation of ice-induced vibrations and told me "first you have to read all the papers, then you can start writing", maybe I started writing a bit too early.

I am greatly indebted to Dr Lennart Fransson, Luleå University of Technology who taught me about ice mechanics and offered me information about Swedish Lighthouses which I never have seen elsewhere. Thanks to Professor Andrew C. Palmer, University of Cambridge for a pleasant and instructive stay in Cambridge in January 2004.

I would also like to thank the coordinators of the LOLEIF and STRICE teams, Dr Joachim Schwarz and Dr Walter L. Kühnlein from Hamburg Ship Model Basin (HSVA) for the possibilities to publish this work.

Associate Professor Knut V. Høyland (UNIS) taught me about ice ridges; his knowledge and friendly attitude led to many long and interesting discussions. Likewise, Basile

Table of Contents

1 Introduction

1.1 General

What is meant by ice actions on an offshore structure? Why do people still study these phenomena after many years of research? How can sea ice represent such a great hazard to structures and why do structures start to vibrate as a result of ice actions?

For the average person, ice research is often related to climate research on glaciers, research on ice accumulations or problems with icy roads. This study has another focus, namely, the analysis of drifting first-year ice in seas and the actions of such ice on the infrastructure in offshore and near shore areas.

Problems due to sea ice have been reported since the days when Nansen (1897) reported his experiences with the vessel "Fram" in the Arctic Basin (Fig. 1.1). The earliest attempts were often based on "trial and error" methods and there is no doubt that the first researchers in the Arctic were bold explorers, taking significant risks to achieve their goals. This study might give the reader an insight into how arctic research programmes are conducted nowadays, and give ideas about where new knowledge might be needed.

Figure 1.1. The research and exploration vessel "Fram" frozen
into arctic ice in the late 19th century (Nansen, 1897).

1.2 Structure of the thesis

The intent of this work has been to contribute to knowledge about ice actions on fixed offshore structures in general and study ice-induced vibrations and actions from ridged

ice in particular. This work has involved the interpretation of full-scale data from the Norströmsgrund lighthouse together with in-situ and laboratory testing of the mechanical properties of arctic ice. The main objectives of the thesis are:

Design ice loads acting on fixed structures:

- Summary of selected full-scale measurements
- Influence of the structural width in ice load prediction

Dynamic ice-structure interaction:

- Applications of the continuous wavelet transform on ice load signals
- Use of the cross-wavelet spectra to detect intervals with high common energy in signals
- Occurrence of ice actions of resonant character with special attention paid on the onset phase and the dependence on drift speed, ice thickness and temperature.

Actions caused by ridged ice:

- Analyses of 14 incidents of ridge interaction with the vertical sided Norströmsgrund lighthouse with special emphasis on the geometry of ridges, the failure mode of ridges and contributions from the ridge keel to the highest loads
- Investigations of ice from first-year ice ridges during uniaxial compression strength, salinity and ice temperature measurements.

The thesis has an introductory chapter (Chapter 1), a chapter that presents the scope of the work (Chapter 2) and a chapter that summarizes some selected full-scale measurements (Chapter 3). This is followed by six chapters, which are papers that have been or will be submitted to international journals or conference proceedings (Chapter 4 to 9).

Chapter 2 presents the different parameters used in this study together with the various zones where the ice conditions differ significantly. Three different theoretical methods are presented to predict ice loads on structures.

Chapter 3 summarizes 31 selected pieces of work, which report global ice pressure on fixed structures. In general, ice load data are known to scatter significantly while this chapter tries to explain some of the scattering by categorization of data with respect to measuring devices, structural characteristics and geographical location.

Chapter 4 presents information on how changing failure modes of the ice may control the ice loads on a structure. Most ice load prediction formulas describe how there is lower effective ice pressure for larger structures due to the occurrence of non-simultaneous local load peaks and scale effects. The current work indicates what happens when simultaneous local load peaks are occurring related to the prediction of design ice loads to structures.

Chapter 5 shows an application of continuous wavelet transforms (CWT) on ice load signals. The purpose of the analyses was to detect the intervals which had an influence on the loading signal considering the structural characteristics such as mass and stiffness. Intervals with load signals that are dominated by the fundamental frequency of the structure are detected and checked for consistency against the measured dynamic response of the structure.

Chapter 6 shows the further applications of CWT using cross-wavelet spectra. The measured response and ice pressure on a structure during ice actions have been analysed, and intervals with high common power are detected in the time and frequency domains.

Chapter 7 handles further analyses of intervals with ice-induced vibrations. Corresponding parameters such as drift speed and ice thickness are considered to see if ice-induced vibrations are more frequent in thick or warm ice. Mechanisms that trigger ice-induced vibrations are investigated.

Chapter 8 presents analyses of 14 incidents caused by the actions of ridged ice on the Norströmsgrund lighthouse. Both the keel-to-sail ratio, loads from ridges and the different failure modes of ridges are studied.

Chapter 9 summarizes in-situ and laboratory investigations on level ice and a first-year ice ridge, respectively. Investigations were conducted during the winter 2003 in the Van Mijen fjord on Svalbard and in the north-western Barents Sea, respectively. The main focus of this chapter is on the crushing strength of the ice. Level ice is compared to consolidated ice in ridges and vertical and horizontal ice samples are compared.

1.3 Readership

The present work deals with ice actions on fixed structures which is one of the major environmental treats to structures located in ice-infested waters. The primary readership for this thesis as a whole and for some particular parts are students, engineers and scientists working with:

- The design of structures for hydrocarbon production and development in ice-infested waters
- Ice research with focus on ice actions on fixed structure in general and the ice-induced vibrations and actions of ridged ice in particular
- The design of all kinds of fixed slender structures in ice such as offshore wind-turbines.

2 Motivation and scope of the work

2.1 What is ice action?

The term "Ice actions on structures" means in this study the failure scenario between floating ice features and fixed or floating structures. Such ice features can be all kinds of ice from icebergs and multi-year sea-ice to thin freshwater ice. Possible structures could be fixed structures such as platforms for the production of hydrocarbons, wind-turbine foundations, pipelines, breakwaters or quays where floating structures could be floating platforms or ships operating in ice-infested waters.

The physical environment varies significantly from sea to sea in the Northern hemisphere. Egorov and Spichlin (1993) and Mironov (1996) presented data from the Barents Sea divided into 6-7 different zones with respect to environmental conditions. Bourke and Garett (1987) gave an overview analysis of the distribution of keel depths in arctic ice. Using their results, the arctic ice extent can be approximated as shown by the solid line named Zone II in Fig. 2.1. Although the environmental conditions within Zone II vary, structures located within Zone II will typically have to withstand first-year ice with possible inclusions of multi-year features and icebergs. Løset et al. (1999a) reported a comparison between environmental conditions in the North American Beaufort Sea and the Russian arctic seas, respectively. The thickest first-year level ice in Zone II ranges from 1.6 m in the Pechora Sea (Mironov et al., 1994) to 2.1 m in the Beaufort Sea (API RP 2N, 1995). The inner solid line named Zone I, indicates the area where multi-year ice is present. The thickness of typical ice in Zone I is approximately 3-4 m (Maykut and Untersteiner, 1971).

The dashed outer line named Zone III in Fig. 2.1 is a sub-arctic area where only first-year ice is present. The ice thickness varies significantly from about 0.4 m in the Bohai Sea (Yang, 2000) to about 1.0 m in the Gulf of Bothnia (Leppäranta et al., 1995). Other areas with ice-infested waters in Zone III are the Caspian Sea in Kazakhstan, the Sea of Okhotsk in Russia, Cook Inlet in Alaska and several rivers and lakes in Scandinavia, Russia and North America.
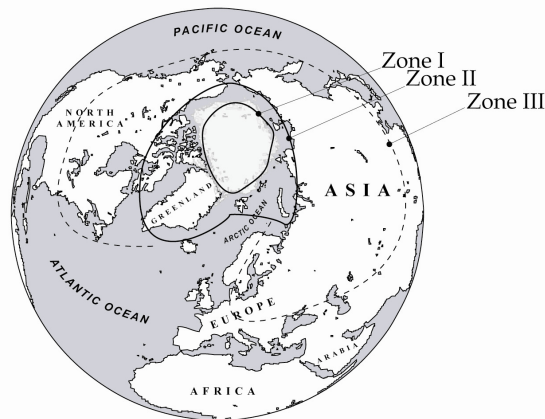
Figure 2.1. The Northern hemisphere with three zones indicated to describe the severity of ice conditions.

Structures exposed to the actions of drifting ice features are categorized as floating or fixed; this study will pay attention to structures that are fixed to the seabed. Fig. 2.2 shows a selection of five different types of fixed structures that already have been used in ice-infested waters. It should be mentioned that the structures shown in Fig. 2.2 have been used in relatively light ice conditions in sub-arctic regions (Zone III) except for the caisson structure. Except for the bridge pier and the vibration isolated channel marker, structures shown have also experienced severe ice-induced vibrations. Other types of structures than the ones shown in Fig. 2.2, which could be needed in arctic waters in the future are offshore wind-turbine foundations, loading towers for the export of hydrocarbons as well as artificial islands.

Lighthouse   Jacket   Channel marker   Bridge pier   Caisson
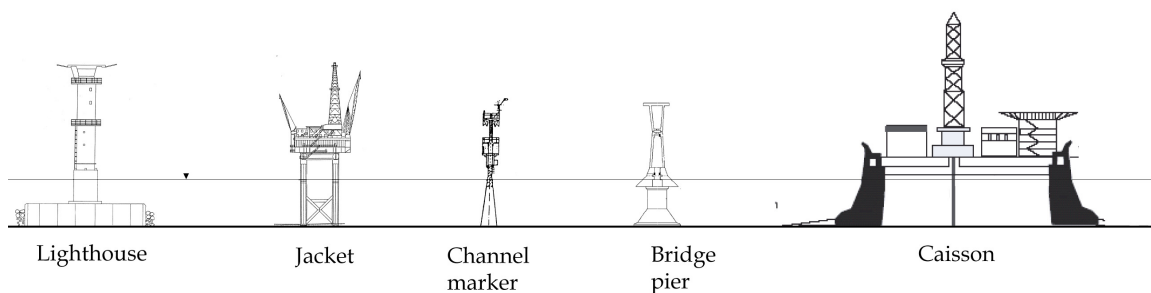
Figure 2.2. Various structure types used in different arctic regions during the last four decades (not to scale).

An ice sheet is a three-dimensional body with a surface area A (Fig. 2.3) and an ice thickness h (Fig. 2.4). Ice floats in seawater because the density of ice is about 90 % of the

density of seawater. Typically, seawater has a salinity of about 34 ppt. However, this study will also mention structures located in waters with less salinity.

Ice features need horizontal forces to come into motion. These forces are applied from mainly two sources; wind (τ_w) and current (τ_c) stresses. Due to weak zones in the ice cover or totally ice-free areas in a largely ice covered sea, floating ice sheets can start drifting due to the transfer of energy from wind and/or currents. The drift speed is connected to the "in-water" and "in-air" drag forces on the ice sheet during motion as indicated in Figs. 2.3 and 2.4.
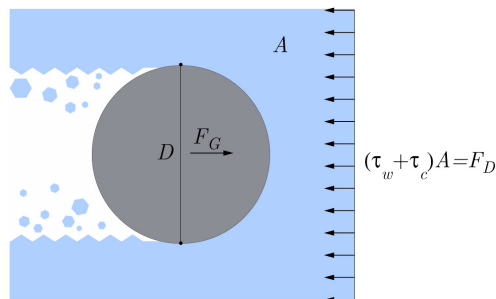
Figure 2.3. A circular cross section of a marine structure under action from an ice sheet stressed by wind and current (plan view).

During the interaction between floating ice and offshore structures, the surface piercing breadth is of special interest. Fig. 2.3 indicates how the width D of the surface piercing part could be measured. The assumption that A is much larger than the cross sectional area of the structure is generally correct for narrow structures. When applying that assumption, one can presume that the driving forces on the ice sheet from the wind and currents (F_D) are significantly larger than the reaction force (F_G) from the penetrating structure ($F_D >> F_G$).

Fig. 2.4 shows the side view of the circular cross section in Fig. 2.3, the ice thickness h can be seen as the distance from the ice-water interface to the ice-air interface. Any possible

snow cover is usually excluded from the measured h. In most cases both the top surface and the sub-surface of the ice floe are uneven, in those cases the parameter h describes an average ice thickness. The ice temperature will usually change linearly between the surface temperature T_S against the water temperature T_W during the ice growth season. The linear distribution during ice growth is changed to a C-shaped distribution when the ice growth stops and the ice starts melting. As shown in Fig. 2.4, a sea-ice floe consists of an isotropic top layer of granular ice above a thicker layer that consists of mainly orthotropic columnar ice with vertical brine channels between plates of pure ice. During ice growth, a skeleton layer forms at the ice-water interface. The skeleton layer is significantly weaker than the columnar and the granular ice (Weeks and Ackley, 1986).

The parameter v_i designates the drift speed of the ice floe while in special cases the drift speed can be divided into a far field and a near field drift speed, where v_i usually represents the far field drift speed. The global load F_G on the structure is caused by the actions of the moving ice sheet. Further, loads designate ice pressure to a structure multiplied with a certain area while actions means load effects from ice including the global integrity of the structure.
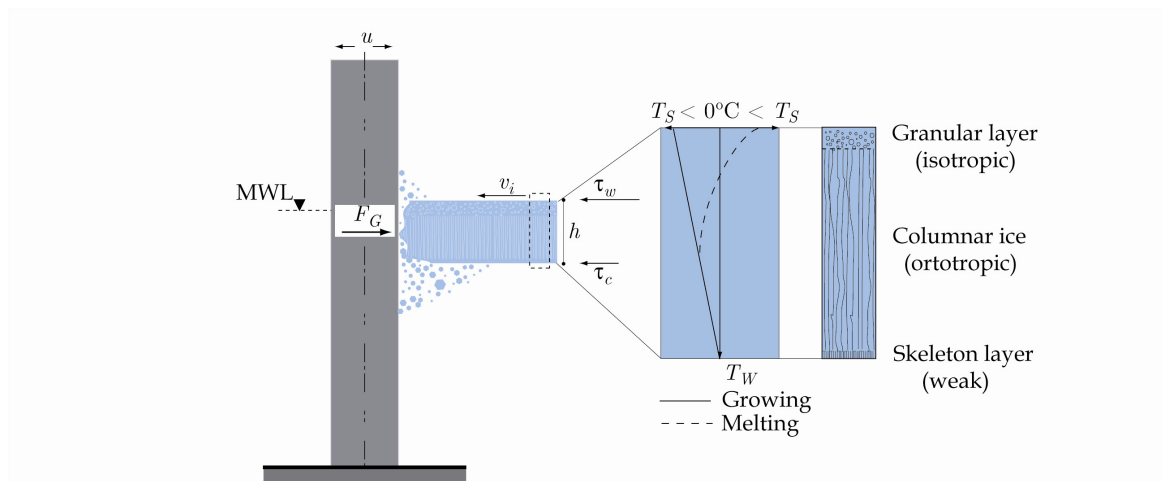
Figure 2.4. A vertical sided structure under sea-ice action (side view).

The parameter u in Fig. 2.4 indicates the structural displacement and could be once or twice differentiated with respect to the time to get the velocity and the acceleration of the structure, respectively.

The distribution of ice loads within the ice-structure contact area Dh is not very well depicted in the literature. However, some information was gained from ice-edge indentation tests by Takeuchi et al. (2000). A servo-controlled flat indentor instrumented with load sensors of size 10 mm × 10 mm was pushed into an ice edge. Fig. 2.5 shows a sample from a test where the ice thickness was $h = 0.4$ m and the width of the indentor $D = 2.0$ m.
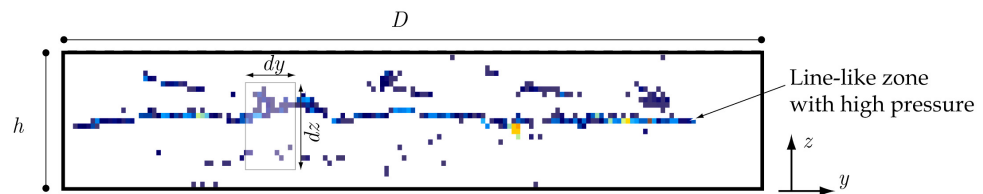
Figure 2.5. Spatial distribution of ice pressure within an ice-indenter contact area. Data provided to the author by the National Maritime Research Institute in Japan.

As investigated by Joensuu and Riska (1988), a significant portion of the ice load tends to be applied to the structure through a line-like zone in the middle part of the ice sheet. The breadth of this line-like zone in the z-direction might depend on different parameters such as the drift speed of the ice and the ice temperature. The global ice load applied to the indenter can be formulated as

$$F_G = \int\limits_{0}^{D} \int\limits_{0}^{h} p_L \, dzdy \qquad\qquad (2.1)$$

where p_L is the pressure measured on an area $dzdy$ (Fig. 2.5). A parameter which is discussed later in this work is the global pressure p_G, which could be defined as the global ice load in Eq. (2.1) divided by the nominal contact area (Dh) as

$$p_G = \frac{F_G}{Dh} \qquad\qquad (2.2)$$

As can be observed in Fig. 2.5, the "pressure intensity" differs significantly within the contact area, hence the highest local pressure p_{Lmax} is usually higher than the global pressure ($p_{Lmax} > p_G$). The following chapter will handle different sources of measured p_G to structures during field investigations around the world.

2.2 Motivation and objectives

Among the scientists and engineers working on the description of ice loads and actions from ice on structures, there are a handful of different methods which produce significantly different design loads given the same input values. Comparative studies have been outlined during the last twenty years for example by Sanderson (1988), Shkhinek et al. (1994) and Croasdale and Kennedy (1996), where the latter study shows that different methods have a scatter with a factor of more than ten in predicting F_G on an offshore structure. This section presents briefly three different and popular approaches to predict ice loads on structures, namely; empirical pressure relationships, physical models, and stochastic models.

2.2.1 Empirical pressure relationships

A well-known approach to predict ice loads on offshore structures was presented by Masterson and Frederking (1993). A work which was considered for design code purposes in both API RP 2N (1995) and CSA (2004). They collected the most available data and fitted an upper bound power law to represent the nominal pressure as a function of the contact area (Fig. 2.6). The number 8.1 represents the level of pressure where the $(Dh)^{-0.5}$ is applied to let the nominal ice pressure decrease with increasing contact area.
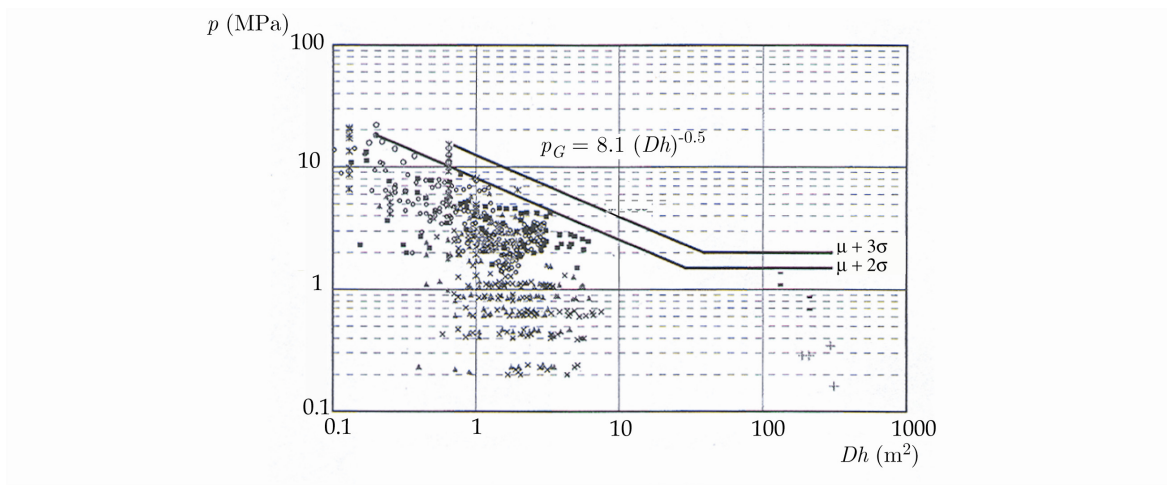
Figure 2.6. An upper bound pressure-area relationship presented by Masterson and Frederking (1993) (μ= mean, σ = standard deviation).

An intuitive problem with pressure-area relationships in general is that an ice sheet with thickness h = 1.0 m crushing against a structure of width D = 100.0 m most probably gives a different load than an ice feature with thickness h = 100.0 m crushing against an obstacle of width D = 1.0 m although the contact area should be the same. Afanasiev et al. (1971) addressed this problem by presenting ice pressure as a function of the aspect ratio (D/h) instead of the contact area. Empirical curves such as the one shown in Fig. 2.6 have also been outlined for effective pressure as a function of aspect ratio (D/h).

Recently, an empirical design formula was presented by Løset et al. (1999b), where the pressure dependence of the aspect ratio and contact area were combined in a way such that separate factors were proposed for the pressure dependence of structural width and the ice thickness, respectively. Their formula reads

$$p_{G,\max} = KD^m h^n \qquad\qquad (2.3)$$

where K is a constant that is dependent on the mechanical properties of ice, and m and n are reduction factors for structural width and ice thickness, respectively. The latest contributions within this field are connected to the magnitude of the factors m and n. Jochmann and Schwarz (in review) together with Kärnä and Qu (in review) discuss the magnitudes of m and n based on analyses of data from the Norströmsgrund lighthouse in Sweden while Bjerkås (2004) discusses the magnitude of m with respect to possible failure modes during ice-structure interaction.

Generally, an empirical design curve such as the one represented by Eq. (2.3) is appreciated because it is easily accessible for most readers of design codes. However, to prove the applicability of such an empirical formula, physical models are needed to reproduce the loads calculated by the formula. Because the curve is fitted to a large amount of data measured under varying and thereby different conditions, it is a considerable challenge to obtain a physical model which can represent all data by the use of one formula only. That challenge should be recalled during the use of empirical design curves. Therefore, designers using empirical pressure relationships must always ask whether the applied empirical formula is obtained from conditions which are comparable to a new design case or not.

2.2.2 Physical models

A considerable amount of physical models have been presented to describe the ice-structure interaction phenomenon. An idealized physical failure scenario is usually assumed based on observations from small or large-scale measurements. An early

attempt was presented by Tryde (1973) where it was assumed that the ice sheet has a wedge shape in the ice-structure contact zone. Furthermore, it was supposed that the horizontal force could be predicted by summing the needed shear stresses to maintain the wedge at a certain angle. Later, a number of reporters have written about the simulation of the ice-structure interaction using simplified models and the finite element (Derradji-Aouat, 2005) or finite difference (Shkhinek et al., 1999) approaches. Moreover, the discrete element approach has been applied by Selvadurai and Sepehr (1999) to model two-dimensional ice-structure interactions.

Recently a contribution by Dempsey et al. (2001) builds on definitions presented by Jordaan (2001) and Sodhi (2001). As a starting point, they define two different crushing scenarios, one with few localized hot spots in a relatively thick ice sheet and another with a line-like concentration of hot spots concentrated in the middle third of the ice sheet (Fig. 2.6). The development of pressure in the hot spots was proposed to be limited by the apparent fracture toughness (K_Q) of ice.
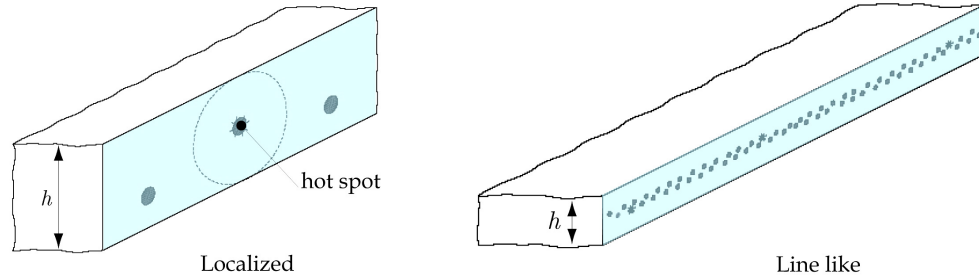

Figure 2.6. Hotspots in the ice-structure contact zone as proposed
by Dempsey et al. (2001).

The ice load was derived from the failure of these hot spots with a diameter a, based on localized and line-like pressure distributions. The model of Dempsey et al. (2001) proposed that the effective ice pressure on a structure during level ice interaction was dependent on ice thickness as

$$p_{\max} = \Omega \frac{h^{3/2}}{a^2} \sqrt{EG_c^{scale}} \quad \text{(Localized)}$$
$$p_{\max} = \Psi \frac{h^{1/2}}{a} \sqrt{E'G_c^{scale}} \quad \text{(Line-like)}$$

(2.4)

where Ω and Ψ are constants. Then E and G_c^{scale} are Young's modulus and a critical energy-release-rate at the actual scale, respectively. So far, it has not been presented comparisons to full-scale data or other analyses that can be used to predict the magnitudes of Ω and Ψ in Eq. (2.4).

If a physical model is able to reproduce the various observations from field conditions, it might be assumed that such a model could be the most reliable way of predicting ice loads on a structure. However, such a model is not yet presented and physical models have so far not been very trusted in the prediction of ice loads to vertical sided structures. Further work is needed on the derivation of models that have to be connected to measured and observed scenarios in the field in a clear way. However, the first questions which need an answer before the derivation of new sophisticated models can start is when and under which conditions do the highest ice loads occur?

2.2.3 Stochastic models

Stochastic models is the third approach that is used to predict ice loads. This applies probabilistic theories and the ideas behind random processes (Reddy et al., 1975). The two main assumptions behind such models are no interaction between the structure and the ice crushing process and second that dynamic ice crushing is a stationary process. The zonal failure approach has been applied from these two assumptions. The zonal ice forces F_i as shown in Fig. 2.7, could be divided into separate components which are:

$$F_i = F_m + F_d$$

(2.5)

where F_m is a stationary mean value, and F_d is the fluctuating dynamic part of the ice load. The value F_m is derived from data on the maximum resistance to in-plane indentation, while F_d is formulated by assumptions from Kry (1978) stating that

independent linear processes exist during ice crushing. From those ideas, either ice loads or ice-induced response signals or both have been transformed into the frequency domain and represented by frequency spectra of various shapes often dependent on ice conditions such as drift speed and ice thickness. Recently Qu et al. (2003) presented analyses of data from the Bohai Sea in China, where ice loads on cone structures were modelled as random processes in the frequency domain.

Ice load models based on the theory of random signals are preferred and applicable. First, the theory is easily accessible for engineers, as the same ideas frequently have been applied for wind and wave actions on structures. Second, it can be implemented into commercial finite element (FE) software used in structural design. On the other hand, neither of the two assumptions behind stochastic models have been proven to be fulfilled during ice-structure interaction. For example the influence of structural vibrations on ice loads has already been proven to occur on structures from narrow channel markers to wide caisson structures (see Chapter 4) though none of the stationary ice load signals have been proven to reproduce the highest ice loads on structures. Nevertheless, stochastic models are useful, because the fluctuating part of ice loads can be well represented and applied in design to reveal associated fatigue problems in offshore structures due to ice actions.
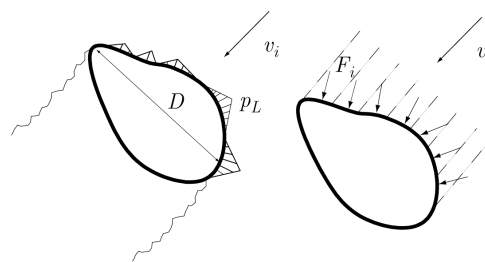

Figure 2.7. A zonal failure approach used as a basis
for stochastic modelling of ice forces.

2.2.4 Ice actions of a resonant character

A special type of ice actions occurs in cases when the structural vibrations start to influence the ice action. Ordinarily, the global ice load consists of a summation of local

load components which usually are not in phase with each other along the water-line perimeter. Two models have been proposed to explain why the loads F_i get in-phase with the structural vibrations. Namely a model based on self excitation (Määttänen, 1988) and a model that relies on forced vibrations (Sodhi, 1988).

The present work includes three papers that discuss aspects of ice-induced vibrations. First, Bjerkås et al. (in review) and Bjerkås (2006) present the use of continuous wavelet transforms, a method that can extract information about the occurrence of characteristic frequencies in the load signals during ice crushing. Such information might be important because load signals from full-scale measurements can be long with short intervals where some dominant frequencies are present. Another aspect of ice-induced vibrations studied by Bjerkås and Skiple (Chapter 7) is the starting procedure of the intervals with ice-induced vibrations. Such information might be needed when it should be decided if a structure is vulnerable to ice-induced vibrations at its present location.

2.2.5 Ice actions from ridged ice

Another scenario with ice actions on offshore structures is when ridged ice hits a structure. Ice ridges are established either due to compression or shear in the ice cover and consist of a consolidated layer together with parts which are partly consolidated or not consolidated. Loads on structures due to the actions of ridged ice are complex and little information exists on full-scale ice loads from ice ridges. The current work includes two papers that contribute information about geometry, failure modes and loads from ice ridges (Bjerkås and Bonnemaire, in progress). Subsequently, work that handles the mechanical properties of ridged ice and level ice in the Barents Sea and in the Van Mijen fjord on Svalbard is included (Høyland et al., 2004).

2.3 Summary and conclusions

This chapter introduces the reader to some research topics related to first-year ice actions on fixed offshore structures. Parameters frequently used later in the work are defined where the Northern Hemisphere is divided into three different zones to help categorizing field measuring programmes summarized in the following chapter.

Three different approaches for calculations of ice loads were presented. First, empirical pressure relations derived from measured data were discussed. It was concluded that empirical functions are easy to apply, but have limitations that are more difficult to control. Second, physical models were presented with a description of a model based on pressure controlled by the fracture toughness of ice. The physical models are a challenging way to treat ice loads, since many details about the ice-structure interaction phenomenon are still unknown. The third approach was ice loads modelled as stochastic processes, which is a preferred way for engineers, as they already know similar methods from wind and wave engineering. It was found that it is unclear if the basic assumptions behind the theory of stochastic signals are satisfied during ice actions on structures. From the discussions concerning the three different approaches to predict ice forces, it follows that more theoretical and empirical research is needed, before a unified method can be trusted to properly predict realistic ice forces on offshore structures.

The main contributions in the present work are divided into three different parts, which are all related to ice actions. The first part is the occurrence of the highest ice pressures on structures which focuses on how they have been measured during field tests and how they are influenced by structural width. The next topic addresses the detection of ice-induced vibrations with a particular study of how they occur. The last item is ice ridge actions on structures with emphasis on the mechanical properties of ridged ice.

References

Afanasiev, V.P., Dolgopolov, Y.V. and Shyeishtein, Z.I. (1971), Ice pressure on separate supporting structures in the sea, Trudy Institute, Vol. 300, pp. 61-80 (In Russian).

API RP-2N (1995), Recommended Practice for Planning, Designing, and Constructing Structures and Pipelines for Arctic Conditions, American Petroleum Institute, p. 82.

Bjerkås, M. (2004), Global design ice loads' dependence on failure mode, International Journal of Offshore and Polar Engineers, Vol. 14, No. 3, pp. 189-195 (Chapter 4).

Bjerkås, M. and Bonnemaire, B. (in progress), Loads from ridged ice on the Norströmsgrund lighthouse, (Chapter 8).

Bjerkås, M., Skiple, A. and Røe, O.I. (in review), Applications of Continuous Wavelet Transforms on Ice Load Signals, Engineering Structures (Chapter 5).

Bjerkås, M. and Skiple, A. (in review), Occurrence of continuous and intermittent crushing during ice-structure interaction, Proc. International conf. on Port and Ocean Eng. under Arctic Cond. (POAC), Potsdam, NY, USA, Vol. 3, (Chapter 7).

Bjerkås, M. (2006), Wavelet transforms and ice actions on structures, Cold Regions Science and Technology, Vol. 44, pp. 159-169, (Chapter 6).

Bourke, R. and Garett, R. (1987), Sea ice thickness distribution in the Arctic Ocean, Cold Regions Science and Technology, Vol. 13, pp. 259–280.

CSA (2004), General requirements, design criteria, the environment, and loads, Canadian Standards Association, S471-04, 94 p.

Dempsey, J.P., Palmer, A.C. and Sodhi, D.S. (2001), High pressure zone formation during compressive ice failure, Engineering Fracture Mechanics, Vol. 68, pp. 1961-1974.

Derradji-Aouat, A. (2005), Explicit FEA and constitutive modeling of damage and fracture in polycrystalline ice – simulations of ice loads on offshore structures, Proc. International Conf. on Port and Ocean Eng. under Arctic Cond. (POAC), Potsdam, NY, USA, Vol. 1, pp. 225-238.

Egorov, A. and Spichkin, V. (1993), Division into Districts of the Russian Arctic Seas on the Base of the Ice Indications, Proc. of the First International Conference on Development of the Russian Arctic Offshore RAO-93, St. Petersburg, Russia, pp. 21–24.

Jochmann, P. and Schwarz, J. (in review), The Influence of Individual Parameters on the Effective Pressure of Level Ice Against Lighthouse Norströmsgrund, Proc. International Conf. on Port and Ocean Eng. under Arctic Cond. (POAC), Potsdam, NY, USA, Vol. 3.

Høyland, K.V., Bjerkås, M. and Vernyayev, S. (2004), Mechanical properties of ice ridges and level ice, in-situ and laboratory testing 2003, Proc. IAHR Ice Symposium, St. Petersburg, Russia, Vol. 1, pp. 69-75, (Chapter 9).

Jordaan, I.J. (2000), Mechanics of ice-structure interaction, Engineering Fracture Mechanics, Vol. 68, pp. 1923-1960.

Joensuu, A. and Riska, K. (1989), Jään ja raketeen välinen vuorovaikutus. Mittaustulokset yhtesustä jään murskausjokeista Wärtsilän Arktisen Teknologiakeskuksen kanssa keväällä 1988 (In Finnish). Laboratory of Naval Architecture and Marine Engineering, Helsinki University of Technology, Espoo, Finland, Report M-88.

Kärnä, T. and Qu, Y. (in review), Pressure-Area Relationships Based on Enhanced-Quality Field Data, Proc. International Conf. on Port and Ocean Eng. under Arctic Cond. (POAC), Potsdam, NY, USA, Vol. 3.

Kennedy, K.P. (1995), A 1995 perspective on global design ice loads, Proc. of Offshore mechanics and arctic engineering conference, Copenhagen, Denmark, Vol. 4, pp. 9-16.

Kry, P.R. (1978), A statistical prediction of effective ice crushing stresses on wide structures. Proc. IAHR Symposium on Ice Problems, Luleå, Sweden. Vol. 1, pp. 33-47.

Leppäranta, M., Lensu, M., Kosloff, P. and Veitch, B. (1995), The life story of a first-year sea ice ridge, Cold Regions Science and Technology, Vol. 23, pp. 279-290.

Løset, S., Shkhinek, K.N., Gudmestad, O.T., Strass, P., Michalenko, E., Frederking, R.M.W. and Kärnä, T. (1999a), Comparison of the physical environment of some Arctic seas, Cold Regions Science and Technology, Vol. 29, pp. 201-214.

Løset, S., Shkhinek, K.N. and Uvarova, E. (1999b), An overview of the influence of structure width and ice thickness on the global ice load, Proc. International Conf. on Port and Ocean Eng. under Arctic Cond. (POAC), Helsinki, Finland, Vol. 1, pp. 425-434.

Masterson, D.M. and Frederking, R.M.W. (1993), Local contact pressure in ship and structure/ice interactions, Cold Regions Science and Technology, 21, pp. 169-185.

Maykut, G.A. and Untersteiner, N. (1971), Some results from a time dependent thermodynamic model of sea ice, Journal of Geophysical Research, Vol. 76, No 6, pp. 1550-1575.

Mironov, E., Spinchkin, V.A. and Egorov, A. (1993), Season Variability and Their Variations in the Region of Mastering of the Barents and Kara Seas Offshore, Proc. of the First International Conference on Development of the Russian Arctic Offshore RAO-93., St. Petersburg, Russia, pp. 110–121.

Mironov, E. (1996), Uniform Ice Regions of the Barents Sea Ice Regime. Proc. IAHR Ice Symposium, Beijing, China, Vol. 1, pp. 361-368.

Määttänen, M. (1988), Ice-induced Vibrations in Structures – Self-Excitation, IAHR Ice Symposium, Sapporo, Japan, Vol. 2, pp. 658-665.

Nansen, F. (1897), Some results of the Norwegian Polar Expedition 1893-96, Proc. Am. Phil. Soc., Vol. 36, pp. 442-463.

Qu, Y., Yue, Q.J., Bi, X.J. and Kärnä, T. (2003), Random Ice force on conical structure, Proc. International Conf. on Port and Ocean Eng. under Arctic Cond. (POAC), Trondheim, Norway, Vol. 1, pp. 259-271.

Reddy, D.V., Swamidas, A.S.J. and Cheema, P.S. (1975), Ice force response spectrum modal analysis of offshore towers, Proc. International Conf. on Port and Ocean Eng. under Arctic Cond. (POAC), Fairbanks, Alaska, USA, Vol. 2, pp. 887-910.

Sanderson, T.J.O. (1988), Ice mechanics-risks to offshore structures, Graham and Trotman, London, 253 p.

Selvadurai, A.P.S. and Sepehr, K. (1999), Two-dimensional discrete element simulations of ice-structure interaction, International Journal of Solids and Structures, Vol. 36, pp. 4919-4940.

Shkhinek, K.N., Blanchet, D., Croasdale, K., Matskevitch, D.G. and Bhat, S.U. (1994), Comparison of the Russian and Foreign Codes and Methods for Global Load Estimations, Proc. of Offshore Mechanics and Arctic Engineering Conference (OMAE), Houston, TX, USA, Vol. 4, pp. 75– 82.

Shkhinek, K.N., Kapustiansky, S., Jilenkov, A. and Kärnä, T. (1999), Numerical simulation of ice failure process, Proc. International Conf. on Port and Ocean Eng. under Arctic Cond. (POAC), Helsinki, Finland, Vol 2., pp. 877-887.

Sodhi, D.S. (1988), Ice-induced vibrations of structures, IAHR Ice Symposium, Vol. 3, pp. 625-657.

Sodhi, D.S. (2001), Crushing failure during ice-structure interaction, Engineering Fracture Mechanics, Vol. 68, pp. 1889-1921.

Takeuchi, T., Sakai, M., Akagava, S., Nakazawa, N. and Saeki, H. (2000), On the factors influencing the scaling of ice forces, In "Scaling Laws in Ice Mechanics and Ice Dynamics" (Eds. J.P. Dempsey and H.H. Shen), IUTAM Proc, Fairbanks, Alaska, pp. 149-160.

Tryde, P. (1973), Forces exerted on structures by ice floes, Proc. XXIIIrd International Navigation Congress, Ottawa, Subject 4, pp. 31-44.

Weeks, W.F. and Ackley, S.F. (1986), The growth, structure and properties of sea ice, In Geophysics of Sea Ice (ed. N. Untersteiner), Plenum, New York, pp. 9-164.

Yang, G. (2000), Bohai Sea Ice Conditions, Journal of Cold Regions Engineering, Vol. 14, No. 2, pp. 54 – 67.

3 Summary of selected measurements of ice actions against fixed structures

3.1 General

This chapter contains a summary of selected parts from the existing literature on full-scale ice-structure interaction field tests. Neither new data nor new interpretations are presented in this chapter. The second section presents different ways to measure ice actions on structures whereas the third section presents some of the early known investigations with structures in ice-infested waters. The fourth part presents Russian research basically focused on studies conducted in Siberian Rivers by Korzhavin and colleagues, while the fifth section presents Scandinavian studies together with one work conducted in Germany. The sixth section presents programmes from North America where the seventh section is about research done on ice actions in China and eastern Russia. The eighth section summarizes and discusses the mentioned data sources, while the ninth section concludes the chapter.

3.2 Methods to record ice actions

3.2.1 Introduction

Different methods and procedures to collect data from ice-structure interactions have been applied. Generally, each one of the methods can record displacements of the ice floe or displacements of the structure during ice-structure interaction. This section gives a short description of different methods and devices used in selected programmes mentioned further in this chapter.

3.2.2 Interfacial methods

Interfacial methods include devices for measuring ice loads at the ice-structure interface using flat steel platens frequently named as ice load panels. An ice load panel is generally a square-shaped plate (1.0-2.0 m edge length; a few centimetres thick) and has a material of known stiffness sandwiched between two steel plates. An ice load panel operates by measuring the displacement x of the plates during ice actions. An ice load panel is usually

so stiff that the inertia effects during motions of the panels gives neglectable load effects. Originally, ice load panels were designed to be placed in ice slots, which required panel stiffness comparable to the ice stiffness. Thus, a general problem with load panels is that they are softer than the parent structure and deflects more during ice loading than the structure itself.

A special type of ice load panel is the MEDOF (MEtge, DOme, Fenco) panel (Metge et al., 1983), which consists of a steel box filled with a calcium chloride solution including a stand pipe behind where ice pressure can be registered either manually or by a pressure transducer. A hinged beam is another interfacial method, which is simpler than a load panel. The hinged beam is usually constructed with a load cell in the upper end and a hinge in the lower end. Hinged beams are usually applied in places where the ice drift direction does not vary significantly as e.g. in rivers and channels.

Data obtained from interfacial methods are assumed as a measure of the static ice pressure because dynamic effects of the device itself usually are ignored. However little research has been conducted to support such an assumption. To obtain a magnitude of ice load, a summation of the load cells supporting a load panel or a summation of moments around the hinge in a hinged beam is conducted. The installation of interfacial devices usually requires underwater operations with equipment that have to sustain in a harsh environment. Calibration of load cells is usually conducted before installation and after dismantling of the interfacial device. Generally, ice load panels are measuring normal forces only; however, some panels have been aimed to measure tangential shear forces (Wessels et al., 1989).

Panels supported by load cells have usually better resolution than the MEDOF panels, because the liquid inside the MEDOF panels has a response time which limits the temporal resolution to about 1 Hz. The resolution of data obtained by panels supported by load cells depends on the storing capacity and logging routines. The data resolution of hinged beam systems depends largely on the width and number of beams installed. Temporally, the resolution depends on response time of the whole load cell and hinge system.

Due to the costs related to design and installation of load panels, wide structures are rarely completely covered with ice load panels in the water line. Calculation of global ice loads from incompletely covered structures is not straightforward. Difference in stiffness between the interfacial device and the supporting structure makes it difficult to obtain realistic values on the global ice load. If a hinged beam covers a whole bridge pier width, then the global ice load can be assumed to be recorded. However, dynamics of the bridge pier and the hinged beam have to be measured separately to figure out if a dynamic amplification is included in the measured load or not.

3.2.3 Structural response

The structural response can be recorded as a measure of the deflection of a structure due to an applied ice load. By recording the structural response, the structure itself acts as a load cell. However, in such a case, the motion of the structure is not ignorable and the modal mass and the damping have to be predicted together with the stiffness of the structure. In principle there are different ways to record the structural response e.g. by accelerometers, strain gauges, tiltmeters or pendulums. By measuring the structural response, the ice drift direction is not as critical as with use of interfacial methods, given that the structural stiffness in different directions is well predicted. The accuracy of measured data is much dependent on the accuracy of the measuring device and the dynamic characterization of the structure.

When using the structural response as a measure of the global ice load, it is important to recall that the response of the structure contains a dynamic amplification. This is important for structures vulnerable to ice induced vibrations, especially during so-called frequency locked-in ice loads. Monitoring the structural response is often preferable because it is usually cheaper than applying interfacial methods. Installation of devices can be completed in safe and dry conditions, as well as it can be inspected during the ongoing measurements. A physical description of the structure is needed for transformation of measured responses to applied loads. Such information can be obtained from a pull test with load control, FEM analyses, or by analytical calculations.

By use of accelerometers, deflections of the structure can be predicted by numerical integration. Due to unknown constants, only the dynamic part of the displacement can be predicted from acceleration records, however with additionally inclinometers installed, the complete displacement history might be predicted. To eliminate dynamic contributions in tiltmeter signals, records must be low pass filtered. Frederking (2005) recommended use of a seven second running average filter from experiences on the Norströmsgrund lighthouse. To remove potential drift in integrated displacements and velocities from measured accelerations, a so called baseline correction approach can be applied (Boore et al., 2001).

3.2.4 Hindcast calculations

Hindcast methods are well established concepts in wave prediction; however, in the current context, hindcast implies back calculation of ice loads from former incidents of ice actions. Usually permanent deformations are required to link previous ice actions to a level of ice load. Typical incidents could be failure of an offshore structure, or other situations including permanent cracks or sliding of gravity based structures along the seabed. Dependent on the geometrical characteristics of the structure and the seabed, hindcast calculations are not sensitive to ice drift directions.

Generally, hindcast calculations give the maximum global ice load. Local maxima can be obtained from local deformations of the structure as local bending of plate girders. The global load predicted, might include a dynamic amplification, hence care should be taken when calculating static ice pressure from loads obtained by hindcast methods. If a gravity-based structure is sliding along the seabed, an applied force can be predicted by assuming a friction coefficient between the soil and the concrete foundation. When applied in such situations, a dynamic amplification is generally not included in the estimated load.

Costs related to applications of hindcast calculations are related to transport of people to the site for registration of damages of the structure together with possible laboratory

investigations on the broken structure. However, operational challenges can be met during inspections of failed structures. First, it is preferred to know when the structure failed because the ice thickness and the failure scenario must be estimated in-situ. If the structure damages have been caused by interaction with level ice, the ice thickness can be measured in the wake behind the damaged structure. On the other hand, if a pile-up or pressure ridge has caused the incident, the situation is more complex and only a rough estimate of the ice thickness might be obtained. When predicting an applied ice load from failure of a slender structure, one should always recall that the structure could have failed due to dynamic effects and not due to static ice pressure only.

3.2.5 Newton's second law

To predict ice loads from measurements of ice floe deceleration is perhaps the most elegant way to quantify ice loads. The method uses straightforward Newton's second law ($F = m\ddot{x}$), where m is the ice feature mass and $\ddot{x}$ is deceleration of the ice feature during interaction with a structure. This method requires that the driving forces on the ice feature are of comparable size with the interaction force, such that the ice-structure interaction influences the far field drift speed. This requirement is usually satisfied during ice actions on islands or interaction between ice floes in rivers and bridge piers.

The application of Newton's second law is generally not costly and is precise if the mass and the deceleration of the ice floe is predicted accurately. One problem in prediction of the ice feature mass is the effect of added masses on the rigid body in motion. This might not be a big uncertainty in the case of a level ice sheet and if the ice floe is much thinner than the water depth (Dunwoody, 1982). Because an ice floe is not a perfectly rigid body, another pitfall is that the deceleration in the middle of the ice feature might not be the same as on the edge hitting a structure. These uncertainties can be accounted for by installing an array of accelerometers on an ice floe.

3.2.6 Internal ice stress measurements

Measurements of stresses in an ice cover by means of pressure sensors can be performed by two types of devices, a thin flat sensor and a stiff cylindrical sensor (Duckworth and Westermann, 1989). The thin flat sensor is always much wider than its thickness and is usually installed in pre-cut slots in ice through the entire ice thickness. Another type of sensor is the disk shaped sensor filled with liquid where its diameter is usually in the range of $D = 0.1$ m while the stiffness is as high as possible. The second type of sensor is the thick walled stiff cylindrical sensor installed through a hole in the ice.

Ice stress sensors are measuring normal stresses, hence three sensors have to be deployed in a rosette to get information about the principal stresses in a biaxial stress field (Prinsenberg et al., 1987). If the aspect ratio of the sensor is greater than 10, the stiffness of the sensor does not really matter if the stiffness is greater or comparable to the ice sheet stiffness (Sanderson, 1988).

It is not straightforward to predict loads on structures from measurements of stresses in the surrounding ice. Internal ice stress measurements are commonly used around structures located in stable ice covers. Such structures are often surrounded by grounded ice rubble, which might transmit energy both to the seabed and to the structure simultaneously. Because the knowledge about how ice rubble interacts with the seabed during grounding is sparse, it is a major challenge to figure out the magnitude of ice loads that could be transmitted from drifting ice through grounded rubble to the structure. Another uncertainty with internal ice stress measurements is that the ice quality might vary significantly over small areas, hence stresses measured at one location could differ from other locations not far away because the ice properties could vary much over small distances. To obtain the global ice load to a structure from internal ice stress measurements, different interpolation methods have been proposed. One of the methods is a surface integral method developed by Johnson (1983) to predict loads on a Caisson Retained Island (CRI) at Kadluk site in the Beaufort Sea (Fig. 3.28).

To summarize, ice load measurements have been divided into five categories in this section. To separate hinged beams and load panels, the interfacial methods are divided in two separate groups. Methods mentioned in this section are referred to in the next sections together with the description of different data sources. For comparison purposes, symbols from $\mathcal{A}$ to $\mathcal{F}$ are connected to each of the methods as indicated in Table 3.1.

Table 3.1. Six methods to record ice actions against structures.

$\mathcal{A}$	-	Interfacial methods
$\mathcal{B}$	-	Hinged beams
$\mathcal{C}$	-	Structural response
$\mathcal{D}$	-	Hindcast calculations
$\mathcal{E}$	-	Newton's 2nd Law
$\mathcal{F}$	-	Ice stress measurements

3.3 The earliest investigations of ice actions

Since Runeberg (1888) reported on different kinds of ice actions on steam boats in the Baltic Sea and Leonard (1898) reported on an ice damage incident with a pier under construction in Canada, a great deal of experience with ice actions have been obtained in different areas around the world (Fig. 3.1).
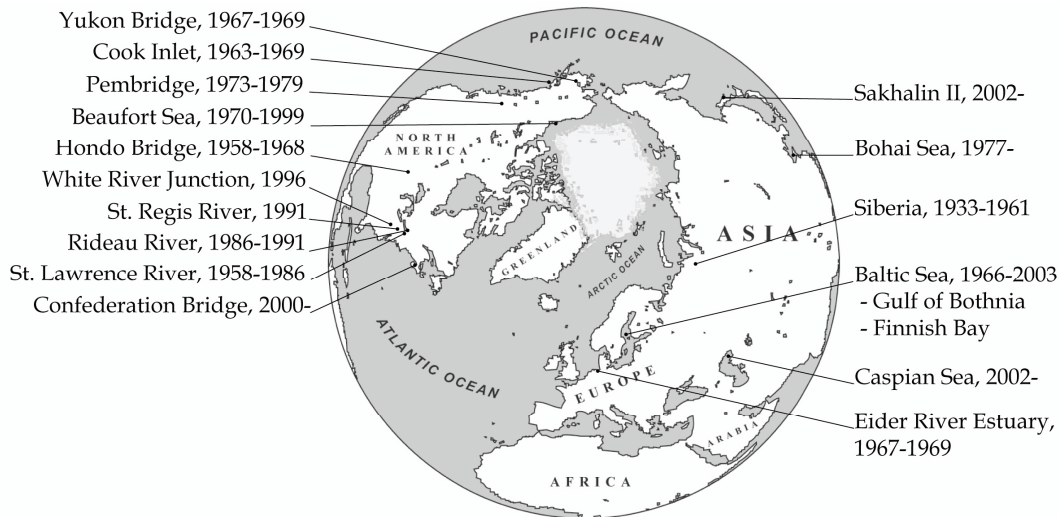
Figure 3.1. The locations of some selected sources of instrumented
full-scale ice-structure interactions.

An extensive Russian bibliography shows that studies dating back to the 19th century have been conducted in Russia while model tests using artificial ice were apparently conducted as early as 1930. The first measurements of ice forces on a full-scale pier were conducted in 1945-1946 reported by Gamayunov (1947). An English-language literature has developed partly based on translations of earlier Russian works, but also in form of new investigations.

The earliest approaches treated ice pressure as a static load and studies conducted from the mid 1960ties shed light on the dynamic effects of ice actions. Full-scale data measured first in Cook Inlet and then in Eider River Estuary and at bridges in Alberta showed that rapid force fluctuations of considerable amplitude normally occur, an aspect of ice actions that had been largely overlooked in earlier analytical studies. Another key question that concerned the researchers was why the global effective pressure p_G usually seemed to be lower than the laboratory measured uni-axial compressive strength (σ_c) of ice.

Considerable amounts of field tests have been reported at two international conferences established in the early 1970ties, namely the "Port and Ocean engineering under Arctic Conditions" (POAC) and the "Ice Symposium" organized by the International

Association of Hydraulic Research (IAHR). Other conferences with some focus on engineering challenges in polar regions are e.g. "International conference and exhibition on performance of ships and structures in ice (ICETECH)", "International Conference on Technology for Polar Areas (POLARTECH)", "International Offshore and Polar Engineering Conference (ISOPE) " and the "International Conference on Offshore Mechanics and Arctic Engineering (OMAE) ".

Including contributions submitted to several international journals, reporters to POAC, IAHR Ice Symposium, POLARTECH, ICETECH, ISOPE and OMAE have presented most of the latest research related to the integrity of structures in ice-infested waters. A map showing the locations of selected measurements on full-scale structures is indicated in Fig. 3.1. A brief description of different data sources follows in the next sections.

3.4 Measurements on bridge piers and hydropower plants in Siberia 1934-1966

Investigations in Russia have been the starting point for a considerable amount of later research on ice actions against fixed structures. One of the works are selected for further descriptions, namely a work by Professor K.N. Korzhavin from Novosibirsk State Technical University conducted in Siberian Rivers (Fig. 3.2).

Siberia is located between 55°N and 65°N (Zone III) including the rivers Ob, Yenisey and Angara as shown in Fig. 3.2. Due to an increasing activity on hydro-electric power projects in the late 1950ties, effects of ice due to annual ice runs, ice jams and ice packs in the rivers mentioned above were studied in more detail (Korzhavin, 1962).
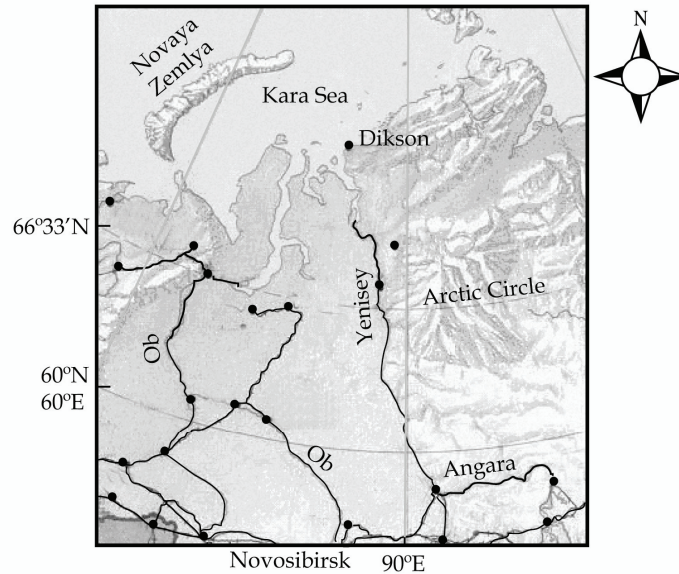
Figure 3.2. Map of Siberia with the rivers Ob, Yenisey and Angara used by
Korzhavin (1962) for investigations on ice forces on structures.

During the period 1945-1958, ice runs were filmed and analyzed where it was found that ice floes were cut into pieces of 0.1-0.5 m causing local compression as well as it was discovered that inclined bridge piers could prevent from ice jamming. Before the ice runs started, the ice thickness was investigated by drilling on cross sections in the river ice cover. Motion picture cameras were installed on bridge piers to obtain pictures of decelerating ice floes. Observers were investigating the size of the ice floe when the floes were drifting against the structure. The drift speeds of ice were investigated by cameras and ice forces were calculated using Newton's second law (Section 3.2.5). Ice floes were photographed and a grid was drawn on the photo (Fig. 3.3) to predict the speed of the ice floe. It is not known if the structural response was monitored during these measurements.

Korzhavin (1959) reported after tests of some 1500 ice samples that the bending strength of ice seems to be reduced as much as three times in the late spring. The local compression failure was found to reduce the global ice load as much as 2.0-2.5 times. As the rate of indentation speed increases, the compressive strength of ice was discovered to have a decreasing trend. The highest global pressure was measured during slow ice drift at p_G = 0.6 MPa (Korzhavin, 1959).
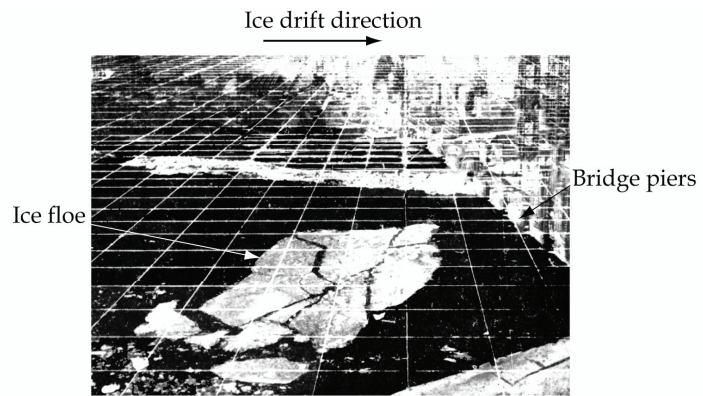
Figure 3.3. Sample image of an ice floe interacting with bridge piers in Siberia (after Korzhavin, 1962).

3.5 Measurements of ice actions in Germany and Scandinavia

3.5.1 Investigation in Eider River Estuary, northern Germany 1967-1969

A study was performed on river ice interaction with a test pile (D = 0.6 m) in Eider river Estuary, northern Germany (Fig. 3.1) (Schwarz, 1970). A pier was instrumented with an encircling shield consisting of 50 separate pressure measuring panels (Fig. 3.4). The ice thickness varied in the range of h = 0.1 - 0.2 m, with the most intensive ice actions from an interval with continuous crushing. The ice drift speed was always less than v_i = 0.40 m/s whereas the highest reported effective pressure was p_G = 0.8 MPa.
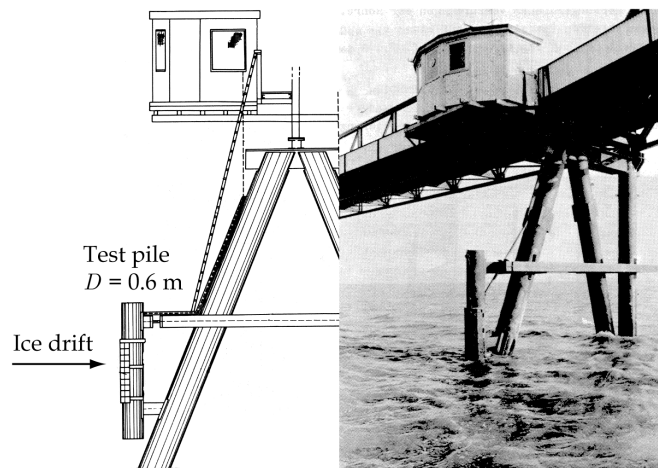

Test pile
D = 0.6 m

Ice drift

Figure 3.4. Experimental setup at the Eider River Estuary, northern Germany with the test pile (D = 0.6 m) (Schwarz, 1970).

One of the main concerns in this study was the ratio p_G / σ_c that was found to increase with thicker ice, an effect addressed to the decreasing aspect ratio (D/h). The aspect ratio (D/h) effect was confirmed by recorded data and explained by occurrence of non-simultaneous load peaks within the contact area (Dh). The strain rate ($\dot{\varepsilon}$) was found to influence on σ_c with decreasing ice strength as the strain rate increased with the highest strength at strain rate $\dot{\varepsilon}$ = 10^{-3} s^{-1}. However, no clear influence of the ice drift speed on p_G was detected. The uni-axial ice strength was found to rise with decreasing ice

temperature (T_i) together with a linearly decreasing σ_c with increasing ice porosity. Laboratory investigations by Hirayama (1974) followed up the work by Schwarz (1970).

3.5.2 Investigations in the Baltic 1966-2003

The Baltic Sea, including the Gulf of Bothnia (GOB) and the Finnish Bay has been a popular area to record ice actions against structures the last four decades. Good accessibility with reliable ice conditions generated a great deal of unique data. Usually, the ice starts to form during late October or early November in the Northern part of GOB while it usually not stays later than May (FIMR, 2005). The ice conditions in this area are sub-arctic (Zone III) dominated by land fast ice close to the shore and drifting level ice including pressure ridges and ridge fields elsewhere. A considerable amount of aid-to-navigation (ATN) structures as lighthouses and channel markers have been instrumented since 1973 (Fig. 3.5). This section concerns investigations in the area displayed in Fig. 3.5 conducted on ten lighthouses (❶❷❸❹❺❻ and ❼), a set of channel markers (❾) and an instrumented bridge pier (❽).

❶ Kemi I and II
❷ Björnklacken
❸ Borussiagrund
❹ Norströmsgrund
❺ Nygrån
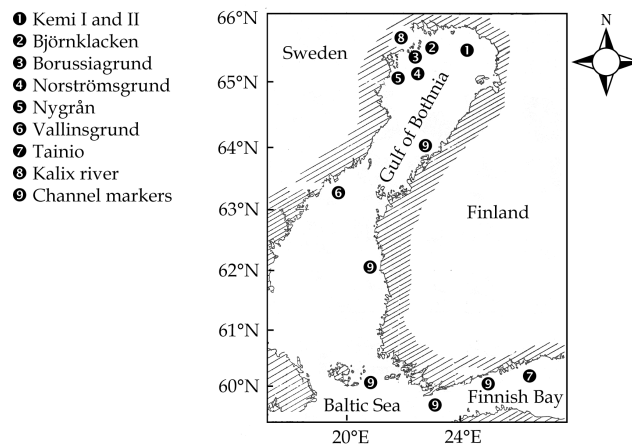❻ Vallinsgrund
❼ Tainio
❽ Kalix river
❾ Channel markers

Figure 3.5. Map of the Gulf of Bothnia with locations of instrumented structures.

Analyses of incidents with two lighthouses Tainio ❼ and Nygrån ❺ were conducted by Reinius et al. (1971) and Bergdahl (1972), respectively. Tainio lighthouse (Fig. 3.6) was

displaced about 14 m towards southeast in February 1967. After an ice pileup, the air temperature had been low for several weeks (-10°C to -26°C) together with winds in the range 10.8-13.8 m/s from northwest, which started the movement of the lighthouse along the seabed. One week later, the pack ice on the western side of the lighthouse had a thickness from 3.5 m to 4.0 m with a sail height of 0.5 m, while the surrounding level ice thickness was h = 0.7 m. The friction between the concrete foundation and the sea bed is unknown; hence, the predictions of applied ice loads must be approximately. The mass of the lighthouse was about 7.8 MN, hence with applications of a friction factor between 0.3-0.6, a horizontal force becomes F_G = 2.3-4.7 MN. An ice pressure can be calculated with an ice thickness h = 0.7 m as p_G = 1.0-1.9 MPa.
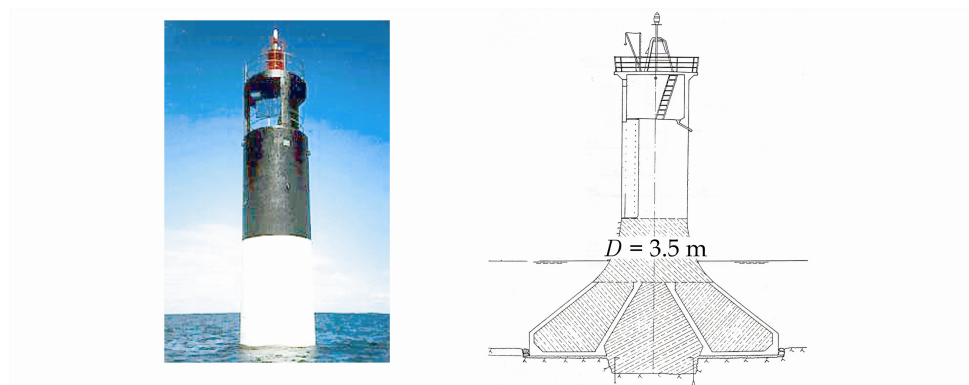

Figure 3.6. Tainio lighthouse (D = 3.5 m) (Finish board of Navigation, 2005).

The Nygrån lighthouse ❺ was constructed in 1958 and failed after ten years in service the winter 1968-69 (Fig. 3.7). Failure occurred due to tension cracks about one meter below mean water line (MWL) within the connection of the tower to the foundation (Bergdahl, 1971). The horizontal design load was F_G = 3.8 MN acting 0.5 m above MWL while in-situ observations registered that ridged ice tended to slide upwards the underwater caisson. With tensile cracks in the wall two meter above MWL, the attack point of the load causing failure was supposed to be higher than 0.5 m above MWL.
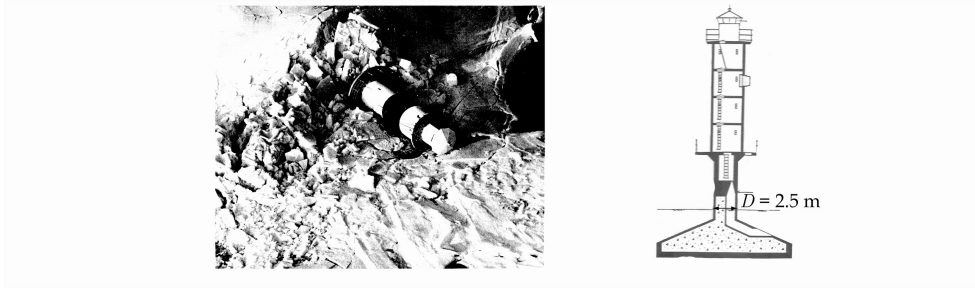
Figure 3.7. The tower of Nygrån lighthouse was broken the winter
1968/1969 (D = 2.5 m) (Reininus et al., 1972).

The Nygrån incident is a slightly different case compared to other failures due to ice loads in the same area. Nygrån lighthouse illustrates that not only the horizontal load capacity in MWL gives the global integrity of a structure. Especially in shallow waters, the geometric shape of the structure around MWL has to be considered. Nominal ice pressure is not calculated in this instance because the special circumstances during the failure.

The twin lighthouses Borrusiagrunden ❸ and Björnklacken ❷ were deployed at the Swedish coast in 1969, in an area with active ice drift most of the winter. During its first spring in service, horizontal displacements less than 0.1 m were observed on both structures (Bergdahl, 1971).
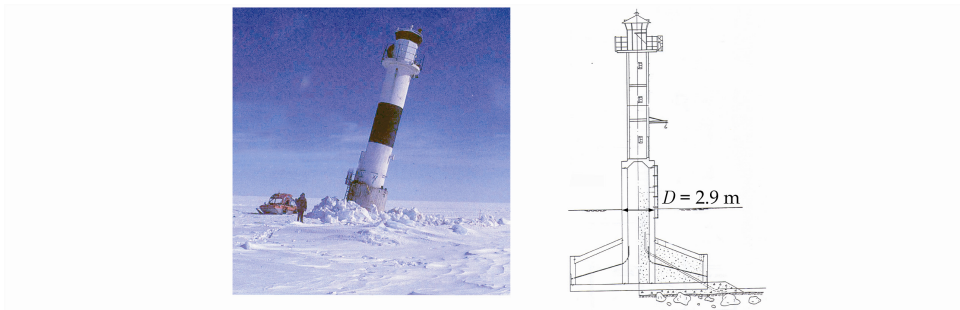

Figure 3.8. Björnklacken lighthouse (D = 2.9 m) after failure in 1985 (photo: L. Fransson).

Later stability of Borrusiagrunden and Björnklacken was increased with tension rock anchors, however, 4 April 1985, Björnklacken lighthouse started to move 17 m along the seabed and got a vertical inclination of 12° (Fig. 3.8) (Fransson and Danielson, 1985). No corrosion or other disabilities were observed on broken rock anchors after failure. Thickness of rafted ice interacting with the lighthouse was h = 1.4 – 1.5 m with ice loads calculated by hindcast methods as F_G = 10.9 MN, possibly including a dynamic amplification. Global ice pressure was calculated p_G = 2.7 MPa (h = 1.4 m).

Vallinsgrund lighthouse ❻ (Fig. 3.9) was constructed in mid 1970ies while in late April 1979, the lighthouse collapsed due to ice actions (Björk, 1981). In a series of damages addressed to ice actions during the period 1976-1979, a collapse was the final incident. The failure was addressed to ice crushing approximately 50 m during ice drift from south while characteristic ice was closed packed with small floes and consolidated ridges. Average ice concentration was about 80 % while the ice thickness was h = 0.5 - 0.7 m. The wind speed varied in the range 1.0-5.0 m/s with direction 340°-90° from North. Designers proposed the design load of the lighthouse to be F_G = 7.0 MN in MWL while pre-stressed rock anchors were supposed to have a strain of 0.7-1.0 m with a lighthouse inclination 10°. A global ice pressure caused by 7.0 MN was p_G = 4.4 MPa (h = 0.6 m).

Figure 3.9. Vallinsgrund lighthouse (D = 2.9 m)
(photo: Swedish Maritime Administration).

Norströmsgrund lighthouse ❹ was deployed in 1971, 60 km south east of Luleå in Sweden (Fig. 3.5). Norströmsgrund (Fig. 3.10) has been one of the major contributors to full-scale data on ice-structure interactions the last three decades. During its first winter in service, Norströmsgrund got cracks in its side walls due to ice actions (Björk, 1981). People working on the structure reported harsh vibrations during ice crushing whereupon the Swedish engineer Alf Engelbrektson installed accelerometers from 1973 to 1989 to determine details about the dynamic ice crushing phenomena. Engelbrektson (1977) reported accelerograms with integrated velocities and displacements, which revealed that the applied ice load had a static and a dynamic component. The static component was supposed to be connected to ice strength whereas the dynamic part was oscillating with a frequency around the natural frequency of the structure. In 1979 video cameras were installed to observe ice crushing. Analyses of video records showed that the ice thickness and drift speed played important roles during ice induced vibrations while it was elaborated that the ice sheet was crushed against the structure during a cycle with a characteristic crushing length. However, Engelbrektson and Jansson (1985) abounded this hypothesis, stating that the frequency of crushing was influenced by the resonant vibration of the structure at its natural frequency. Engelbrektson (1983) indicated that the global ice load could be in the range of F_G = 3.0 MN with an ice thickness h = 0.3-0.5 m, which gives a nominal pressures in the range p_G = 0.8-1.3 MPa.
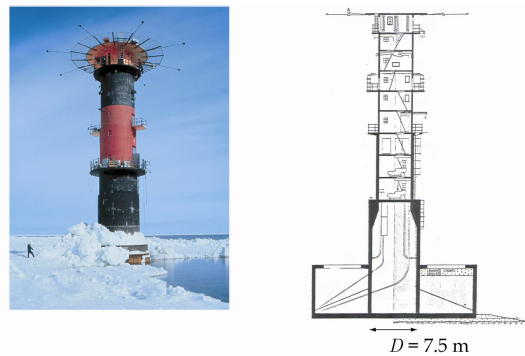

D = 7.5 m

Figure 3.10. Norströmsgrund lighthouse (D = 7.5 m, without panels) about 60 km south east of Luleå, Sweden (photo: Luleå University of Technology, LTU).

In 1986, a joint industry project (JIP) called "Ice Forces against Offshore Structures" was established between several oil companies together with Swedish engineers and scientists. Digital signal storing units were installed together with new inclinometers with an objective of measuring ice induced response on the Norströmsgrund lighthouse. Additionally, a pendulum system was installed to register inclination of the structure. Three ice load panels were installed in 1987 by Hamburg Ship Model Basin (HSVA) to record ice pressure in the water line. This new ice load panels were aimed to measure both normal and tangential forces (Wessels et al., 1989). Individual time series at each panel were measured winter 1989 and local peak pressures were in the range of $p_L = 1.5$ MPa during level ice crushing. Additionally, inclinometers and accelerometers were installed on the lighthouse Farstugrunden not far from Norströmsgrund; however, data from the Farstugrunden lighthouse has not been reported yet.

An aim during the first measurements on Norströmsgrund lighthouse was to derive a model for global ice loads by means of recordings from accelerometers and inclinometers. The first analyses of recorded accelerations included a disturbing drift in the integrated velocities and displacements. To get rid of the drift, new analyzing methods were introduced. Shortly, it was used a low pass filter on the inclinometer recordings and a high pass filter on acceleration signals. Then inclinometer recordings were used as a base line correction during stepwise integration of acceleration signals. From these investigations, a numerical ice load formula was derived based on data from Norströmsgrund (Engelbrektson, 1989) while a last refinement of the model was presented by Engelbrektson (1997).

A partly EU-funded and partly industrial funded project named "LOw LEvel Ice Forces" (LOLEIF) installed a new measuring setup at Norströmsgrund in 1998. LOLEIF installed nine individual ice load panels covering 167° of the MWL perimeter in 1998 while accelerometers and inclinometers were installed from 2001 to 2003. Together with ice thickness recordings from an electromagnetic (EM) device, a laser device and a sonar device, additionally four video cameras were installed to observe the ice-structure interactions. In 2001 a new project named "Measurements on STRuctures in ICE" (STRICE) was established which continued the LOLEIF project for three more years.

Schwarz (2001) presented first results from the LOLEIF project with pressures from level ice crushing in the range p_G = 1.4 MPa as the highest global pressure and p_L = 2.1 MPa as the highest pressure on one single load panel (D = 1.2 m).

An ice load panel was installed on a bridge pier in Kalix River ❸ with the aim of measuring ice forces during spring break-up (Fransson and Hoseth, 1999). Measurements were conducted for two years (1997 and 1998) while useful records of ice pressure were achieved from the last year only. The breadth of the bridge pier and the panel was D = 1.3 m and D = 0.3 m, respectively, while the nominal contact area of the panel was 0.1 m². The maximum panel pressure was p_G = 3.0 MPa whereas the highest forces were measured five minutes before fracturing of the whole ice cover. It was reported fluctuations of the ice load signal assumed to be caused by vibrations of the bridge. On the other hand, recorded responses of the bridge during the measurements were not reported. Corresponding the measurements on the bridge in Kalix River, ice samples were collected and the uni-axial strength was investigated. The highest strength measured was σ_c = 1.0 MPa.

Different ATN devices located along the Finnish coast have been instrumented to gain information about ice-structure interaction. This work concerns structures named Kemi I and Kemi-II/Kemi-2 located north in the GOB together with a set of channel markers situated along the Finnish coast.

The first Kemi I lighthouse ❶ (Fig. 3.11) was a steel structure deployed in 1973 which failed during its first winter in service. Failure was assumed to be due to ice actions of lock-in type and thereafter high static loads due to interaction with ridged ice (Määttänen, 1974). The largest accelerations recorded was 3.2g, which caused a dynamic ice force of F_{dyn} = 2.9 MN, a load exceeding the capacity of Kemi I steel lighthouse. From hindcast calculations, an ice pressure in the range of p_G = 5.0 MPa was derived from the current meteorological conditions at the site of Kemi I steel lighthouse the actual year

(Määttänen, 1974). It should be remarked that the aspect ratio (D/h) could approach one or less on the old Kemi I steel lighthouse.

The Kemi I concrete lighthouse (Fig. 3.12) was deployed in 1975 as a substitute of the failed Kemi I steel lighthouse. The lighthouse was instrumented with ice force measuring devices as pressure transducers and accelerometers from 1976. Altogether 30 pressure transducers organized in six rows and five columns were installed with the lowest row 3.8 m below MWL and the highest row 1.0 m above MWL. Accelerometers were installed at two different levels to collect information about the dynamic response during ice actions. To measure total bending moment, four rods were installed inside shield tubes, free to move in relation to the concrete structure. The relative movements of rods were sensed by strain-gauge transducers (Määttänen, 1977) while two data storing systems were in use, one that collected hourly peak measurements together with an analogue telemetry system transferring data to the University of Oulu.

Figure 3.11. Inclined superstructure of the Kemi I steel lighthouse
in the spring 1974 (D ~ 1.0 m) (photo: M. Määttänen).

The first analyses of data from Kemi I concrete lighthouse were reported by Määttänen (1977), which calculated maximal local pressure p_L = 2.5 MPa thus reduced to p_G = 1.8 MPa as global pressure. Reasons for this reduction were supposed to be non-simultaneous local load peaks. Frequencies of ice actions in the range of the fundamental

42

Figure 3.7. The tower of Nygrån lighthouse was broken the winter
1968/1969 (D = 2.5 m) (Reininus et al., 1972).
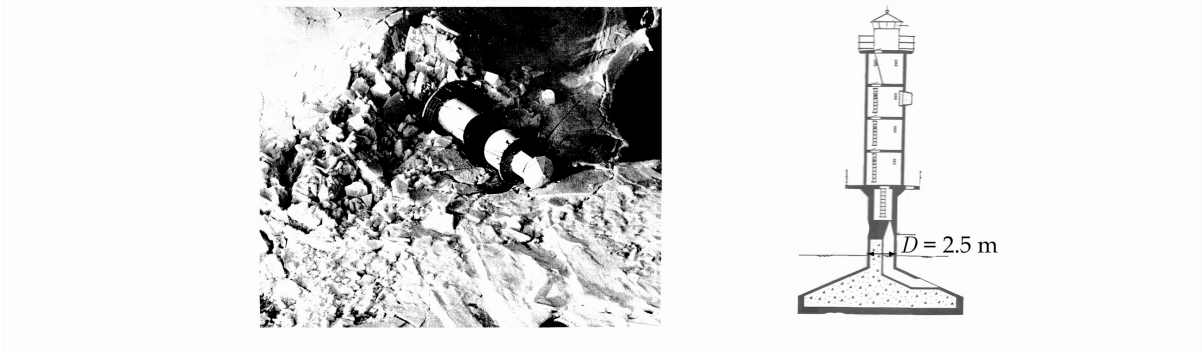
The Nygrån incident is a slightly different case compared to other failures due to ice loads in the same area. Nygrån lighthouse illustrates that not only the horizontal load capacity in MWL gives the global integrity of a structure. Especially in shallow waters, the geometric shape of the structure around MWL has to be considered. Nominal ice pressure is not calculated in this instance because the special circumstances during the failure.

The twin lighthouses Borrusiagrunden ❸ and Björnklacken ❷ were deployed at the Swedish coast in 1969, in an area with active ice drift most of the winter. During its first spring in service, horizontal displacements less than 0.1 m were observed on both structures (Bergdahl, 1971).
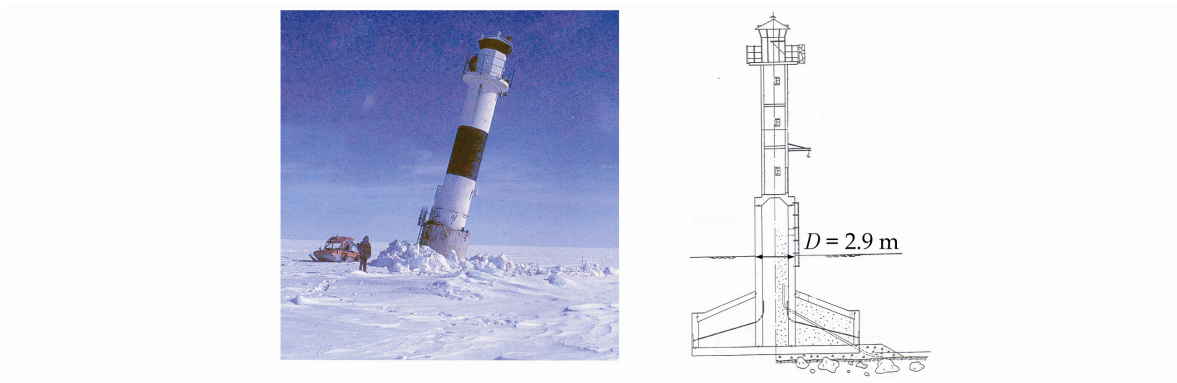

Figure 3.8. Björnklacken lighthouse (D = 2.9 m) after failure in 1985 (photo: L. Fransson).

Later stability of Borrusiagrunden and Björnklacken was increased with tension rock anchors, however, 4 April 1985, Björnklacken lighthouse started to move 17 m along the seabed and got a vertical inclination of 12° (Fig. 3.8) (Fransson and Danielson, 1985). No corrosion or other disabilities were observed on broken rock anchors after failure. Thickness of rafted ice interacting with the lighthouse was h = 1.4 – 1.5 m with ice loads calculated by hindcast methods as F_G = 10.9 MN, possibly including a dynamic amplification. Global ice pressure was calculated p_G = 2.7 MPa (h = 1.4 m).

Vallinsgrund lighthouse ❻ (Fig. 3.9) was constructed in mid 1970ies while in late April 1979, the lighthouse collapsed due to ice actions (Björk, 1981). In a series of damages addressed to ice actions during the period 1976-1979, a collapse was the final incident. The failure was addressed to ice crushing approximately 50 m during ice drift from south while characteristic ice was closed packed with small floes and consolidated ridges. Average ice concentration was about 80 % while the ice thickness was h = 0.5 - 0.7 m. The wind speed varied in the range 1.0-5.0 m/s with direction 340°-90° from North. Designers proposed the design load of the lighthouse to be F_G = 7.0 MN in MWL while pre-stressed rock anchors were supposed to have a strain of 0.7-1.0 m with a lighthouse inclination 10°. A global ice pressure caused by 7.0 MN was p_G = 4.4 MPa (h = 0.6 m).

Figure 3.9. Vallinsgrund lighthouse (D = 2.9 m)
(photo: Swedish Maritime Administration).

Norströmsgrund lighthouse ❹ was deployed in 1971, 60 km south east of Luleå in Sweden (Fig. 3.5). Norströmsgrund (Fig. 3.10) has been one of the major contributors to full-scale data on ice-structure interactions the last three decades. During its first winter in service, Norströmsgrund got cracks in its side walls due to ice actions (Björk, 1981). People working on the structure reported harsh vibrations during ice crushing whereupon the Swedish engineer Alf Engelbrektson installed accelerometers from 1973 to 1989 to determine details about the dynamic ice crushing phenomena. Engelbrektson (1977) reported accelerograms with integrated velocities and displacements, which revealed that the applied ice load had a static and a dynamic component. The static component was supposed to be connected to ice strength whereas the dynamic part was oscillating with a frequency around the natural frequency of the structure. In 1979 video cameras were installed to observe ice crushing. Analyses of video records showed that the ice thickness and drift speed played important roles during ice induced vibrations while it was elaborated that the ice sheet was crushed against the structure during a cycle with a characteristic crushing length. However, Engelbrektson and Jansson (1985) abounded this hypothesis, stating that the frequency of crushing was influenced by the resonant vibration of the structure at its natural frequency. Engelbrektson (1983) indicated that the global ice load could be in the range of F_G = 3.0 MN with an ice thickness h = 0.3-0.5 m, which gives a nominal pressures in the range p_G = 0.8-1.3 MPa.
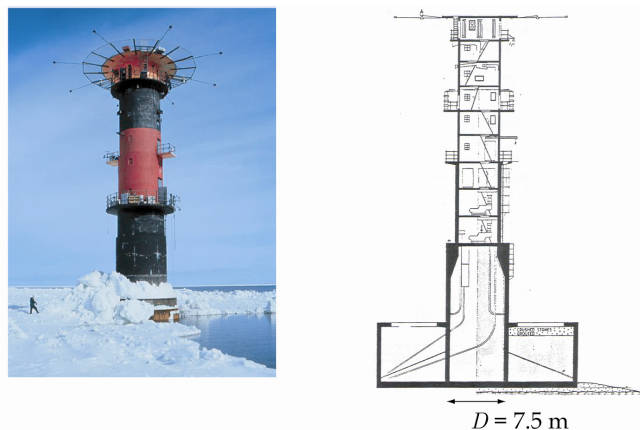

D = 7.5 m

Figure 3.10. Norströmsgrund lighthouse (D = 7.5 m, without panels) about 60 km south east of Luleå, Sweden (photo: Luleå University of Technology, LTU).

In 1986, a joint industry project (JIP) called "Ice Forces against Offshore Structures" was established between several oil companies together with Swedish engineers and scientists. Digital signal storing units were installed together with new inclinometers with an objective of measuring ice induced response on the Norströmsgrund lighthouse. Additionally, a pendulum system was installed to register inclination of the structure. Three ice load panels were installed in 1987 by Hamburg Ship Model Basin (HSVA) to record ice pressure in the water line. This new ice load panels were aimed to measure both normal and tangential forces (Wessels et al., 1989). Individual time series at each panel were measured winter 1989 and local peak pressures were in the range of p_L = 1.5 MPa during level ice crushing. Additionally, inclinometers and accelerometers were installed on the lighthouse Farstugrunden not far from Norströmsgrund; however, data from the Farstugrunden lighthouse has not been reported yet.

An aim during the first measurements on Norströmsgrund lighthouse was to derive a model for global ice loads by means of recordings from accelerometers and inclinometers. The first analyses of recorded accelerations included a disturbing drift in the integrated velocities and displacements. To get rid of the drift, new analyzing methods were introduced. Shortly, it was used a low pass filter on the inclinometer recordings and a high pass filter on acceleration signals. Then inclinometer recordings were used as a base line correction during stepwise integration of acceleration signals. From these investigations, a numerical ice load formula was derived based on data from Norströmsgrund (Engelbrektson, 1989) while a last refinement of the model was presented by Engelbrektson (1997).

A partly EU-funded and partly industrial funded project named "LOw LEvel Ice Forces" (LOLEIF) installed a new measuring setup at Norströmsgrund in 1998. LOLEIF installed nine individual ice load panels covering 167° of the MWL perimeter in 1998 while accelerometers and inclinometers were installed from 2001 to 2003. Together with ice thickness recordings from an electromagnetic (EM) device, a laser device and a sonar device, additionally four video cameras were installed to observe the ice-structure interactions. In 2001 a new project named "Measurements on STRuctures in ICE" (STRICE) was established which continued the LOLEIF project for three more years.

Schwarz (2001) presented first results from the LOLEIF project with pressures from level ice crushing in the range p_G = 1.4 MPa as the highest global pressure and p_L = 2.1 MPa as the highest pressure on one single load panel (D = 1.2 m).

An ice load panel was installed on a bridge pier in Kalix River ❸ with the aim of measuring ice forces during spring break-up (Fransson and Hoseth, 1999). Measurements were conducted for two years (1997 and 1998) while useful records of ice pressure were achieved from the last year only. The breadth of the bridge pier and the panel was D = 1.3 m and D = 0.3 m, respectively, while the nominal contact area of the panel was 0.1 m². The maximum panel pressure was p_G = 3.0 MPa whereas the highest forces were measured five minutes before fracturing of the whole ice cover. It was reported fluctuations of the ice load signal assumed to be caused by vibrations of the bridge. On the other hand, recorded responses of the bridge during the measurements were not reported. Corresponding the measurements on the bridge in Kalix River, ice samples were collected and the uni-axial strength was investigated. The highest strength measured was σ_c = 1.0 MPa.

Different ATN devices located along the Finnish coast have been instrumented to gain information about ice-structure interaction. This work concerns structures named Kemi I and Kemi-II/Kemi-2 located north in the GOB together with a set of channel markers situated along the Finnish coast.

The first Kemi I lighthouse ❶ (Fig. 3.11) was a steel structure deployed in 1973 which failed during its first winter in service. Failure was assumed to be due to ice actions of lock-in type and thereafter high static loads due to interaction with ridged ice (Määttänen, 1974). The largest accelerations recorded was 3.2g, which caused a dynamic ice force of F_{dyn} = 2.9 MN, a load exceeding the capacity of Kemi I steel lighthouse. From hindcast calculations, an ice pressure in the range of p_G = 5.0 MPa was derived from the current meteorological conditions at the site of Kemi I steel lighthouse the actual year

displaced about 14 m towards southeast in February 1967. After an ice pileup, the air temperature had been low for several weeks (-10°C to -26°C) together with winds in the range 10.8-13.8 m/s from northwest, which started the movement of the lighthouse along the seabed. One week later, the pack ice on the western side of the lighthouse had a thickness from 3.5 m to 4.0 m with a sail height of 0.5 m, while the surrounding level ice thickness was h = 0.7 m. The friction between the concrete foundation and the sea bed is unknown; hence, the predictions of applied ice loads must be approximately. The mass of the lighthouse was about 7.8 MN, hence with applications of a friction factor between 0.3-0.6, a horizontal force becomes F_G = 2.3-4.7 MN. An ice pressure can be calculated with an ice thickness h = 0.7 m as p_G = 1.0-1.9 MPa.
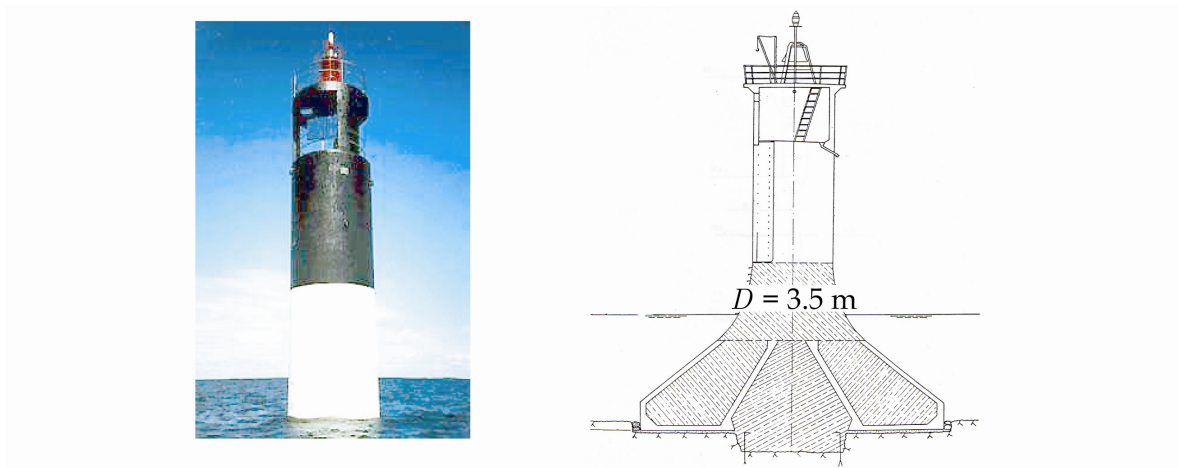

Figure 3.6. Tainio lighthouse (D = 3.5 m) (Finish board of Navigation, 2005).

The Nygrån lighthouse ❺ was constructed in 1958 and failed after ten years in service the winter 1968-69 (Fig. 3.7). Failure occurred due to tension cracks about one meter below mean water line (MWL) within the connection of the tower to the foundation (Bergdahl, 1971). The horizontal design load was F_G = 3.8 MN acting 0.5 m above MWL while in-situ observations registered that ridged ice tended to slide upwards the underwater caisson. With tensile cracks in the wall two meter above MWL, the attack point of the load causing failure was supposed to be higher than 0.5 m above MWL.

(Määttänen, 1974). It should be remarked that the aspect ratio (D/h) could approach one or less on the old Kemi I steel lighthouse.

The Kemi I concrete lighthouse (Fig. 3.12) was deployed in 1975 as a substitute of the failed Kemi I steel lighthouse. The lighthouse was instrumented with ice force measuring devices as pressure transducers and accelerometers from 1976. Altogether 30 pressure transducers organized in six rows and five columns were installed with the lowest row 3.8 m below MWL and the highest row 1.0 m above MWL. Accelerometers were installed at two different levels to collect information about the dynamic response during ice actions. To measure total bending moment, four rods were installed inside shield tubes, free to move in relation to the concrete structure. The relative movements of rods were sensed by strain-gauge transducers (Määttänen, 1977) while two data storing systems were in use, one that collected hourly peak measurements together with an analogue telemetry system transferring data to the University of Oulu.

Figure 3.11. Inclined superstructure of the Kemi I steel lighthouse
in the spring 1974 ($D \sim 1.0$ m) (photo: M. Määttänen).

The first analyses of data from Kemi I concrete lighthouse were reported by Määttänen (1977), which calculated maximal local pressure p_L = 2.5 MPa thus reduced to p_G = 1.8 MPa as global pressure. Reasons for this reduction were supposed to be non-simultaneous local load peaks. Frequencies of ice actions in the range of the fundamental

frequencies of the structure were discovered. However, such events were rare and not many details were reported.

Later, new analyses (1978-1981) were conducted with the purpose of estimating vertical distribution of pressure during ridge-structure interaction. Hoikkanen (1984) reported that the highest local pressure from consolidated parts of pressure ridges could be p_L = 7.5 MPa whereas the maximum global pressure from level ice (h = 0.8 m) was estimated as p_G = 1.7 MPa.
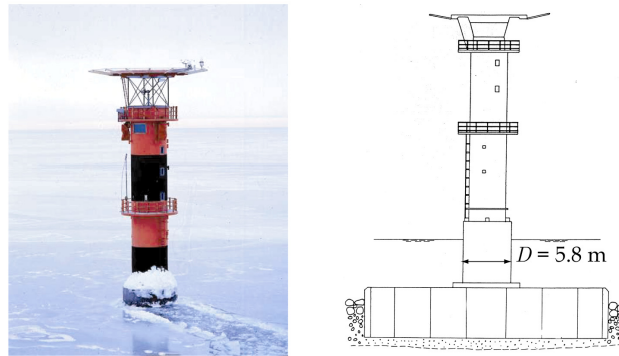

Figure 3.12. Kemi I concrete lighthouse (D = 5.8 m) with vertical sides
(photo: Finnish Board of Navigation).

During a JIP including Finnish ship industry and American oil companies, a steel cone was installed on the Kemi I concrete lighthouse from 1984 to 1987. This project aimed to investigate the behaviour of sea ice loads on a conical structure (Määttänen et al., 1996). The thickest level ice was reported as h = 0.9 m where rafted ice was reported h = 1.5 m.

Laboratory investigations reported σ_c from 1.7 MPa to 2.4 MPa and flexural strength (σ_f) from 0.4 MPa to 0.6 MPa with E-modulus from 3.0 GPa to 6.4 GPa. It was discovered from visual observations that accumulation of ice rubble in front of the cone was dependent on the drift speed while a rubble pile in front of the structure was more frequent with an ad-frozen snow cover on the ice or without a snow cover. Multimodal failure behaviour was discovered with bending, crushing and shearing modes present. Highest nominal pressure from level ice was found to be p_G = 0.3 MPa for D = 10.0 m.

The Kemi I test cone project offered for the first time reliable full-scale data of sea ice interaction with a conical structure.

The Kemi II ❶ lighthouse was constructed in 1973. The superstructure of the lighthouse failed due to dynamic ice loads during its first winter in service (1973/1974). Later, numerical simulations with an assumed forcing function showed that the acceleration might have been as high as 8g (Määttänen, 1974). The remaining parts of the superstructure were removed, and the first vibration isolated superstructure was installed on the original Kemi II foundation in 1976. However, in 1980 the original foundation was overloaded probably due to loads from a pressure ridge. The foundation got a tilt of 10° from that event. The vibration isolated superstructure was reinstalled on top of the new Välikivikko edge marker, where it is still in service. A completely new lighthouse named "Nukkujan matalan majakka" (Fig. 3.13) with a vibration isolated superstructure was constructed in 1981 (renamed 1986 to Kemi-2). The Kemi-2 was designed with 6 % modal damping which seemed to be suitable in the GOB to avoid ice-induced vibrations. Structures like the Kemi-2 lighthouse was the first to prove that vibration isolated structures were able to mitigate ice-induced vibrations. However, in 2000 a German ship collided with Kemi-2 and destroyed the superstructure. A new superstructure with a cone at waterline and vibration isolated lantern/battery pack was installed in 2001 on top of the remaining foundation pile. The name of the new lightpier is "Kemi-2 Radar Beacon".

Kemi-2 lighthouse was instrumented with strain gauges and accelerometers including a remote control system transmitting real time data to University of Oulu. The highest global recorded ice load was F_G = 3.9 MN, which gave p_G = 4.3 MPa (h = 0.9 m) (Määttänen, 1987). Ice thickness and drift speed were hindcasted from environmental parameters as wind speeds and air temperatures. Määttänen (1987) reported experiences from two other lighthouses of similar type as the Kemi-2, namely Kokkola test lighthouse and Välikiviikko lighthouse.
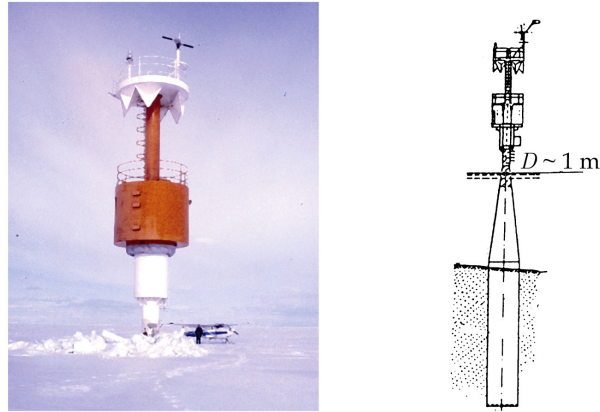
Figure 3.13. The Kemi-2 steel lighthouse (D = 1.0 m) (Määttänen, 1987).

Measurements on different channel markers ❾ (Fig. 3.14) located along the Finnish coast were conducted during winter 1987/1988 (Nordlund et al., 1988). The focus in this study was the occurrence of ice-induced vibrations and development of less costly channel markers. Little attention was paid on reporting global ice pressure. Due to remote location of channel markers, an automatic measuring procedure was developed which recorded 29 events with accelerations exceeding 0.1g. The highest accelerations were reported to be about 1.0g-2.0g with extreme events as high as 5.2g.

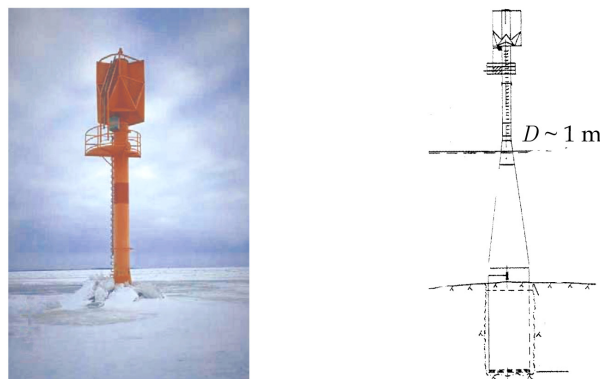Figure 3.14. Channel markers (D = 0.9 m) located along the coast
of Finland (Nordlund et al., 1988).

3.6 Explorations in North America

3.6.1 Measurements in Cook Inlet, Alaska, 1963-1976

Offshore structures in Cook Inlet, Alaska, were generally steel jackets or of the monopod type, located in a sub-arctic (Zone III) area including drifting first-year sea ice between November and early March. A common ice thickness was h = 0.4 m but could reach maximum h = 0.7 m during January and February (Peyton, 1966). Strong winds and tidal actions caused that few ice floes were remaining in Cook Inlet for more than 30 days. Furthermore interactions with coastlines resulted in a high density of low consolidated pressure ridges.
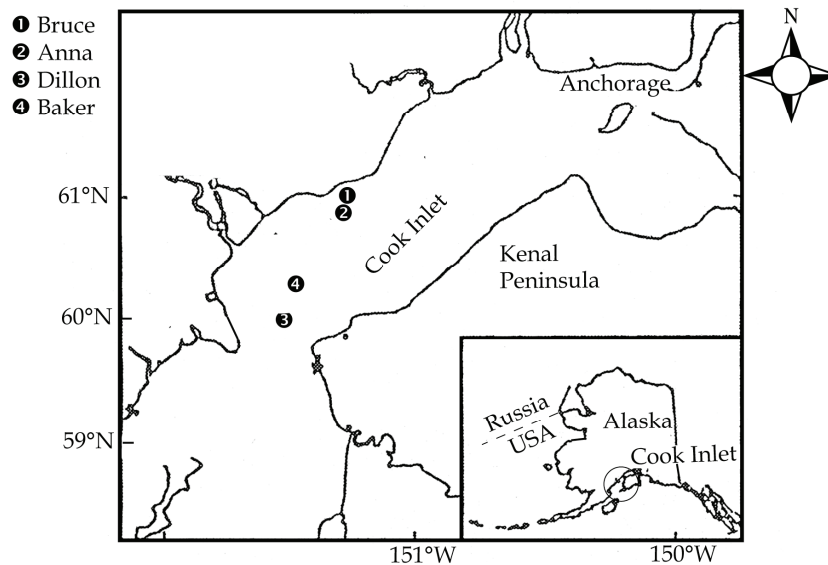
Figure 3.15. A map with the locations of four instrumented platforms in Cook Inlet, Alaska.

Several structures in Cook Inlet, including a specially designed test pile, were instrumented with strain gauges to measure ice forces from 1963 to 1976. Vibrations of structures complicated the analyses of measured time series because measured loads could possibly include dynamic amplification. Loads from pressure ridges were predicted as two-three times higher than loads from level ice sheets while typical results from a cylindrical platform leg (D = 4.3 m) (Fig. 3.16) showed that steady loads from level

ice crushing could be from $F_G = 0.3$ MN to $F_G = 1.4$ MN ($h = 0.4$ m) with corresponding pressure $p_G = 0.2$-0.8 MPa (Blenkarn, 1970). Dynamic loads were reported in the range $F_d = 1.8$-3.8 MN with static loads from ridges $F_m = 0.9$ - 2.2 MN. Principal sources of data from analyses of Cook Inlet data are Blenkarn (1970) and Peyton (1968) which did not report pressures exceeding $p_G = 1.0$ MPa. More recently, Bhat and Cox (1995) presented analyses of records from the platforms Anna, Bruce (Fig. 3.16) and Dillon from a statistical point of view. They reported that ice pressure seems not to exceed $p_G = 2.0$ MPa for ice thickness $h = 0.7$ m, it is not clear if that pressure includes dynamic amplification or not.
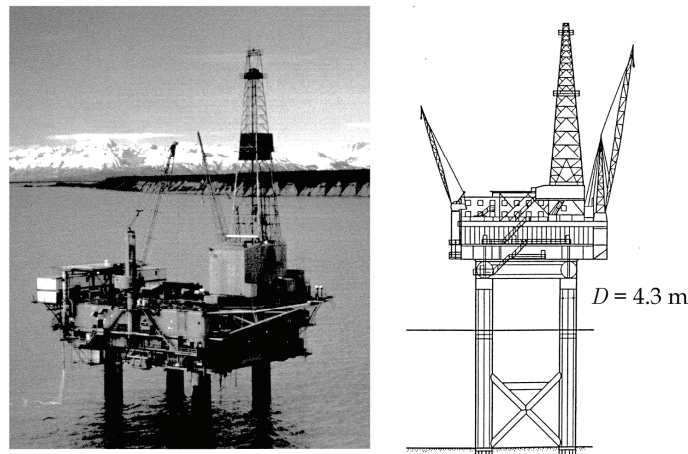
Figure 3.16. Four-legged steel jacket platform "Bruce" ($D = 4.3$ m) as it looked in Cook Inlet, Alaska (photo: Cook Inlet Regional Citizens Advisory Council).

3.6.2 Ice load measurements in St. Lawrence River, Canada, 1958-1989

ATN structures in St. Lawrence River (Fig. 3.17) have been instrumented to record ice actions. Most structures have cone interfaces in the water line as shown on the Prince Shoal lighthouse (Fig. 3.18) while they usually are steel shell structures with a concrete core supported by piles. Measurements have been conducted on structures located between St. Lawrence River Estuary not far from Quebec and Lake Ontario. Ice conditions is of first-year freshwater type (Zone III) with the thickest ice $h = 0.8$ m

reported by Danys (1981). Ice in the St. Lawrence River and its surrounding lakes are usually broken into pieces by winter navigation.

Figure 3.17. Map of St. Lawrence River with location of lighthouses (after Frederking et al., 1991).

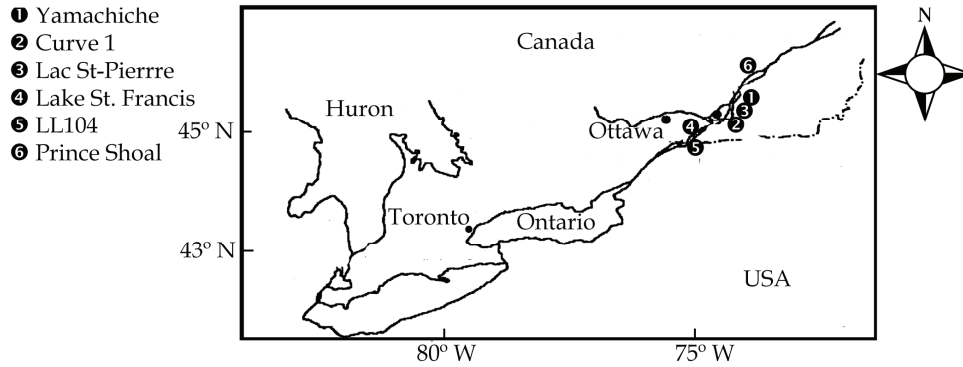Three programmes have presented analyses of ice actions in St. Lawrence River water systems. First, 22 offshore light piers were analysed, of which seven had been damaged or destroyed by ice (Danys, 1975). All damaged piers were found analytically incapable to withstand ice pressure greater than p_G = 0.7 MPa, whereas structures without damages were found to withstand at least p_G = 2.1 MPa.

Results from a second programme were reported by Danys (1981), which describes instrumentation of three light piers. These structures were Yamachiche Bend, Curve 1 and Curve 3 light piers. All structures had characteristic widths in the range from D = 4.0-5.0 m, where ice load panels were installed in the water line together with accelerometers on the structure top side. Global ice pressures were reported as p_G = 0.8 MPa, approximately 20-40 % less than maximal local panel pressures. Experiences obtained on light piers in St. Lawrence River were applied during instrumentation of the Kemi I lighthouse during the earlier mentioned "Test cone project".

Third, a joint programme between Canadian Coast Guard and National Research Council Canada (NRC) reported ice actions from five different light piers during eight years

(Frederking et al., 1991). The level ice thickness was h = 0.6 m while lighthouses in this programme had much the same instrumentation as reported by Danys (1981). The light piers instrumented had two different slope angles 45° and 76°, measured from horizontal, however no clear difference was predicted between the magnitudes of ice loads measured on these two slope angles. The highest measured ice pressures were in the range of p_G = 0.5-0.7 MPa, considerably higher than recommended by the Canadian Standards Association (1988).
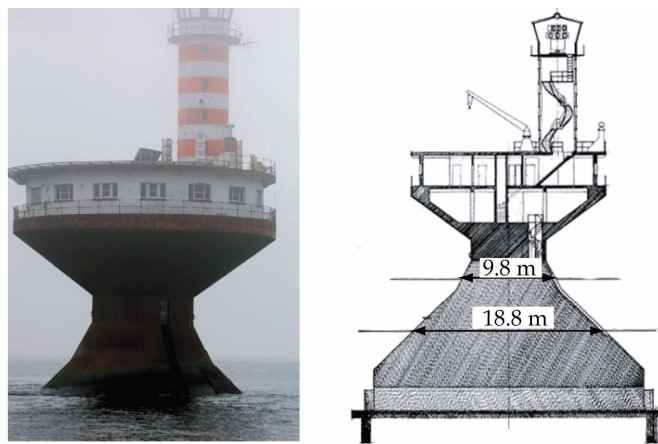
Figure 3.18. Prince Shoal lighthouse (D = 9.8-18.8 m, MWL) in the
St. Lawrence river, Canada (Danys, 1971).

3.6.3 Experiences with ice actions against Canadian bridges, 1966 - present

The instrumented bridge pier at Hondo (Fig. 3.19) in Athabasca River, Alberta is a massive concrete structure inclined 67° from horizontal and instrumented during construction in 1966 (Sanden and Neill, 1968). Ice conditions are first-year freshwater ice with maximum thickness h = 1.1 m (Montgomery and Lipsett, 1980). Most dominant failure modes were reported to be crushing and bending during interaction with level ice.

Montgomery and Lipsett (1980) conducted measurements on the bridge pier to predict its dynamic structural properties where they performed controlled load tests to determine the stiffness and the damping of the pier. Natural frequency and damping ratio relative to critical were found to be 8.9 Hz and 19 %, respectively. The bridge pier was first

instrumented with a hinged beam system in 1966 for direct measurements of ice forces while accelerometers were installed in 1978 to figure out dynamic response of the structure. The agreement between direct applied forces and loads derived from deconvolution of measured response was acceptable, which suggests there was little interaction between structure and ice.

Ice runs at Hondo were divided into three stages where the first stage was concerned with an ice break-up in the vicinity of Hondo. The second run involved thicker ice found between Hondo Creek and Rourke Creek, whereas the last stage happened when ice upstream Rourke passed Hondo. The highest pressure reported by Montgomery and Lipsett (1980) was p_G = 1.9 MPa.
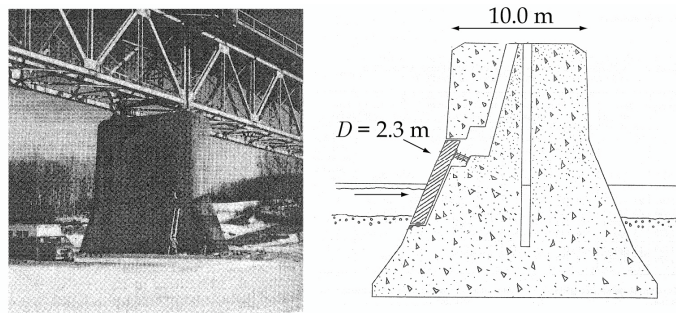
Figure 3.19. Hondo bridge pier (D = 2.3 m) in
Athabasca River, Alberta (after Neill, 1970).

A steel structure named Pembridge is crossing Pembina River in Alberta. Ice conditions are first-year freshwater with ice actions associated with spring break-up. The thickest ice floes were reported as h = 0.6 m.

Two measuring programmes were conducted on Pembridge (Fig. 3.20), the first in 1969 and 1970, reported by Neill (1970), and the second from 1973 to 1979, described by Lipsett and Gerard (1980). Pembridge was first instrumented with strain gauges to measure bending strains inside a vertical hollow steel pipe. However, the steel pipe was early damaged by ice actions and a new hinged beam (D = 0.9 m) as shown in Fig. 3.20 was installed in 1969. Neill (1970) mentioned that ice actions on the hinged beam were dominated by spikes due to drift of broken ice floes. The maximum ice pressure reported

was p_G = 2.7 MPa while no details were reported on the dynamic amplification of this load. However, due to the test pile geometry, vibrations might have taken place during ice actions.
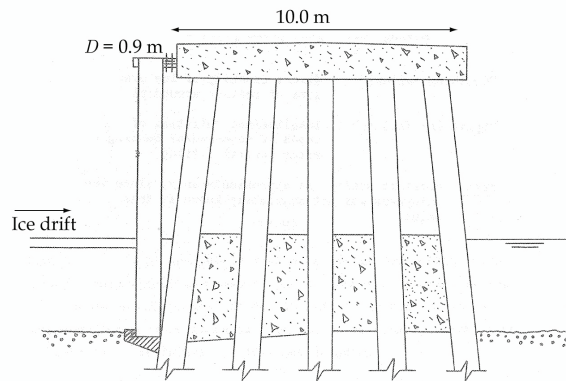
Figure 3.20. Principal sketch of the Pembridge structure in Pembina River with its instrumented pile (D = 0.9 m) (after Neill, 1970).

At Rideau River, Ontario a bridge pier with a V-shaped cross section (D = 2.1 m) was instrumented from 1986 to 1991. First-year freshwater ice in this river has a characteristic thickness h = 0.6 m (Frederking and Sayed, 1992). The river ice in Rideau River is commonly blasted by the City of Ottawa to prevent flooding. NRC took advantage of this blasting to have controlled ice-structure interaction events. The bridge pier is a part of Minto Bridge in Ottawa, and was instrumented with strain gauge panels from 1986 to 1987 and with additionally fluid filled panels in 1988. Local pressures about p_L = 6.0 MPa were recognized on small areas by hindcast calculations of destructed structural members while the highest global pressure on the pier was p_G = 0.6 MPa (Frederking and Sayed, 1992).

3.6.4 Investigations of ice forces in American rivers

All measurements in American rivers were conducted on first-year freshwater ice (Zone III) while the ice thickness differs significantly between e.g. the White River Junction on the east coast of USA and in the Yukon River in Alaska.

A joint project between NRC and Cold Regions Research and Engineering Laboratory (CRREL) named "Measuring ice forces on the St. Regis River, Hogansburg, NY" reported ice forces measured on a bridge pier in St. Regis River (Haynes et al., 1991). The ice thickness was measured as h = 0.2 m while ice pressures during spring break-up were investigated by a hinged beam (D = 1.2 m) in the winter of 1990/1991 and gave six load time series with maximum pressure p_G = 1.5 MPa.

Another bridge pier (Fig. 3.21) (D = 1.2 m) located near White River Junction, Vermont, USA was instrumented with the purpose of collecting data on ice loads and ice scouring. The thickest ice during the winter 1992/1993 was h = 0.5 m (Zabilansky, 1996) while one inclined bridge pier was instrumented with a load panel as shown in Fig. 3.21. Due to drift of small ice floes in the river during spring break-up, ice load time series were characterized with short spikes of maximum pressure p_G = 0.3 MPa (Zabilansky, 1996).
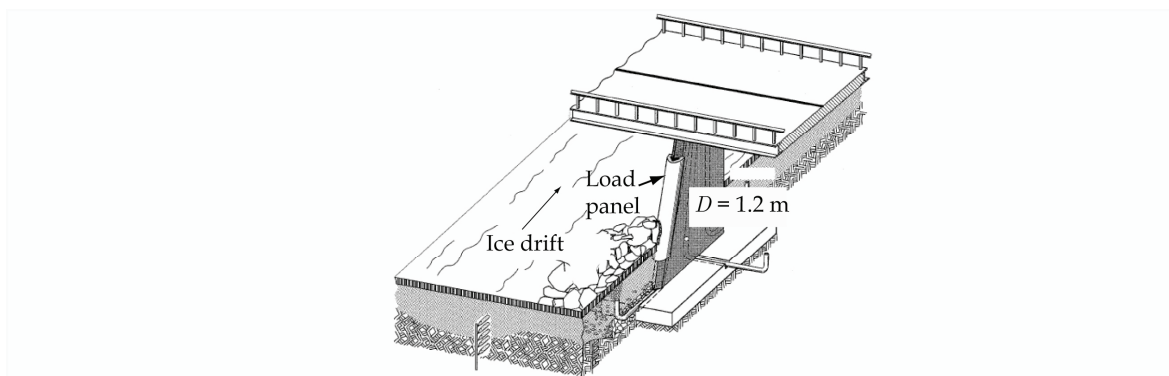

Figure 3.21. A bridge pier near White River Junction, Vermont, USA

(D = 1.2 m) (Zabilanski, 1996).

Bridge piers (D = 2.7 m) on Yukon River Bridge (Fig. 3.22) located at the North Slope Haul Road, west of Fairbanks, Alaska were instrumented for recording ice actions. The ice conditions in this river were first-year freshwater with thickest ice h = 1.5 m. Drift speed of the ice runs was about v_i = 3.0 m/s during four spring break-ups studied by MacFadden et al. (1981) from 1977 to 1980. Ice loads were measured by load cells mounted in front of one pier with accelerometers mounted on two of the piers while the ice thickness was measured by use of a radar pulse technique. Ice loads were derived from acceleration signals with the transfer function approach and with a load frame mounted on the bridge pier. Problems were revealed with the load frame, however, estimates of F_G = 1.3 MN (p_G = 0.5 MPa) were presented as the highest force from crushing of an ice floe with mean thickness h = 1.1 m (MacFadden et al., 1981).
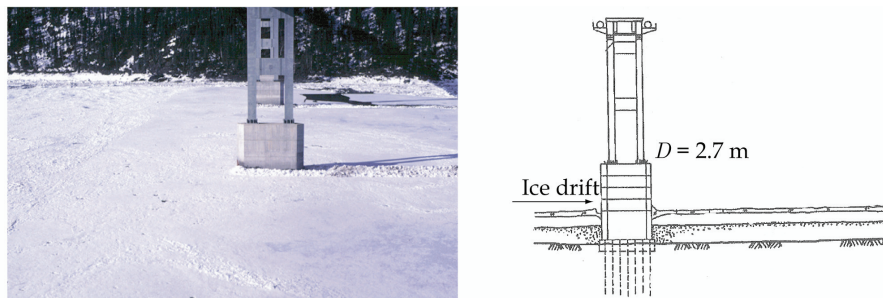
Figure 3.22. The Yukon River Bridge located in Alaska, USA (Sodhi, 1988).

3.6.5 Measurements on the Confederation Bridge, Canada 1997 - present

The Confederation Bridge is crossing Northumberland Strait between Prince Edward Island and New Brunswick (Fig. 3.23). Sea ice in that area is of first-year type (Zone III) with maximum ice loads caused by ice thickness h = 0.7 m (Brown, 2001). Because the ice are moving due to winds and currents, a large number of pressure ridges interacts with the bridge piers every winter. Two bridge piers as shown in Fig. 3.24 were instrumented in 1997. They have a cone in the water line to enable drifting ice floes to fail by bending instead of pure crushing. Tiltmeters and ice load panels were installed to measure the total and local ice loads, respectively. Sonars and Acoustic Doppler Current Profiler were

installed to measure a underwater profile of the interacting ice features (Bruce and Brown, 2001).
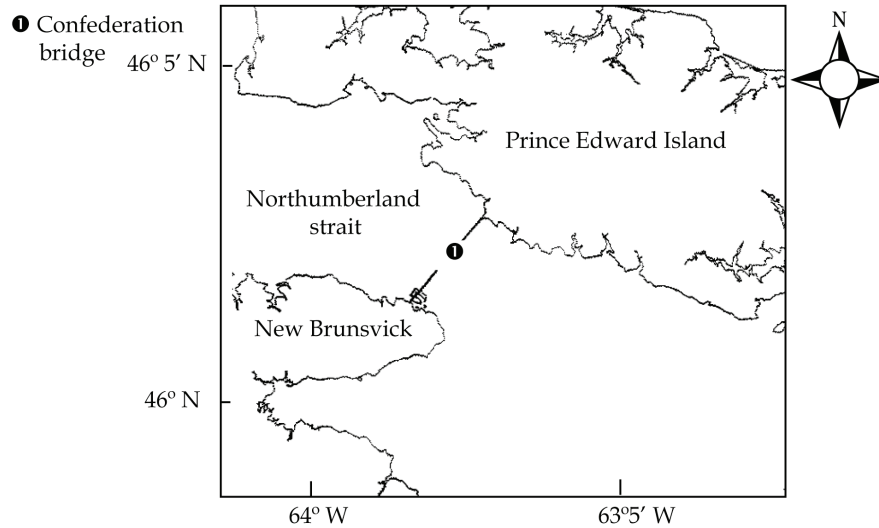
Figure 3.23. The location of the Confederation Bridge between Prince Edward Island and New Brunswick in Canada.

Lemee and Brown (2005) presented analyses of pressure ridge interactions where they reported loads of about F_G = 3.8 MN from ridges with keel depths of 17 m. No connections were detected between keel depths and global loads on the bridge piers. Based on observations of algae growth on piers, loads from unconsolidated ice in ridge keels were supposed to be minor. The highest load reported by Brown (2001) from the period 1997 to 2001 was in the range of F_G = 4.8 MN, which gives a pressure p_G = 0.7 MPa.
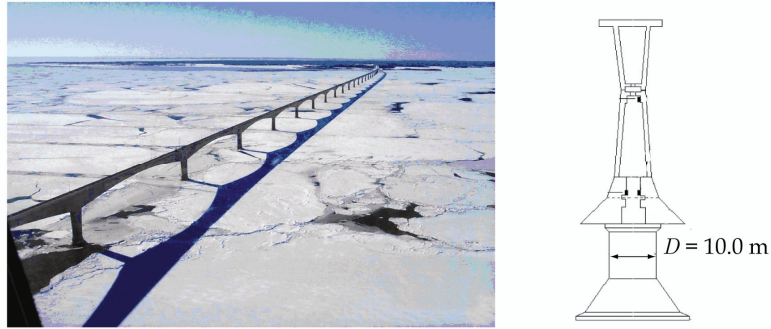
Figure 3.24. The Confederation Bridge with an instrumented
bridge pier (Lemee and Brown, 2005).

3.6.6 Field investigations in the Beaufort Sea, 1970 - 1990

During 1970ies and 1980ies, activities on oil exploration in Canadian and American parts of the Beaufort Sea took place (Fig. 3.25). The Beaufort Sea contains both first-year and multi-year ice features (Zone II), which have motivated use of caisson structures and artificial islands in this area. Initially, the knowledge about actual ice loads on wide structures was sparse, whereas many of the structures were instrumented to measure ice loads. Typical design first-year ice thickness in the Beaufort Sea is h = 1.8 m (Blanchet and DeFranco, 1996), while Timco and Burden (1997) reported that first-year ridge keel depths between 20 m and 30 m could occur.

Investigations on the following structures are mentioned; Tarsiut N-44 Caisson, Single-Steel Drilling Caisson (SSDC), Caisson-Retained Island (CRI) and Mobile Arctic Caisson (MAC) Molikpaq. Information presented in this section is compiled from reviews by Blanchet and Kennedy (1996), Timco and Johnston (2003, 2004) and Johnston and Timco (2003).

❶ Uviluk
❷ Amerk
❸ Amauligak
❹ Kogyuk
❺ Isserk
❻ Kaubvik
❼ Kadluk
❽ Tarsiut, N-44
❾ Tarsiut (Molikpaq, P-45)
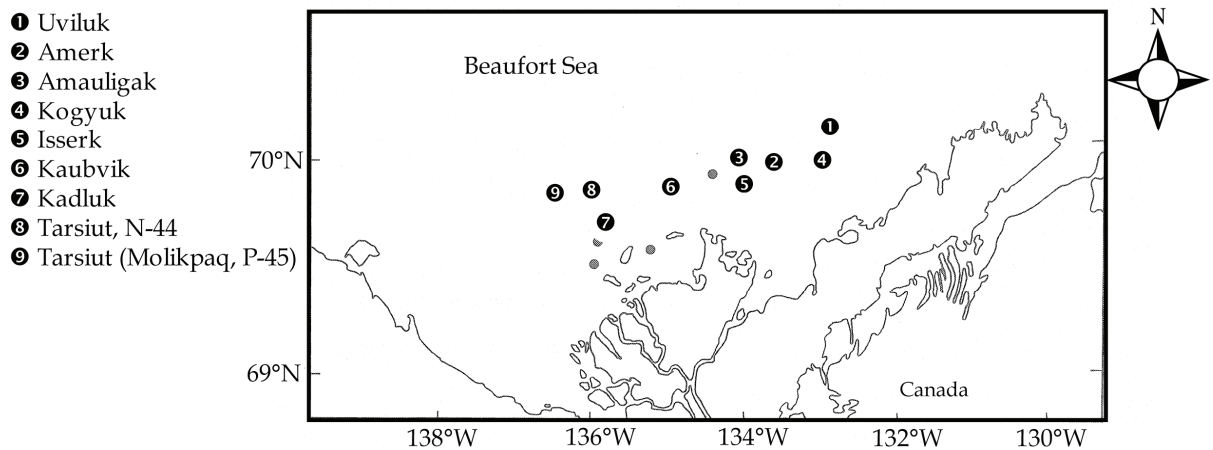
Figure 3.25. Overview showing deployments of caisson structures
in the Canadian Beaufort Sea.

The Tarsiut N-44 caisson (Fig. 3.26) was the first caisson structure used in the Arctic. It consisted of four individual ten meter high concrete caissons (Fitzpatric and Stenning, 1983) with total width D = 110.0 m. In 1982-1983, Tarsiut N-44 was used for observational purposes and studies of ice-structure interactions only. The instrumentation consisted of both direct load measurements and indirect response measurements with strain gauges and geotechnical sensors in the core and the foundation. The global ice load was estimated F_G = 140.0 MN, which gives a pressure p_G = 0.7 MPa (h = 1.8 m) (Blanchet and Kennedy, 1996), a load measured directly at the caisson and after transmitting through grounded rubble. Timco and Wright (1999) have discussed four selected ice loading events from Tarsiut N-44.
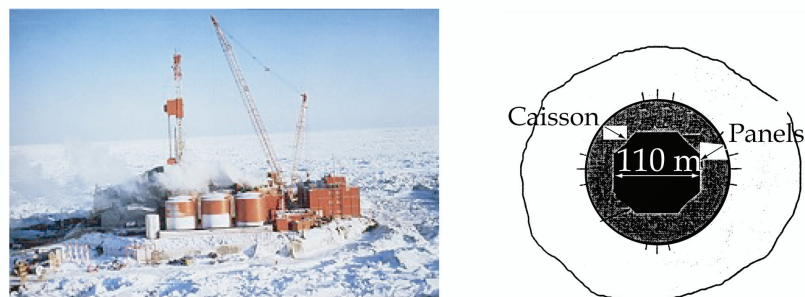
Figure 3.26. Tarsiut N-44 caisson in the Canadian Beafort Sea (EBA, 2005).

The Single-Steel Drilling Caisson (SSDC) is a super tanker (Fig. 3.27) that has undergone extensive modifications to adapt it for use as a support structure for year-round exploratory drilling in the Beaufort Sea. The structure was 162.0 m long, 53.0 m wide at the stern, 38.0 m at the bow, 25.0 m high and all sides were vertical at the waterline. SSDC was initially designed to rest in nine meter water depth. It was deployed at four different sites, Uviluk (Fig. 3.25) and Kogyuk, in the Canadian Beaufort Sea and Phoenix and Aurora, offshore Alaska in the American Beaufort Sea. The structure had different instrumentations at each of the four sites described by Johnston and Timco (2003). At Uviluk and Phoenix sites, liquid filled MEDOF panels were placed both on the structure and in surrounding ice. Remote measuring systems of ice conditions as well as in-situ thermistorstrings were used to monitor the ice conditions surrounding SSDC. Reliable ice load measurements were only obtained at Phoenix and Aurora sites. The highest reported global pressure was p_G = 1.2 MPa (Johnston and Timco, 2003).
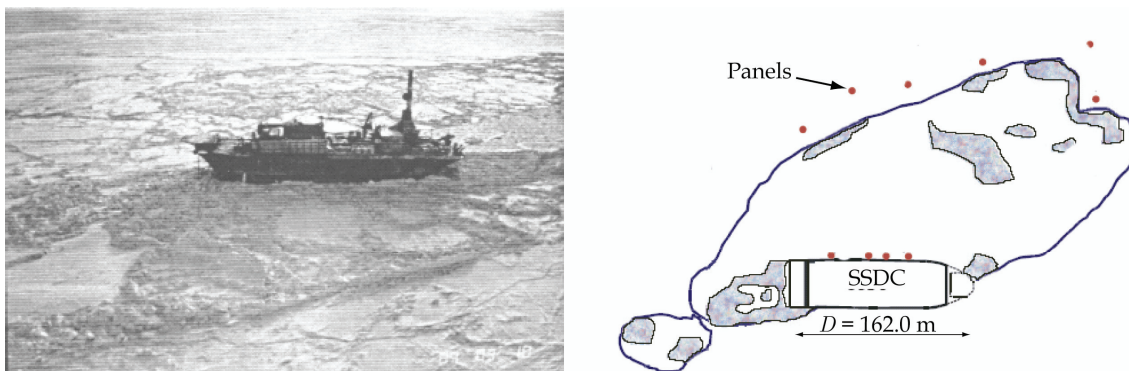
Figure 3.27. Single-Steel Drilling Caisson (SSDC) (D = 162.0 m) drilling unit at the Phoenix site (Johnston and Timco, 2003).

CRI is an segmented (Fig. 3.28), 12.0 m high octagonal shaped steel structure of size D = 117.0 m across the flats and an outer face which are inclined 30º from vertical (Blanchet and Kennedy, 1995). CRI was built by means of reducing dredge quantities compared to traditional sand islands. The caisson was built in 1982–1983 and deployed in the summer 1983. The CRI has eight individual caissons (43.0 m long, 12.2 m high and 13.1 m wide) in a ring, which is pre-stressed by steel wire cables holding the caissons together. Central core is filled with sand to provide stability against applied loads. The CRI was deployed

in the period 1983-1987 at three different sites, namely the Kadluk, Kaubvik and Amerk sites (Fig. 3.25). Three different types of direct ice load sensors were in use (Hawkins et al. 1983), as well as several sensors located in surrounding ice (Sayed et al., 1986). No time series are available from 1983 to 1985 whereas in the winter 1986-1987, an extensive programme was initiated. Croasdale et al. (1988) have summarized these attempts and reported low global ice loads in the range of only F_G = 10.0 MN while Johnson (1983) presented line integral analyses of ice pressure where he found global ice loads of about F_G = 150.0 MN, which gives p_G = 0.7 MPa. Another finding from this programme was that ice pressure measured through the ice sheet thickness indicated that ice loads was transmitted non-uniformly over the thickness.
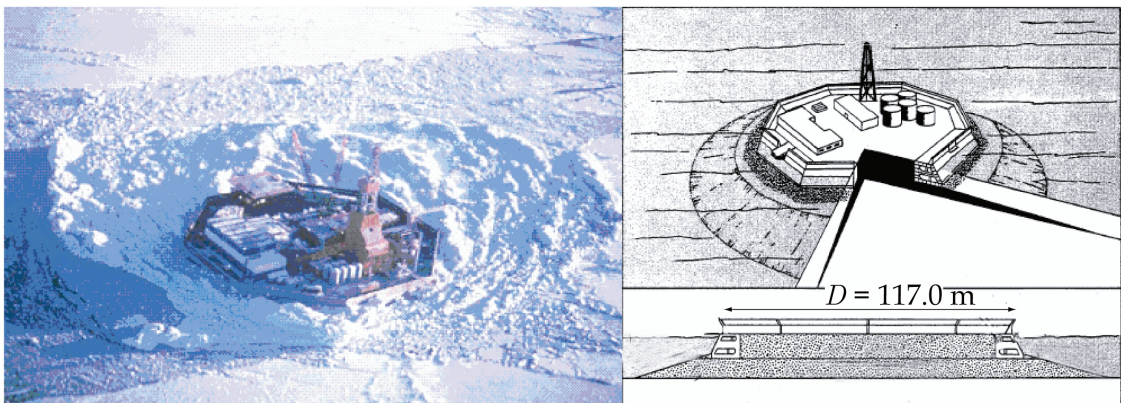
Figure 3.28. Caisson Retained Island (CRI) (D = 117.0 m) surrounded by grounded ice rubble in the Beaufort Sea and a cross sectional drawing (Croasdale, 1985).

Molikpaq was operating in the Beaufort Sea (Fig. 3.29) on four different sites, namely Amauligak I-65, Amauligak F-24, Isserk and Tarsiut from 1984 to 1990 (Fig. 3.25). Molikpaq deployments had considerable ice actions from multi-year ice features together with different kinds of first-year ice. The caisson consisted of a continuous steel annulus filled with sand and ballasting water while the side walls were inclined from 8° to 23° from vertical, depending on the water depth.
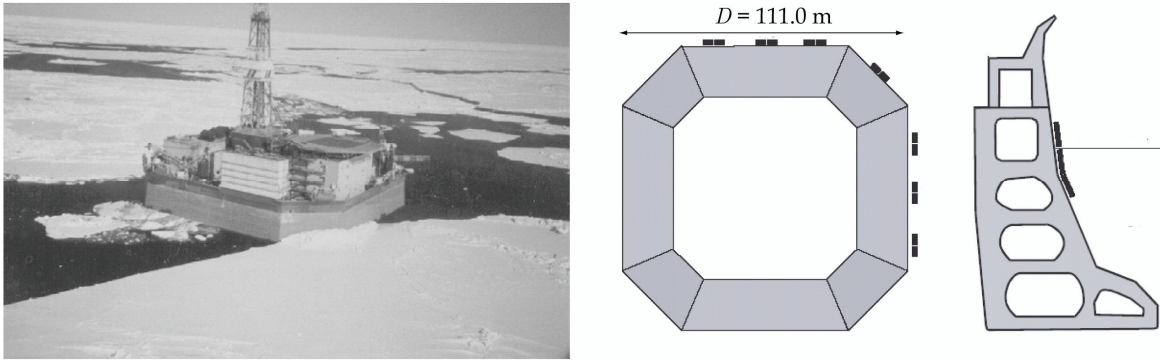
Figure 3.29. Molikpaq under ice actions (Timco and Johnston, 2003).

Exposed water line width of the caisson was D = 111.0 m (Rogers et al., 1986). Molikpaq was instrumented with clusters of MEDOF panels, strain gauges on the caissons main bulkheads and extensometers that sensed the overall deformation of the structure (Wright and Timco, 2001). Despite a large number of measuring devices, MEDOF panels provided the most useful information about ice pressure (Timco and Johnston, 2003) while if frequency resolution of more than 1 Hz was needed, strain gauges gave valuable information (Klohn-Crippen, 1998).

Measured data conducted on the Molikpaq in Beaufort Sea have been an extensive source of information on ice-structure interactions. Several studies have been conducted on analyses. However, two major concerns are selected, namely dynamic effects due to resonance-like ice crushing and first-year ice ridge actions on the Molikpaq.

Before 12 April 1986, it was believed that resonance-like ice crushing should be considered only on narrow structures with low aspect ratios (D/h). This was doubted after Molikpaq got significant vibrations during ice actions (Jefferies and Wright, 1988).They reported that a large multi-year ice feature was drifting against the Molikpaq with a speed of v_i = 0.06 m/s, causing global loads higher than F_G = 500.0 MN. Jefferies and Wright was the first to show that local loads could be synchronized on a wide structure during ice crushing and it was concluded that the dynamic response was due to the unloading phase and not the loading phase. Timco et al. (2005) showed new interpretations of data from an event 12 May 1986. During this event, a large first year ice

floe with inclusions of multi-year features was crushing into the caisson with an initial speed of v_i = 0.18 m/s, and slowing down to zero speed. Peak loads from this event measured on the north side of the caisson were about F_G = 250.0 MN. This event also showed vibration of the structure with a change in frequency as the ice floe slowed down.

Loads from first-year ice ridges on the Molikpaq were reported by a series of papers written by scientists at different companies. Among others, these works were compiled in a summarizing paper by Wright and Timco (2001), describing the most knowledge about ridge failure modes and applied loads from ridges to wide structures. The keel loads were estimated from load panels covering only parts of the entire ridge keel. Comparisons with existing codes were also conducted in this work, which showed that most codes are over-predicting the loads from unconsolidated ridge keels.

Recently, most data recorded at the Molikpaq in the Beaufort Sea became public where Timco and Johnston (2004) presented an overview analysis of measured loads. Important conclusions were that global ice loads seemed to increase with ice thickness and that global ice pressure from first-year ice not exceeded p_G = 1.5 MPa for the significant loads while p_G = 1.8 MPa was calculated for few events with low global loads and thin ice (Timco and Johnston, 2003).

To summarize, full-scale measurements on twelve structures located in North America have been mentioned in this section. Out of this, one series of measurements conducted on piled steel jacket structures, another on light piers with a cone interface, five bridge piers with different shapes and at last four structures of caisson type.

3.7 Present and future measurements in Eastern waters

3.7.1 Investigations in Bohai Sea, China, 1977 - present

Bohai Sea is an eastern extension of the Yellow Sea in China (Fig. 3.30). The climate is sub-arctic (Zone III) with level ice thickness rarely more than h = 0.6 m and rafted ice seldom thicker than h = 1.0 m (Yang, 2000). Interactions between offshore structures and pressure ridges are infrequently a case in Bohai Sea. The ice season extends typically from December to March and the ice drift speeds are relatively high, with reported values of v_i = 1.50 m/s (Yang, 2000). Ice problems related to offshore structures in the Bohai Sea have been for the most part due to vibrations of structures during ice crushing.
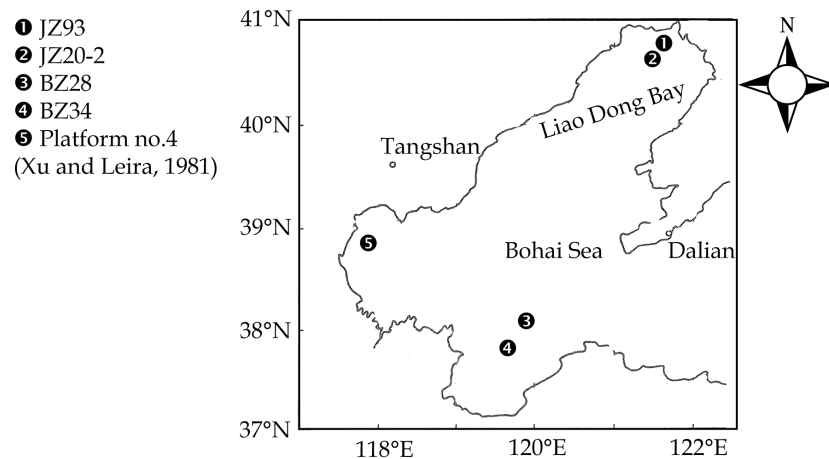
Figure 3.30. Map of the Bohai Sea with the locations of oil fields where platforms have been involved in ice-structure interactions.

An early attempt to study ice-induced vibrations of structures in the Bohai Sea was reported by Xu et al. (1983) from an incident in the spring 1977 with a four-legged accommodation platform (❺ in Fig. 3.30). A mechanical "vibrationmeter" was mounted on the deck for measuring displacements while ice forces were estimated from frequency domain analyses. It was pointed out that ice-induced vibrations were more probable for thicker than thinner ice sheets (Xu and Leira, 1981). Neither maximum ice forces nor nominal pressures were reported in the study by Xu et al. (1981, 1983).

During a joint project between German and Chinese engineers, full-scale ice load measurements were carried out in 1989 and 1990 at one of four legs on the wellhead platform JZ20-2-1 in the Liao Dong Bay in the northern Bohai Sea (❷ in Fig. 3.30). One leg of the platform was instrumented with load panels together with strain gauges on the topside of the structure. Due to the dimensions of the platform leg (D = 1.7 m), a polygonal steel shield (D = 2.0 m) was installed in the water line to make a plane mounting base for the load panels possible. Each of the four panels was 1.5 m × 0.6 m supported by four strain gauged load cells sampling with a rate of 30 Hz. The panels were the same as applied by Wessels et al. (1989) on the Norströmsgrund lighthouse, which enabled to measure both normal and tangential ice forces. Results have been reported by Wessels and Jochmann (1991) with maximal panel pressure p_L= 1.2 MPa. More recently a 50 seconds load sample was analyzed by Johnston et al. (2000), to investigate how the total load on a multi legged platform should be calculated based on load panel measurements. Only low nominal pressures (p_G < 0.1 MPa) were reported in this study.

Recently, Yue and Bi (2000) installed twelve and six accelerometers in the platforms MUQ (Fig. 3.31) and MNW, respectively. The intention of this programme was to measure dynamic response during ice actions on cone structures. The platforms were located at the JZ20-2 oil field (❷ in Fig. 3.30) and instrumented with an array of sensors (0.5 m × 0.2 m) arranged in three rows and eleven columns. Additionally, video cameras were installed on the platforms to give visual information about ice thickness and ice drift speed. Furthermore, load panels and six accelerometers were installed on the MS platform, where no cones were installed in the water line. One of the main purposes behind this programme was to investigate whether the cones could reduce ice induced vibrations or not. Ice induced vibrations was found to occur with both a sloping and a vertical shaped structure (Yue and Bi, 2000).

Recently, Duan et al. (2002) reported ice loads on a vertical leg (D = 1.7 m) of one of the Bohai Sea platforms at the JZ20-2 oil field. They observed loads from various ice

thicknesses with the highest ice load from an ice thickness of h = 0.2 m. This resulted in a reported maximum ice load of F_G = 0.7 MN, with a nominal pressure p_G = 2.1 MPa. An active group at Dalian University of Technology (DUT) is still working out analyses of data from structures at JZ20-2 oil field.
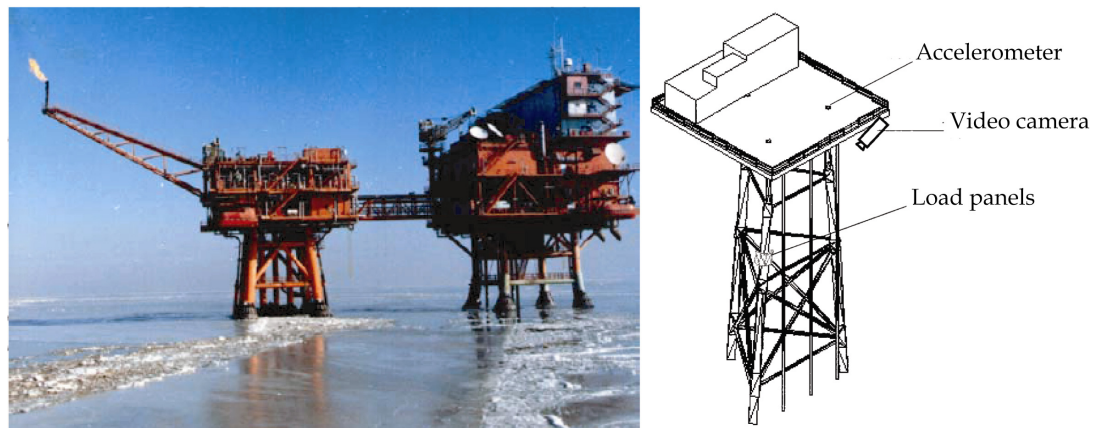
Figure 3.31. Photo of the JZ20-2 MUQ platform (left) and the MS platform (D = 1.7 m) (right) in the Bohai Sea (Yue and Bi, 2000).

3.7.2 Investigations in the Caspian Sea, Kazakhstan, 1999 - present

The Caspian Sea represents the biggest inter-continental basin in the world (Fig. 3.32) (Zone III). The Northern Caspian Sea has an average water depth of 4.4 m with maximums around 10.0 m (Küehnlein, 2002). The ice motion is generally wind driven and generally the ice starts to form mid November in the north eastern regions.
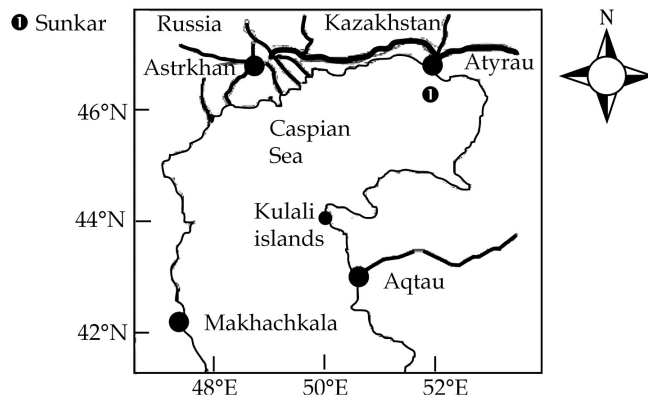
Figure 3.32. Map of the Northern Caspian Sea with one of the Sunkar deployments indicated (after Granneman and Goris, 2001).

By mid January the ice cover has its maximum extent where the area North of Kulali Island (Fig. 3.32) is usually ice covered, while from mid April the Northern Caspian Sea is usually ice free. A drilling barge named "Sunkar" (Fig. 3.33) is employed in the North Eastern Caspian Sea (Fig. 3.32).

At the first deployment of "Sunkar" in the northern Caspian Sea, ice force reducing piles were installed as shown in Fig. 3.33. The piles were instrumented for two years, however time records are still confidential (2005). On a new deployment of "Sunkar" in 2002, ice barriers were installed instead of piles. During February 2002, strong western winds compacted the ice masses in the Eastern Caspian Sea and the barge was barely avoided from drifting ice by the ice barriers (Kouraev et al., 2004).
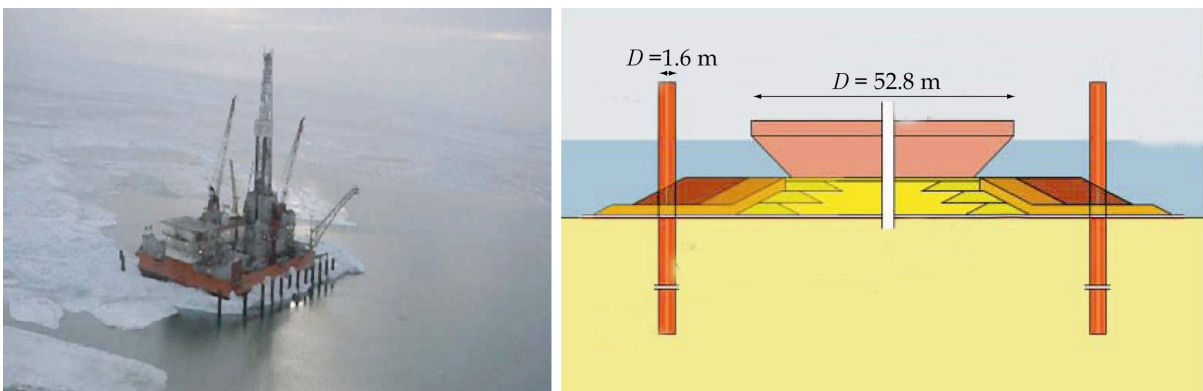
Figure 3.33. "Sunkar" during ice actions in Northern Caspian Sea. Remark piles around the structure at this deployment (Grannemann and Goris, 2001).

64

One of the ice barriers was pushed 120 m along the seabed by ice drift, while no further analyses have been presented from this incident. The maximum level ice thickness has been estimated around $h = 0.6$ m whereas the structure was designed for $h = 1.3$ m rafted ice with drift speed $v_i = 1.00$ m/s (Evers et al., 2001). The barge is manned with ice advisors, however instrumentations with respect to ice actions are not reported.

3.7.3 New deployments at Sakhalin Island, Russia, 2000 - present

In 1998 the Molikpaq caisson was transported from the Canadian Beaufort Sea to an area in the Sea of Okhotsk close to Sakhalin Island in Russia where it was deployed in September 1998 (❷ in Fig. 3.34). The goal was year round production of hydrocarbons in ice-infested waters around Sakhalin Island (Fig. 3.35). Sea ice in the present area starts to form in the northern part of Sea of Okhotsk, where the level ice is typically $h = 1.6\text{-}1.7$ m (Zone II). Truskov (2004) reported that the thickest rafted ice features could be as thick as $h = 2.5 – 4.0$ m with an average thickness $h = 1.0$ m, additionally second year stamukhas have been reported to interact with structures in the Sea of Okhotsk (Truskov, 2004).
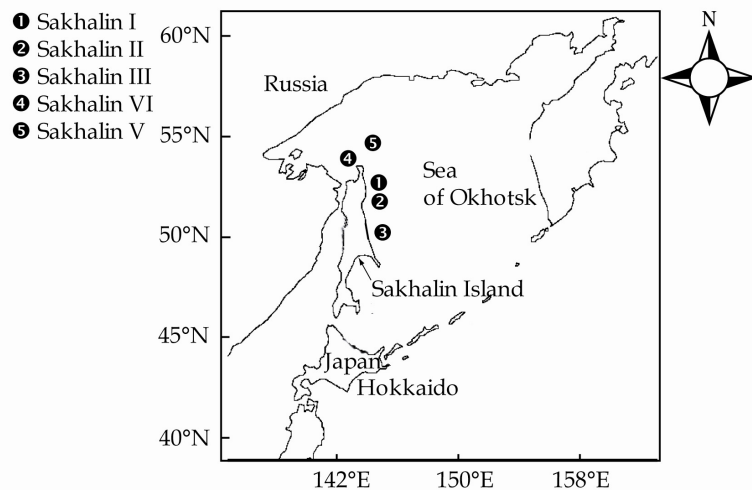
Figure 3.34. Map showing oil fields being planned to be developed in the Sea of Okhotsk around Sakhalin Island.

The ice drift in this area is typically cyclone driven; hence, ice tends to circulate (Truskov, 2004). The mean diurnal drift speeds calculated from observations of individual floes, where on average v_i = 0.30 m/s in January/February and up to v_i = 0.12 m/s in April. Average and design values of drift speeds are mentioned by Truskov (2004) to v_i = 0.60 m/s and v_i = 1.70 m/s, respectively. Compressive strength of the ice is reported to be in the range of σ_c = 1.5-2.0 MPa. The Molikpaq caisson are instrumented with new load panels for the Sakahlin deployment as described by Frederking et al. (2002). An overview of the latest instrumentation of Molikpaq is described by Weiss et al. (2001), henceforth the new deployment of Molikpaq at Sakhalin will provide new data from new environmental conditions than obtained earlier. So far, data from Sakhalin deployments of Molikpaq are not published due to confidentiality agreements.

Figure 3.35. The caisson structure Molikpaq under ice actions at
Sakhalin II deployment in the Sea of Okhotsk, Russia.

3.8 Summary and discussions

3.8.1 General

Altogether 31 magnitudes of ice pressure measured on structures in the field are summarized in this chapter. One programme conducted in Germany is mentioned together with thirteen magnitudes of pressures recorded in Scandinavia. Further one programme conducted in Siberian Rivers is mentioned together with five magnitudes obtained on caisson structures in the North American Beaufort Sea are summarized. Two works are mentioned which have analyzed ice actions on Cook Inlet structures, while one group are reporting ice crushing against a bridge in Yukon River, both situated in Alaska. Two bridges in Alberta and two in Quebec, both in Canada are furthermore mentioned. A bridge in Vermont, USA, together with the Confederation Bridge in Canada and forces on light piers in the St. Lawrence River are summarized. Additionally, investigations on platforms in Bohai Sea are summarized as well as two offshore structures, one barge in the Caspian Sea and one caisson structure located near Sakhalin Island in the Sea of Okhotsk are mentioned.

3.8.2 Summary

Numerical values of ice pressure from the locations mentioned above are reported in Table 3.2. The first column describes the geographical location of the measurements while, the second and third columns indicate which type of structures and which type of measuring devices that have been involved in the measurements, respectively. Symbols used in the third columns refer to definitions established in Table 3.1. The fourth and the fifth column describes the ice thickness and the structural width associated with reported magnitudes of pressure, respectively, while the sixth column indicates the current range of aspect ratios (D/h). Ice drift speeds and the highest of the reported ice pressures are listed in column seven and eight, respectively. Column eight are denoted p without a sub index because it represent both global and local pressures as described above. The ninth column cites a source of literature where the reported pressure could be found. Other sources that reports different values might exist but are not mentioned herein.

Table 3.2. Selected data from full-scale ice-structure interactions (Note that '+' in column 3 from the left hand side means that corresponding laboratory tests exist).

	Structure	Type	h m	D m	D/h	v m/s	p MPa	Reference
Eider	Bridge	$\mathcal{A}$+	0.2	0.6	4.0	< 0.4	0.8	Schwarz (1970)
Kemi I, steel	Lighth. (pile)	$\mathcal{DC}$	0.9	> 1.0	1.0	-	5.0	Määttänen (1974)
Kemi I, concrete	Lighth. (caisson)	$\mathcal{AC}$	0.9	5.8	6.4	-	1.8	Määttänen (1977)
		$\mathcal{AC}$	0.8	5.8	7.3	-	1.7	Hoikkanen (1984)
	Lighth. (cone)	$\mathcal{AC}$+	0.9	10.0	11.0	-	0.3	Määttänen et al. (1996)
Kemi II	Lighth. (pile)	$\mathcal{D}$	0.9-1.5	~1.0	1.0	-	-	Määttänen (1974)
Kemi-2	Lighth. (pile)	$\mathcal{CD}$	0.9-1.5	~1.0	1.0	-	4.3	Määttänen (1987)
Channel markers	Pier	$\mathcal{C}$	0.1-0.3	0.9	1.0	< 0.1	-	Nordlund et al. (1988)
Norströms-grund	Lighth.	$\mathcal{C}$	< 1.0	7.5	>7.5	< 0.6	1.3	Engelbrektson (1985)
		$\mathcal{A}$	0.3	0.8	2.4	-	1.5	Wessels et al. (1989)
		$\mathcal{AC}$+	0.3	7.5	30	0.2	1.4	Schwarz (2001)
				1.2	4.8		2.1	
Tainio	Lighth.	$\mathcal{D}$	0.7	3.5	7.0	-	1.9	Reinius et al. (1971)
Nygrån	Lighth.	$\mathcal{D}$	0.7-0.9	2.5	2.8-3.9	-	-	Bergdahl (1971)
Vallins-grund	Lighth.	$\mathcal{D}$	0.5	2.9	2.9	-	4.8	Björk (1981)

Table 3.2. Continue.

	Structure	Type	h m	D m	D/h	v m/s	p MPa	Reference
Björn-klacken	Lighth.	$\mathcal{D}$	1.2	2.9	2.4	-	2.7	Fransson and Danielson (1985)
Kalix river	Bridge pier	$\mathcal{A}+$	< 0.5	0.3	< 0.5	1	3.0	Fransson and Hoseth (1999)
Siberia	Bridge	$\mathcal{E}+$	-	-	-	-	0.6	Korzhavin (1959)
Beaufort Sea	Molikpaq Amaul.	$\mathcal{AC}$	< 3.0	90.0	> 30.0	-	1.5	Timco and Johnston (2003)
	SSDC Phoenix	$\mathcal{DF}$	< 1.6	162.0	> 87.0	low	1.2	Johnston and Timco (2003)
	CRI Kadluk	$\mathcal{AF}$	< 1.8	117.0	-	-	0.3	Johnson (1983)
	CRI Amerk	$\mathcal{F}$	< 1.8	117.0	-	-	0.2	Sayed et al. (1986)
	Tarsiut N-44	$\mathcal{AF}$	< 2.7	100.0	> 37.0	-	0.9	Fitzpatric and Stenning (1983)
Cook Inlet	Steel jackets	$\mathcal{C}+$	0.7	4.3	7.0	2.1	1.1	Blenkarn (1970)
		$\mathcal{C}+$	0.7	4.3	7.0	-	2.0	Bhat and Cox, (1995)
Alberta	Hondo bridge	$\mathcal{B}$	0.4-1.1	2.3	< 2.2	0.4-2.9	1.9	Montgom. and Lipsett (1980)
	Pem-bridge	$\mathcal{B}$	0.6	0.9	1.4	1.0-1.9	2.7	Lipsett and Gerard (1980)
Ontario	Rideau (V-shape)	$\mathcal{A}$	0.3-0.6	2.0	3.3	0.8-1.3	0.6	Frederking and Sayed (1992)
	St. Regis	$\mathcal{B}$	0.3-0.2	1.2	6.1	-	1.5	Haynes et al. (1991)

Table 3.2. Continue.

	Structure	Type	h m	D m	D/h	v m/s	p MPa	Reference
Alaska	Yukon	$\mathcal{BC}$	1.0	2.7	2.7	-	0.5	MacFadden et al. (1979)
Vermont	White river	$\mathcal{B}$	0.5	1.2	2.7	-	0.3	Zabilansky (1996)
Conf. Bridge	Bridge	$\mathcal{AC}$	1.0	10.0	10	-	0.7	Brown (2001)
St.Law. River	Lighth. (cone)	$\mathcal{A}$	0.8	4.0	5	-	0.8	Danys (1981)
		$\mathcal{AC}$	0.6	4.0	6.7	-	0.7	Frederking et al. (1991)
Bohai Sea	Multileg. platforms	$\mathcal{C}$	0.6	0.6	1.1	< 1.5	-	Xu et al. (1983)
		$\mathcal{AC}+$	0.6	0.7	1.1	< 1.5	1.2	Wessels and Jochmann (1991)
		$\mathcal{AC}$	0.2	1.7	8.7	< 1.5	2.1	Duan et al. (2002)
Sakhalin	Molikpaq	$\mathcal{AC}$	1.7	90.0	53.0	< 1.7	-	Truskov (1999)
Caspian	Sunkar	?	1.3	85.0	> 65.0	< 0.1	-	Kouraev et al. (2004)

An overview of the data presented in Table 3.2 is achieved by plotting 31 magnitudes of ice pressures against the logarithm of the effective structural width in Fig. 3.36. Ice pressure data are grouped with different symbols according to structure types. From the selection, five values are obtained on caisson structures, ten from lighthouses, four from cone structures, eight from bridge piers and four from platform legs. The data are further divided into categories by shaded areas numbered from ① to ⑥ counting from the right to left hand side in Fig. 3.36. Data within a shaded area could be obtained from different

types of structures, but might have similarities with respect to the ice actions scenario, environmental conditions and/or structural characteristics.
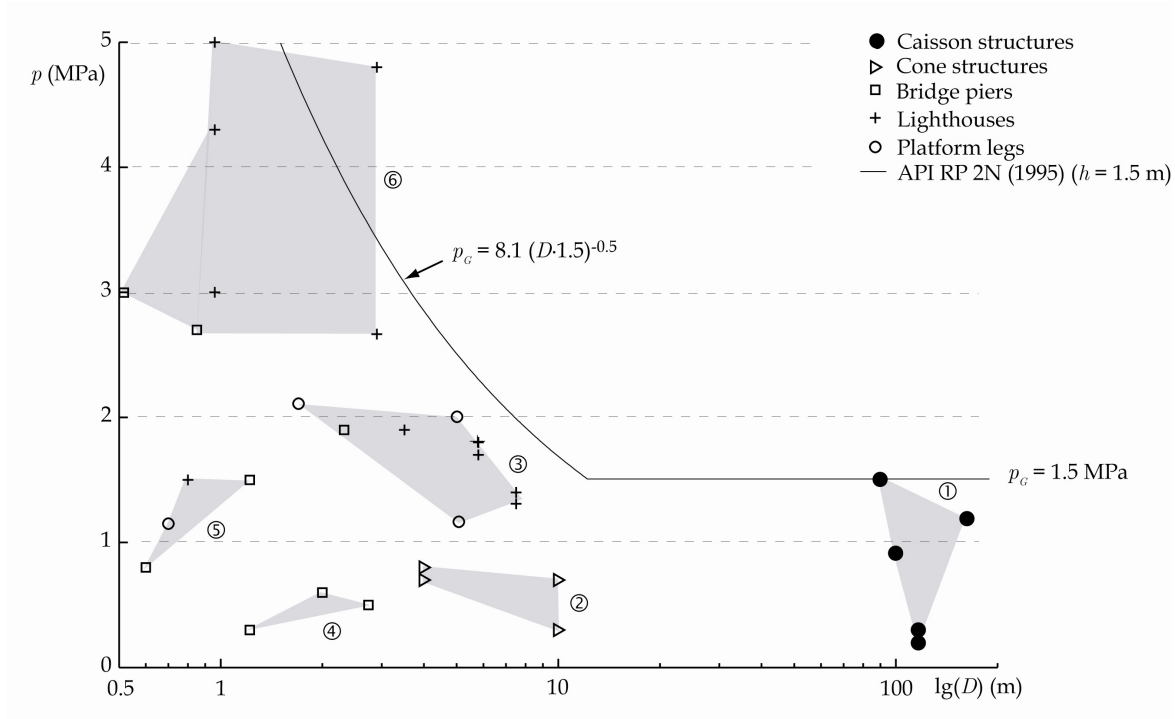
Figure 3.36. The highest ice pressure (p) reported in different measuring programmes versus structural width (D).

3.8.3 Discussion

Investigations of ice actions on full-scale structures have been summarized. Compilation of the highest values of ice pressure recorded on different structures shows that global ice pressure varies widely. Previous studies have presented comparisons of data as Sanderson (1988), Masterson and Frederking (1993) (Fig. 2.6) and Blanchet and DeFranco (1995) with large amounts of data whereupon mathematical curves were fitted as upper bounds.

The present study presents 31 magnitudes of ice pressure where the amount of data points is lower than in previous studies. A difference between the current study and the earlier works is that the previous studies collected most available ice load data from a

wide selection of sources where the current work handles public data obtained on structures in the field only. A key point in the present study was to investigate the highly scattered data reported in the literature by studying each of the data points one by one. The first approach to organize the data was to group the selected data by structure type while the next attempt was to categorize the reported magnitudes of pressure into six categories.

Category ① consists of data measured on wide structures of caisson type located in the Arctic (Zone II). The level of pressures ranges from p_G = 0.2 MPa to p_G = 1.5 MPa where the ice actions scenario linked to the reported values differ significantly. The lowest pressures were measured through a grounded rubble berm surrounding CRI, which was supposed to transfer loads both to the sea bed and to the structure during ice actions (Croasdale, 1985). Ice load scenarios associated with the highest pressures were crushing of ice to the near vertical faced Molikpaq (Timco and Johnston, 2004). Loads recorded on CRI were conducted by interfacial load panels while ice actions on Molikpaq were recorded by both load panels and strain gauges. Hence, at least two reasons could be figured out to explain differences between loads measured at CRI and on the Molikpaq, respectively. The first, and probably the most important reason was the presence of the rubble berm around CRI, which were not present on Molikpaq. The occurrence of this rubble berm shielded the CRI and virtually eliminated the ice loads. Another reason might be vibrations of Molikpaq as discussed by Jefferies and Wright (1988), a phenomena which not were reported from CRI. Hence, an explanation to the different levels of pressure could be that global loads derived from strain gauge data on Molikpaq could have included dynamic amplifications.

Structures in Category ②, have a cone interface in the water line with effective water line widths from D = 4.0 m to D = 10.0 m, and cone angles from 45° to 75°. Typical values of pressures measured on the cones are in the range p_G = 0.3 MPa to p_G = 0.5 MPa, ice actions on cone structures have been measured on light piers and on a bridge pier.

Category ③ includes ice pressures on lighthouses and platform legs of widths from D = 1.7 m to D = 7.5 m. The highest and the lowest pressures in this category were p_G = 2.1 MPa and p_G = 1.1 MPa with most of the data located between p_G = 1.5 MPa and p_G = 2.0 MPa. Data in this group were all measured by interfacial methods in a sub-arctic environment (Zone III).

Category ④ consists of measurements conducted during spring break-ups of North American rivers. It was usually remarked that the ice has started to soften before the break-up and measurements started. Typical widths of investigated bridge piers were D = 1.2 - 2.7 m with reported pressures in the range p_G = 0.3 – 0.6 MPa.

Category ⑤ embrace narrow structures or narrow measuring devices used on wider structures. As well, ice pressure on a bridge pier during spring break up is included in this category. Typical structural width in this category were from D = 0.5 m to D = 1.2 m while the highest reported pressure were in the range from p_G = 0.8 MPa to p_G = 1.6 MPa.

The group of data which contains the highest pressures and the widest scatter is Category ⑥, with all magnitudes obtained in a sub-arctic area (Zone III). The level of pressure scatters from p_G = 2.7 MPa to p_G = 5.0 MPa, where the lowest pressure was measured with a hinged beam while the highest value was found by hindcast calculations of an incident on a slender steel lighthouse. It was reported that both the steel lighthouse and the hinged beam vibrated significantly during ice actions. Other measurements covered by the same category are slender gravity based concrete lighthouses in Sweden, a vibration-isolated lighthouse together with a small load panel on a bridge pier. The width of the structures in this group have a range from D = 0.3 m to D = 2.9 m.

All pressures within Category ⑥ were obtained on structures, which either was vulnerable to ice induced vibrations and/or have low aspect ratios (D/h). Ice loads have, except the small load panel and the hinged beam, been predicted by indirect methods

such as measurements of structural response or hindcast calculations. An elucidation of the highest reported magnitudes of pressures might therefore be twofold.

First, for the narrowest structures, as the small load panel and the steel lighthouses, the aspect ratio (D/h) might have approached one or less (see Table 3.2). In such cases the effective ice pressure might be expected to increase due to the change in state of stress from plane stress (D/h = high) to plane strain (D/h = low) (Sanderson, 1988). Second, several of the narrow structures were vulnerable to ice-induced vibrations; hence, ice loads derived from structural response or with hindcast calculations could possibly include a dynamic amplification.

Concerning design of structures against ice actions, Fig. 3.36 can be treated as a first guide to estimate a global ice pressure together with already existing design formulas as the API RP 2N (1995) shown in Fig. 3.36. However, one should recall that Fig. 3.36 is based on the fundamental assumption that static ice loads are increasing with ice thickness. Very little is known about how ice pressure varies with changing ice thickness, hence some of the scatter within the categories might be addressed to the fact that the highest loads in a category could have been caused by different ice thicknesses.

From right to left, it can be seen that API recommends a pressure p_G = 1.5 MPa, which is equal the highest value in Category ①. For widths slightly less than D = 10.0 m, API predicts pressures slightly higher but in the same range as found in the current summary. Concerning widths less than D = 4.0 m, the differences seems to be more significant, and API RP 2N seems to give ice pressure which are significantly higher than found in Category ③ (static ice pressure). On the other hand, API RP 2N seems to be closer to values in Category ⑥, which were assumed to be pressures calculated by dynamic amplified loads or loads from situations with low aspect ratios (D/h).

3.9 Concluding remarks

Selected ice load data measured between the 1950ties and 2001 are summarized in this chapter. Generally, collected data of ice pressure on structures were significantly scattered. However, as shown herein, some of the scatter might be caused by different measuring devices, different structural characteristics and different geographical locations.

The main conclusions from this chapter are:

1. Variability in ice pressures to structures reported from caissons might be caused by differences in the ice action scenario together with application of different measuring devices. Timco and Johnston (2004) have quantitatively shown that the thickness of the ice, the presence of grounded ice rubble, and the ice failure mode significantly affects the global load on the structure. These factors explain the wide variation in ice loads measured on wide structures.

The overall highest estimated ice pressures ranges from 2.7 MPa to 5.0 MPa, possibly caused by two different effects:

2. Low aspect ratios between structural width and ice thickness causing a confined loading situation resulting in high ice pressures
3. Possible dynamic amplification of ice loads due to ice-induced vibrations and hence over estimated static ice pressure

One category of pressures was found on vertical structures of widths from 1.8 m to 7.5 m located in sub-arctic environments. The main conclusions from this category were:

4. Highest measured ice pressures were all conducted by interfacial methods, and did not exceed 2.1 MPa.

Summarized ice pressures were compared with API RP 2N (1995) design formula with the following findings:

5. API RP 2N seems to fit well with pressures associated with the highest loads measured on structures with widths in the range of 100 m, comparable pressure

for widths around 10 m and significantly higher pressures than measured for widths less than 4 m.

Acknowledgements

References

Afanasiev, V.P., Dolgopolov, Y.V. and Shyeishtein, Z.I. (1971), Ice pressure on separate supporting structures in the sea, Trudy Institute, Vol. 300, pp. 61-80 (In Russian).

API RP 2N (1995), American Petroleum Institute, Recommended Practice for Planning, Design and Constructing Structures and Pipelines for Arctic Conditions – 2N, Second Edition, December 1, 1995.

Bergdahl, L. (1972), Two lighthouses damaged by ice, Proc. IAHR Ice Symposium, Leningrad, USSR, pp. 234-238.

Belliveau, D.J., Hayden, H. and Prinsenberg, S. (2001), Ice Drift and Draft Measurements from Moorings at the Confederation Bridge, Proc. International conf. on Port and Ocean Eng. under Arctic Cond. (POAC), Ottawa, Canada, Vol. 1., pp. 349-358.

Bhat, S.U. and Cox, G.F.N. (1995), Ice Loads on Multi-Legged Structures in Cook Inlet, Proc. International conf. on Port and Ocean Eng. under Arctic Cond. (POAC), Murmansk, Russia, Vol. 4, pp. 51-61.

Blanchet, D. and Kennedy, K.P. (1996), Global first-year ice load measurements in the arctic, Proc. of Offshore Mechanics and Arctic Engineering conference (OMAE), Florence, Italy, Vol. 4, pp. 103-113.

Blanchet, D., and DeFranco, S.J. (1996), Global First-year Ice Loads: Scale Effects and Non simultaneous Failure, IAHR Ice Symposium, Beijing, China, pp. 203–213.

Blenkarn, K.A. (1970), Measurements and Analysis of Ice Forces on Cook Inlet Structures, Proc. Offshore Technology Conference (OTC), Houston, TX, USA, pp. 365-377.

Björk, B. (1981), Ice induced vibrations of fixed offshore structures, Part 2: Experiences with Baltic Lighthouses, In: Marine Structures and ships in Ice (Ed. T. Carstens), Rep. 81-06/2, p. 100.

Bruce, J.R., Brown, T.G. (2001), Operating an ice force monitoring system on the confederation bridge, Proc. International conf. on Port and Ocean Eng. under Arctic Cond. (POAC), Ottawa, Canada, Vol. 1, pp. 299–308.

Boore, D.M., Christopher, D.S. and Joyner, W.B. (2002), Comments on Baseline Correction of Digital Strong-Motion Data: Examples from the 1999 Hector Mine, California, Earthquake, Bulletin of the Seismological Society of America, Vol. 92, No. 4, pp. 1543–1560.

Cox, G.F.N. and Johnson, J.B. (1983), Stress measurements in ice, CRREL Report No. 83-23.

Croasdale, K.R. (1985), Ice Investigations at a Beaufort Sea Caisson, Report to National Research Council of Canada, p. 130.

Croasdale, K.R., Graham, B.W., Comfort, G. and Marcellus, R.W. (1986), Evaluation of ice pressure and strain sensors in a large test basin, IAHR Ice Symposium, Iowa, USA, Vol. 3, pp. 213-225.

Croasdale, K.R., Der, C.D., Shinde, S.B., (1988), Ice forces and geotechnical response of the Esso Caisson retained island, 1986– 87. Esso Resources Canada Report, Calgary, Canada.

Croasdale, K.R. and Kennedy, K. (1996), Ice loads consensus study update, Proc. of Offshore Mechanics and Arctic Engineering conference (OMAE), Firence, Italy, Vol. 4, pp. 115-118.

Danys, J.V. (1975), Effect of ice and wave forces on the design of Canadian offshore lighthouses, Canadian Journal of Civil Engineering. Vol. 2, No. 2, pp. 138-153.

Danys, J.V. (1981), Field measurements of ice forces against cylindrical and conical structures, Proc. Canadian Hydrotechnical conference, Fredericton, Canada, pp. 683-703.

Duan, Z., Qu, J. and Spencer, B.F. (2002), Investigation of ice forces on jacket platforms structures: In-situ measured data on JZ20-2-1 Platform in the China Bohai Sea, Proc. of ASCE Engineering Mechanics Conference, New York, USA.

Dunwoody, B. (1982), Energies dissipated on impact of extreme feature with a fixed offshore structure, Internal report to Dome Petroleum Ltd.

Engelbrektson, A. (1977), Dynamic ice loads on a lighthouse structure, Proc. International conf. on Port and Ocean Eng. under Arctic Cond. (POAC), St. Johns, Canada, Vol. 3, pp. 654-663.

Engelbrektson, A. and Jansson, J.E. (1985), Field observations of ice action on concrete structures in the Baltic sea, Concrete international, Vol. 7, No. 8, pp. 48-52.

Engelbrektson, A. (1989), An ice-structure interaction model based on observations in the Gulf of Bothnia, Proc. International conf. on Port and Ocean Eng. under Arctic Cond. (POAC), Luleå, Sweden, Vol. 3, pp. 504-517.

Engelbrektson, A. (1997), A refined ice/structure interaction model based on observations in the Gulf of Bothnia, Proc. of Offshore Mechanics and Arctic Engineering conference (OMAE), Yokohama, Japan, Vol. 4, pp. 373-376.

EBA Engineering Consultants (2005), http://www.eba.ca.

Evers, K-U., Spring, W., Foulkes, J., Kuehnlein, W. and Jochmann, P. (2000), Ice Model testing of an exploration platform for shallow waters in the North Caspian Sea, Proc. International conf. on Port and Ocean Eng. under Arctic Cond. (POAC), Ottawa, Canada, Vol. 1, pp. 254-264.

Fitzpatrick, J. and Stenning, D.G. (1983), Design and construction of Tarsiut Island in the Canadian Beaufort Sea, Proc. Offshore Technology Conference (OTC), Houston, TX, USA, Vol. 2, pp. 51-60.

Finnish Maritime Administration (2005), http://www.fma.fi.

Fransson, L.Å. and Danielsson, G. (1985), Ice conditions and ice properties close to the light pier Björnklacken shortly after failure due to forces from a moving ice sheet. Department of structural eng. Luleå University of Technology, Sweden, Skrift 85:13.

Fransson, L.Å. and Hoseth, K.A. (1999), Ice pressure on a bridge pier during river break-up, Proc. International conf. on Port and Ocean Eng. under Arctic Cond. (POAC), Espoo, Finland, Vol. 1, pp. 412-419.

Frederking, R.M.W., Haynes, F.D., Hodgson, T.P. and Sayed, M. (1986), Static and Dynamic Ice Loads on the Yamachiche Bend Lightpier, 1984-86, IAHR Ice Symposium, Iowa, USA, Vol. 3, pp. 115-126.

Frederking, R.M.W., Sayed, M. and Penny, G. (1991), Measurements of Ice Forces on Light Piers in the St. Lawrence Seaway, Proc. Int. Offshore and Polar Engineering Conf. (ISOPE), Edinburgh, UK, Vol. 2, pp. 499-504.

Frederking, R.M.W. and Sayed, M. (1992), Ice Impact Force Measurements on a vertically Faced Bridge Pier, Journal of Offshore Mechanics and Arctic Engineering, Vol. 114, pp. 63-65.

Frederking, R:M:W, Masterson, D., Wright, B.D. and Spencer, P. (2002), Ice load measuring panels – the next generation, Proc. IAHR Symposium Ice Symposium, Dunedin, New Zealand, pp. 450-457.

Frederking, R.M.W. (2005), Tiltmeter application at Norströmsgrund lighthouse – STRICE project, Proc. International conf. on Port and Ocean Eng. under Arctic Cond. (POAC), Potsdam, NY, USA, Vol. 1, pp. 399-408.

Gamayunov, A. (1947), Determination of ice pressure on bridge piers; and field measurements of ice forces on bridge piers, Russian Journal of Railway Technology (In Russian).

Granneman, C. and Goris, A. (2001), Kazakhstan, Offshore Exploration in the Caspian Sea, Terra et Aqua, No. 82. pp. 20-30.

Haynes, D., Sodhi, D.S., Zabilansky, L.J. and Clark, C.H. (1991), Ice Force Measurements on a Bridge Pier in the St. Regis River, New York, CRREL report 91-14, 11 p.

Hawkins, J.R., James, D.A., Der, C., (1983), Design, construction and installation of a system to measure environmental forces on a Caisson Retained Island, Proc. International conf. on Port and Ocean Eng. under Arctic Cond. (POAC), Espoo, Finland, Vol. 4, pp. 770–779.

Hirayama, K. (1974), An investigation of ice forces on vertical structures, The University of Iowa, Ph.D. Thesis, 152 p.

Hoikkanen, J. (1984), Measurements and Analysis of Ice Pressure against a Structure in Level Ice and in Pressure Ridges, Proc. IAHR Symposium Ice Symposium, Vol. 3, Hamburg, Germany, pp.151-160.

Jefferies, M.G., Wright, W.H. (1988), Dynamic response of Molikpaq to ice –structure interaction, Proc. of Offshore Mechanics and Arctic Engineering conference (OMAE), Houston, TX, USA, Vol. 4, pp. 201– 220.

Johnson, J.B. (1983), A surface integral method for determining ice loads on offshore structures from in situ measurements, Annals of Glaciology, Vol. 4, pp. 124-128.

Johnston, M., Timco, G.W., Frederking, R.M.W. and Jochmann, P. (2000), Simultaneity of measured ice loads on two legs of a multi-leg platform, Proc. of Offshore Mechanics and Arctic Engineering conference (OMAE), Vol. 4, pp. 1-8.

Johnston, M., Timco, G.W. (2003), Ice loads on the SSDC during its Beaufort Sea deployments. Proc. International conf. on Port and Ocean Eng. under Arctic Cond. (POAC), Vol. 1, Trondheim, Norway, pp. 213– 222.

Klohn-Crippen R. (1998), DynaMAC: Molikpaq ice loading experience. PERD/CHC Report 14-62. Calgary, Canada, 96 p.

Kouraev, A.V., Papa, F., Mognard, N.M., Biharizin, P.I., Cazenave, A., Cretaux, J., Dozortseva, J. and Remy, F. (2004), Sea ice cover in the Caspian and Aral Seas from historical and satellite data, Journal of Marine Systems, Vol. 47, pp. 89-100.

Korzhavin, K.N. (1962), Воздействие льда на инженерные сооружения, Издательство Сибирского отделения АН СССР, Новосибирск, 202 p.

Korzhavin, K.N. (1959), Ice affecting engineering structures on the Siberian Rivers during ice-run, Proc. of International Assoc. for Hydraulic Research, Montreal, Canada, Vol. 3, 5 p.

Kuehnlein, W.L. (2002), The North Caspian Project, Proc. Int. Offshore and Polar Engineering Conf. (ISOPE), Kitakyushu, Japan, pp. 13-17.

Lemee, E. and Brown, T. (2005), Review of ridge failure against the confederation bridge, Cold Regions Science and Technology, Vol. 42, pp. 1-15.

Leonard, R.W. (1898), Masonry pier moved by ice and replaced , Transactions of the Canadian Society of Civil Engineers, Vol. 12.

Lipsett, A.W. and Gerard, R. (1980), Field Measurements of Ice Forces on Bridge Piers 1973-1979. Transportation and Surface Water Engineering Department, Alberta Research Council and Alberta Cooperative Research Program in Transportation and Surface Engineering, Report SWE 80-3, 130 p.

MacFadden, T., Haynes, D., Burdick, J. and Zarling, J. (1981), Ice force measurements on the Yukon River Bridge, Proc. Conference on the Northern community, Seatle, USA, pp. 749-776.

Matlock, H., Dawkins, W.P. and Panak, J.J. (1971), Analytical model for ice-structure interaction, Journal of Engineering Mechanics, ASCE, Vol. 4, pp. 1083-1092.

Määttänen, M. (1987), Ten years of ice-induced vibration isolated lighthouses, Proc. of Offshore Mechanics and Arctic Engineering conference (OMAE), Houston, TX, USA, pp. 261-266.

Määttänen, M. (1974), Bottenvikens stålfyrar – Hållfasthetsanalys ock förbätringsförslag (In Swedish), Winter Navigation Board, Report no. 11, 25 p.

Määttänen, M. (1977), Ice-force measurements at the Gulf of Bothnia by the instrumented Kemi I Lighthouse, Proc. International conf. on Port and Ocean Eng. under Arctic Cond. (POAC), St. Johns, Canada, Vol. 2, pp. 730-740.

Määttänen, M. (1988), Ice-induced Vibrations in Structures – Self-Excitation, IAHR Ice Symposium, Sapporo, Japan, Vol. 2, pp. 658-665.

Määtttanen, M., Nortala-Hoikkanen, A. and Avis, J. (1996), Ice failure and ice loads on a conical structure – Kemi-I cone full-scale ice force measurements data analysis, IAHR Ice Symposium, pp. 8-16.

Metge, M., Pilkington, G.R., Strandberg, A.G. and Blanchet, D. (1983), A new sensor for measuring ice forces on structures: laboratory tests and field experience, Proc. International conf. on Port and Ocean Eng. under Arctic Cond. (POAC), Espoo, Finland, Vol. 4, pp. 790-801.

Montgomery, C.J. and Lipsett, A.W. (1980), Dynamic tests and analysis of a massive pier subjected to ice forces, Canadian Journal of Civil Engineering, Vol. 7, pp. 432-441.

Neill, C.R. (1970), Ice pressure on bridge piers in Alberta, IAHR Ice Symposium, Reykjavik, Iceland, pp. 1-7.

Neill, C.R. (1976), Dynamic ice forces on piers and piles. An assessment of design guidelines in the light of recent research, Canadian Journal of Civil Engineering, Vol. 3, pp. 305-341.

Nordlund, O.P., Kärnä, T. and Järvinen, E. (1988), Measurements of ice-induced vibrations of channel markers, IAHR Ice Symposium, Sapporo, Japan, pp. 537-547.

Peyton, H. (1968), Ice and Marine Structures; Part I: The Magnitudes of ice Forces Involved in Design, Ocean Industry 68.

Pilkington, G.R., Blanchet, D., Metge, M., (1983), Full scale measurements of ice forces on an artificial island, Proc. International conf. on Port and Ocean Eng. under Arctic Cond. (POAC), Espoo, Finland, Vol. 4, pp. 818-834.

Reinius, E., Haggård, S. and Ernstson, E. (1971), Experineces of offshore lighthouses in Sweden, Proc. International conf. on Port and Ocean Eng. under Arctic Cond. (POAC), Trondheim, Norway, pp. 657-673.

Rogers, B.T., Hardy, M.D., Neth, V.W. and Metge, M. (1986), Performance monitoring of the Molikpaq while deployed at Tarsiut P-45, Proc. Canadian Marine Geotechnical Conferecnce, St. Johns, Canada, Vol. 1, pp. 363-383.

Runeberg, R. (1888), On steamers for winter navigation and ice-breaking. Proc. Institution of Civil Engineers, Vol. 97, Pt.III, pp. 277-301.

Sanden, E.J. and Neill, C.R. (1968), Determination of actual forces on bridge piers due to moving ice, Proc. Toronto Conv., Canadian Good Roads Assoc (Transport Canada).

Sanderson, T.J.O. (1988), Ice mechanics-risks to offshore structures, Graham and Trotman, London, 253 p.

Sayed, M., Frederking, R.M.W. and Croasdale, K.R. (1986), Ice stress measurements in a rubble field surrounding a caisson-retained island, In "Ice Technology" (Ed. T.K.S. Murphy, J.J. Connor and C.A. Brebbia) Springer-Verlag, pp. 255-262.

Schwarz, J. (1970), Treibeisdruck auf Pfäle, Mitt. Franzius-Inst. Tech. Univ. Hanover, Heft. 34, (In German), 105 p.

Schwarz, J. (2001), Validation of Low Level Ice Forces on Coastal Structures, Proc. Int. Offshore and Polar Engineering Conf. (ISOPE), Stavanger, Norway, Vol. 1, pp. 749-753.

Sodhi, D.S. (1988), Ice induced vibrations of structures, IAHR Ice Symposium, Vol. 3, pp. 625-657.

Timco, G.W. and Burden, R.P. (1997), An Analysis of the shapes of sea ice ridges, Cold regions Science and Technology, Vol. 25, pp. 65-77.

Timco, G.W. and Wright, B.D. (1999), Load attenuation through grounded ice rubble at Tarsiut Island, Proc. International conf. on Port and Ocean Eng. under Arctic Cond. (POAC), Helsinki, Finland, Vol. 1, Espoo, Finland pp. 454– 463.

Timco, G.W., Croasdale, K.R. and Wright, B. (2000), An overview of First-Year Sea Ice Ridges, PERD/CHC Report 5-112, 159 p.

Timco, G.W. and Johnston, M. (2003), Ice loads on the Molikpaq in the Canadian Beaufort Sea, Cold regions Science and Technology, Vol. 37, pp. 51-68.

Timco, G.W. and Johnston, M. (2004), Ice loads on the caisson structures in the Canadian Beafort Sea, Cold regions Science and Technology, Vol. 38, pp. 185-209.

Timco, G.W., Johnston, M. and Wright, B. (2005), Multi-Year Ice Loads on the Molikpaq: May 12, 1986 Event, Proc. International conf. on Port and Ocean Eng. under Arctic Cond. (POAC), Potsdam, NY, USA, pp. 453-462.

Truskov, P. (2004), Metocean Ice and Seismic Conditions Offshore Northeastern Sakhalin Island, Proc. Offshore Technology Conference (OTC), Houston, TX, USA, pp. 383-399.

Weiss, R.T., Wright, B. and Rogers, B. (2001), In-ice performance of the Molikpaq off Sakhalin Island, Proc. International conf. on Port and Ocean Eng. under Arctic Cond. (POAC), Vol. 1, Ottawa, Canada, pp. 211–222.

Wessels, E., Jochmann, P. and Hoffmann, L. (1989), First results of ice force measurements with TIP-panels at Norströmsgrund lighthouse, Proc. International conf. on Port and Ocean Eng. under Arctic Cond. (POAC), Vol. 3, pp. 1428-1439.

Wessels, E. and Jochmann, P. (1990), Determination of ice forces on jacket JZ 20-2-1 by model and full scale tests, Proc. of SMM '90 Conference, Hamburg, Germany, No. 22, pp. 1567-1570.

Wessels, E. and Jochmann, P. (1991), Model/full scale correlation of ice forces on a jacket platform in Bohai-Bay, Proc. International conf. on Port and Ocean Eng. under Arctic Cond. (POAC), St. Johns, Canada, pp. 198-212.

Wrigth, B.D. and Timco, G.W. (2001), First-year ridge interaction with the Molikpaq in the Beaufort Sea, Cold Regions Science and Technology Vol. 32, pp. 27-44.

Yue , Q. and Bi, X. (2000), Ice-induced jacket structure vibrations in Bohai-Sea, Cold Regions Engineering, Vol. 14, No. 2., pp. 81-93.

Zabilansky, L.J. (1996), Ice force and Scour Instrumentation for the White River, Vermont, CRREL report 96-6, Hanover, NH, USA, 61 p.

Xu, J., Shi, Q. and Meng, Z. (1983), Features of frequency and amplitude in ice-induced vibration of a jacket platform, IAHR Ice Symposium, Espoo, Finland, pp. 952-959.

Xu, J. and Leira, B.J. (1981), Dynamic response of a jacket platform subjected to ice floe loads, Proc. International conf. on Port and Ocean Eng. under Arctic Cond. (POAC), Quebec, Canada, Vol. 1, pp. 502-516.

Chapter 4, Paper I

Global Design Ice Loads' Dependence of Failure Mode

By Morten Bjerkås

International Journal of Offshore and Polar Engineers (IJOPE)

September 2004, Vol. 14, Issue 3, pp. 189-195.

Global Design Ice Loads' Dependence of Failure Mode

Morten Bjerkås*

Department of Civil and Transport Engineering, Norwegian University of Science and Technology
Trondheim, Norway

ABSTRACT

This paper addresses the prediction of global design ice loads on offshore structures related to the structural width. Fourteen events from full-scale measurements on the Norströmsgrund lighthouse are analysed to find out how the effective width should be taken into account for estimating ice forces. Simultaneous failure is found during ductile crushing, initial hit and static loading with a drift speed/ice thickness (v/h) ratio from 0 to 0.05 l/s. Brittle crushing of level ice is found in events with v/h in the range of 0.2 to 0.4 l/s. During brittle crushing of level ice, both nonsimultaneous and a quasi-simultaneous failure modes occur. This work indicates that care should be taken in reducing the effective width when calculating global design ice loads.

INTRODUCTION

There is a recurrence of interest in building activities in Arctic and sub-Arctic areas. Oil and gas fields in areas with first-year sea ice such as the Caspian Sea, Pechora Sea and offshore Sakhalin Island are explored and/or under development. As a further example, Germany is planning significant offshore windmill plants in potential ice-covered waters (SKY 2000).

Loads from floating ice sheets induce one of the most significant horizontal loads on offshore structures in areas where only first-year ice features are present. The effective or nominal pressure p is defined as the measured ice load divided by the ice thickness (h) times a structural width (D) as $p = F/Dh$. Already in 1888, Runeberg stated that the pressure from an ice floe on a structure could not exceed the ice strength. Sanderson (1988) collected the available data from ice load measurements and showed how the effective pressure decreases with the nominal contact area. Later, Masterson and Frederking (1993) found the same trend as Sanderson and presented a design curve where the effective pressure scales with the contact area to the power of -0.5 for areas between 0.2 and 20 m². For contact areas greater than 20 m², the design pressure is recommended to be constant at 1.5 MPa.

This paper addresses how the effective structural width used in ice load prediction is affected by changes in the failure mode of the ice sheet to a vertical structure. Special consideration is paid to the alternation between simultaneous and nonsimultaneous failure dependent on a ratio between drift speed and ice thickness. Further, a link is drawn between simultaneous/nonsimultaneous failure and the effective structural width in predicting design ice loads. The work is based on observations and analysis of full-scale data from the Norströmsgrund lighthouse in the Gulf of Bothnia, Sweden.

BACKGROUND

Blanchet and DeFranco (1996) summarised field data obtained from 1966 to 1988 from several full-scale measurements. Their results indicate that the ice force per unit width decreases with the width and depends only slightly on the ice thickness. Løset et al. (1999a and b, 2003) undertook further review studies on the effective pressure p. They proposed that it is convenient to look for a global load F and p in the dimensional form:

$$F = p \cdot D \cdot h \quad \text{where} \quad p = A_k D^m h^n \qquad (1)$$

where m and n are factors and A_k is an experimental parameter that depends on further relevant parameters—ice quality, strength or fracture toughness, temperature, drift speed, etc. (Kärnä and Qu, 2003).

The factor m addresses the uneven contact along the structural width and scale effects in ice crushing. The perimeter effective width used later reads $D_{\text{eff}} = D^m$. The factor n addresses the uneven distribution of pressure through the entire ice thickness.

Fig. 1 shows an arbitrary rigid body with vertical sides. Fig. 1a illustrates how the pressure p is unevenly distributed around the perimeter of the structural width D. Fig. 1b highlights how the
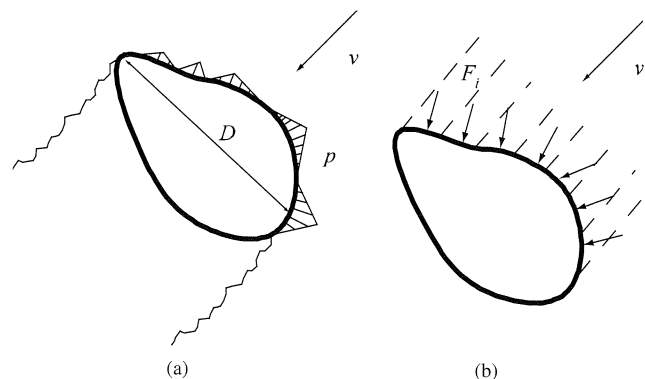

(a) (b)

Fig. 1 Arbitrary rigid body (top view) affected by ice forces: (a) unevenly distributed pressure p, (b) structural width D divided in zones ($D/h \gg 1$) (after Eranti, 1993)

rigid body has independent forces F_i in zones along the ice-structure interaction zone.

Numerous small-scale indentation tests (e.g., Muhonen et al., 1992; Thukuri, 1995; Sodhi, 1998) and a few medium-scale tests (e.g., Fransson and Nyström, 1994; Takeuchi et al., 2000) have been conducted during the last decade. From these tests, it has been stated that a ductile to brittle transition zone occurs with changing indentation speed from low to high. In particular, the analysis by Sodhi et al. (1998) and Takeuchi et al. (2000) from the JOIA tests shows how forces are correlated over large structural widths when the ice fails in the ductile crushing mode. From the tactile sensor data by Sodhi et al. (1998), the contact interface can be observed in detail for different speeds, and the parts of the ice cross-section under significant pressure can be studied in detail.

FAILURE MODES

The failure mode of an ice sheet changes because ice is a highly rate-dependent and temperature-dependent material. As well, the failure mode is affected by discontinuities in the ice cover and generally by the ice properties. This study is based on ice sheets without visible discontinuities and without significant changes of the ice's initial mechanical properties along the ice-structure interaction zone.

For high speed and/or low temperatures, brittle failure occurs, and for low speed and/or high temperatures, ductile and creep failure occurs. The transitions between failure modes due to temperature changes are described by Sodhi and Haehnel (2003) and will not be discussed here. Fig. 3 shows the transition between the ductile and brittle failure with the relative speed between the structure and the ice floe. If the relative speed between the structure and the ice edge (hereafter called indentation speed) changes from slow to fast, the failure mode changes from ductile to brittle.

A commonly used design code for vertical structures is the empirical formula presented by Korzhavin (1962). This formula was derived from small-scale laboratory indentation tests and was initially carried out for bridge piers. Korzhavin's formula has a correction factor, which accounts for the effects of the structural width. Kry (1978) and Ashby et al. (1989) explain this phenomenon as an effect of nonsimultaneous ice crushing and named it the "aspect ratio (D/h) effect."

Fig. 2 shows different cases of simultaneous and nonsimultaneous failure modes. An uneven ice edge causes the nonsimultaneous occurrence of peak loads in independent zones along the structural width. Fig. 2b shows the opposite case with simultaneous occurrence of forces over the whole entire width of the structure. Both these cases are handled below in the light of full-scale observations. Related to the design formula in Eq. 1, the factor m is addressed to take into account the effect of nonsimultaneous failure.
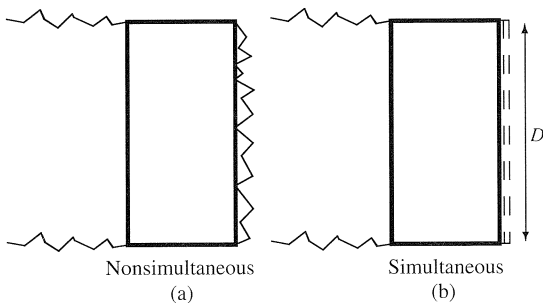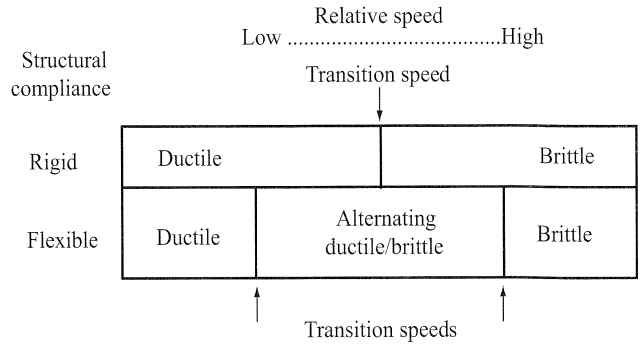

Fig. 3 Principal sketch of ductile to brittle transition during ice-structure interaction (after Sodhi and Haehnel, 2003)

From full-scale measurements, the factor m in Eq. 1 is often obtained empirically from correlation between ice thickness and peak pressure. Common values of the factor m are in the range of -0.3 to -0.1 (Kärnä and Qu, 2003; Blanchet, 1990) for cases where nonsimultaneous failure is assumed to give the design loads on a structure.

Nonsimultaneous Failure

Several authors (Fransson and Nyström, 1994; Takeuchi et al., 2000) have reported from medium-scale tests that load peaks occur nonsimultaneously between spatially discrete points on the face of an indenter. Frederking et al. (1999) also observed this from measurements on the caisson structure Molikpaq in the Canadian Beaufort Sea and recently from the Norströmsgrund lighthouse (Kärnä et al., 2003).

For sufficiently high indentation speeds, ice failure is brittle (Fig. 3) and can be described as stationary random stochastic processes along the ice-structure interaction zone (Kry, 1978). As a first guess, one failure zone is assumed to be limited to an aspect ratio equal to 1. This distribution of failure zones or high-pressure zones is shown schematically in Fig. 4 with w_i as the width of a discrete failure zone. The ice-crushing history inside a zone is independent of what happens in the adjacent zones.

From a design point of view, the above description could yield for structures with high water line stiffness. The time series—such as those in Fig. 7—are assumed to be unaffected by the structural properties as well as the failure in the adjacent zones. If the ice action has no significant influence on the structural properties, then, for example, spectral methods well known from wind and wave engineering can be used to calculate ice loads. Global as well as local loads can be calculated by statistical methods including a load spectrum, mean value and standard deviation.

From this idea, the zonal failure approach can be formulated as shown in Figs. 1b and 4. From measured forces, the time series

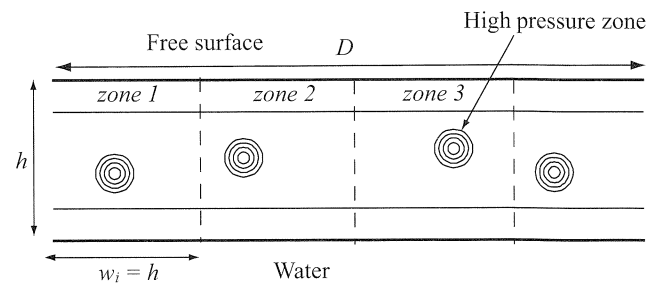Fig. 2 (a) Nonsimultaneous failure, (b) simultaneous failure (top view)

Fig. 4 Assumed distribution of high-pressure zones in ice sheet failing in brittle crushing (front view)

of the local effective pressure in 1 zone reads $p_i = F_i/w_i h$. Kry (1978) formulated the relationship between the global pressure p_G and the mean values μ_i and the standard deviations σ_i of the local effective pressure p_i as:

$$p_G = \mu_i + \sigma_i/\sqrt{n} \tag{2}$$

where G, i and n mean *global, label of the zone* and *number of zones*, respectively. As an example, we can increase the number of zones n from 1 to 10, and reduce the global effective pressure by 40%.

Simultaneous Failure

Simultaneous failure is characterized by load drops at the same time on all spatial points in the ice-structure interaction zone. Simultaneous contact between ice and structure can be caused by at least 4 different scenarios:
- Initial hit
- Static loading
- Ductile crushing
- Phase-locked crushing

The initial hit occurs when a new ice floe is attacking a structure after a period with, say, open water or bending failure. The ice edge is often smooth because of earlier large-scale fractures, melting or erosion. The ice-structure contact is complete before local fracture processes occur and cause an uneven ice edge. If the driving forces are not sufficient to obtain failure of the ice sheet, static forces arise.

If the relative speed between the ice edge and the structure is low, ductile crushing with influences of creep failure occurs. The reason for low drift speed is limiting driving forces (wind and/or currents). As shown in Fig. 3, if the structure is rigid, the border between ductile and brittle crushing is sharp. For example, this is the case with big caisson structures in thin ice.

Phase-locked crushing is also related to the ductile to brittle transition phenomenon (Fig. 3). The phase-locked failure mode is only addressed for structures with a significant compliance in the water line. As discussed first by Sodhi (1988), pointed out earlier by Engelbrektson (1977) and later by Nordlund et al. (1989), all structures have a range of ratios between ice thickness and ice velocities that make them vulnerable to ice-induced vibration and possible simultaneous crushing. Molikpaq in the Canadian Beaufort Sea starts vibrating for a 3-m multiyear ice feature with a drift speed of 0.06 m/s (Jefferies and Wright, 1988). For example, Channel markers in the Gulf of Bothnia start vibrating for 0.2-m-thick ice, and steel lighthouses for 0.5-m-ice thickness. While the phase-locked ice crushing phenomenon is well known, the complete physical explanation is lacking. Määttänen (2001) and Sodhi and Haehnel (2003) give good insights into the present knowledge about dynamic ice-structure interaction.

Table 1 shows how the factor m in Eq. 1 varies with respect to the failure modes discussed above. In a design case, it has to be decided if simultaneous or nonsimultaneous failure should be taken into account for estimating global as well as local ice loads.

Failure mode		m
Simultaneous failure		0
Nonsimultaneous failure	Kärnä and Qu (2004)	−0.28 to −0.1
	Kry (1978)	−0.2
	Blanchet and Kennedy (1996)	−0.5

Table 1   Variation of factor m in Eq. 1

EXPERIMENTAL SETUP

Within the framework of the STRICE (Measurements of STRuctures in ICE) and LOLEIF (LOw LEvel Ice Forces) projects, the Norströmsgrund lighthouse was instrumented for the purpose of measuring ice forces. Jochmann and Schwarz (1999, 2000) give a more complete introduction to the experimental setup at the lighthouse. Only a brief introduction will be presented here.

The Norströmsgrund lighthouse is a cylindrical structure ($D = 7.6$ m) 60 km offshore Luleå in Sweden's Gulf of Bothnia. The lighthouse is usually within the drifting ice zone. During the measurements, ice loads have been measured directly by 9 load panels covering 162° of the perimeter in the waterline. Indirectly, ice loads have been measured by accelerometers, tiltmeters and inclinometers. One of the essential aims of the program was to measure environmental parameters such as ice thickness, wind speeds and air temperatures corresponding to the load measurements. Ice thickness was estimated with a Laser/EM device (Fig. 5). Additionally, continuous video recordings from 4 different cameras were conducted and a detailed log-book was kept during the measurements. For visual observations of the ice-structure interaction zone, the observers have 4 different balconies available. Fig. 5b shows the footprints of 3 of the cameras; the fourth camera is movable and not shown.

Evaluation of data obtained from the dynamic ice-structure interaction during the 1999–2003 measurement campaigns has been undertaken as a joint industry project supported by various companies in addition to the European Union (EU). A confidential agreement has been signed by the various companies, thus restricting the data that can be presented here. Nevertheless, several significant aspects of simultaneous and nonsimultaneous loadings can be shown without the numerical values, and the paper will be argued on this basis. Arrows have been indicated on the various figures to illustrate the peaks (Figs. 7 and 8).

Fig. 6 shows a snapshot of a tool developed for analysis of the ice-load data from Norströmsgrund. This tool plots real-time video and ice-load signals both temporally and spatially. Window ① shows the total load; window ②, panel loads. Real-time video records are in window ③, and a colour intensity plot is in window ④. The label ⑤ displays a compass showing the intensity of forces seen from above. Essential environmental parameters are also given: drift speed, air temperature, drift direction, water stage, wind speed and ice thickness.

The mechanical properties of the brackish sea ice in the northwestern Gulf of Bothnia are reported by Fransson (2003). The salinity is usually in the range of 0.2 to 0.6 ppt. The ice
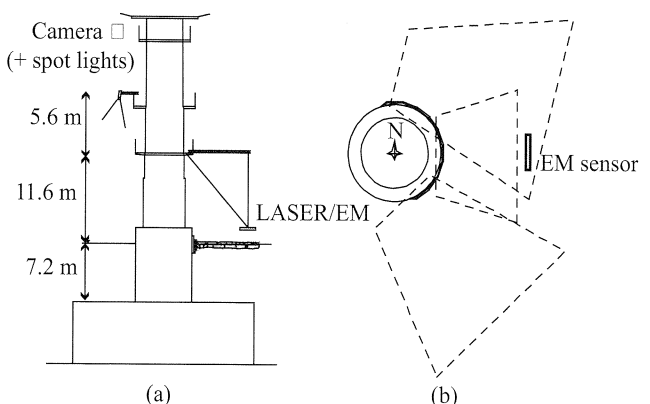

Fig. 5 (a) Norströmsgrund lighthouse with its experimental setup, (b) camera coverage of ice-structure interaction zone
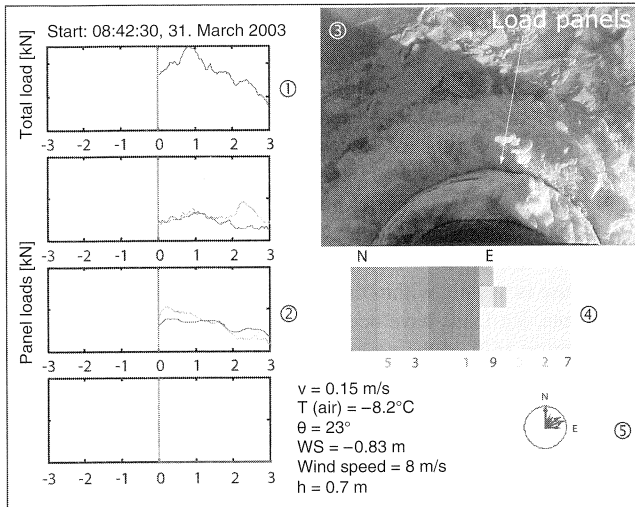
Fig. 6 Snapshot of synchronizing tool developed for studies of effective structural width ① total load, ② panel loads, ③ video record (seen from above), ④ load intensity (front view), ⑤ force intensity (seen from above).

temperature goes from a linear distribution when the weather is stable and cold, to an almost constant temperature close to the water temperature (−0.1°C) when the weather is stable and warm (Bjerkås et al., 2003).

RESULTS

From video records conducted at the measurement site in 2002 and 2001 at the Norströmsgrund lighthouse, 2 discrete periods were selected: 28 February and 31 March, respectively. Table 2 gives their characteristics. Later, 14 sub-events were selected from the 2 discrete periods for detailed analysis, 10 from the 28 February video records and 4 from the 31 March video records. The main purpose of the analysis was to highlight the occurrence of different failure modes, and how the effective width changes due to changes in the failure mode. The focus was on 2 different kinds of failure modes: simultaneous and nonsimultaneous failure. The principal differences between these failures were highlighted above.

A typical picture from the analyses was the transition between the brittle and ductile failure mode due to drift speed and ice thickness. For ratios v/h in the range of 0.33 to 0.5 l/s, nonsimultaneous failure was observed, and for low ratios $v/h = 0$ ($v/h = 0.063$ l/s), static loading and ductile crushing were observed with simultaneous failure.

Event no.	v [m/s]	h [m]	v/h [l/s]	λ	Mode
28020201	0.2	0.53	0.38	2/6	Brittle
28020202	0.2	0.51	0.39	3/6	Brittle
28020203	0.2	0.51	0.39	4/6	Brittle
28020204	0.2	0.51	0.39	4/6	Brittle
28020205	0.2	0.52	0.38	3/6	Brittle
28020206	0.2	0.53	0.38	6/6	Brittle
28020207	0.2	0.47	0.43	3/6	Brittle
28020208	0.2	0.50	0.40	4/6	Brittle
28020209	0.2	0.54	0.37	2/6	Brittle
28020210	0.2	0.59	0.34	4/6	Brittle
31030211	0–0.05	0.8–1.2	0.042–0.063	6/6	Ductile

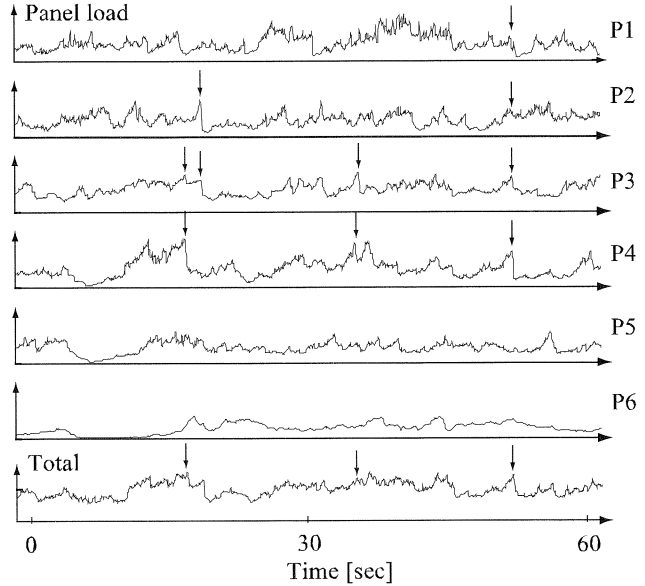Table 2   Characteristics of 2 selected periods

Fig. 7 Loads from 1 min of level ice crushing with peak loads that occurred quasi-simultaneously. This 1-min event occurred at 17:40 on 28 February 2002. Drift speed $v = 0.2$ m/s, ice thickness $h = 0.58$ m ($v/h = 0.35$ l/s). P1 to P6: adjacent panels 1.2 m wide × 1.5 m high.

Fig. 7 shows a typical event which initially was characterized as an event with nonsimultaneous failure. The 6 upper signals (P1 to P6) show forces from different adjacent load panels with characteristic 1.2-m width and 1.5-m height. The lower signal (Total) is the vector sum of the load signal from the large panels. This event is from an 0.58-m-thick level ice flow crushing to the lighthouse with drift speed $v = 0.2$ m/s ($v/h = 0.35$ l/s). From more detailed visual inspections of the time series, some peak loads seems to occur simultaneously. Then 4 discrete events were highlighted with simultaneous failure on as many as 4 adjacent panels (in this case). It was then decided to name this failure mode the quasi-simultaneous failure. Quasi-simultaneous failure had earlier been observed in time series from the caisson structure Molikpaq in the Canadian Beaufort Sea (Frederking et al., 1999). Physical explanations of the quasi-simultaneous failure mode are not addressed here.

Fig. 8 shows a typical event with simultaneous failure. This event is 10 min long; the ice is a 1.2-m-thick rafted ice floe. The failure mode here was initially ductile crushing with low speed ($v = 0.05$ m/s) and then static loading ($v = 0$ m/s) with a smoothly increasing load. From the time series it can be seen that the peak loads simultaneously occurred on all 6 adjacent panels. As in Fig. 7, only approximately 110° of the perimeter was covered with active panels.

Table 2 describes the characteristics of the 2 main periods selected. The parameter λ is the ratio between the number of involved panels in the event (6) and the maximum number of panels with simultaneous peaks.

ANALYSES

From all events analysed in this work, ductile failure with influence of creep seems to occur for ratios v/h in the range of 0 l/s to 0.063 l/s. The limited number of events in the lower range of drift speeds makes it difficult to figure out the transition zone between brittle and ductile failure. Brittle failure has been observed for ratios v/h in the range of 0.33 to 0.5 l/s.
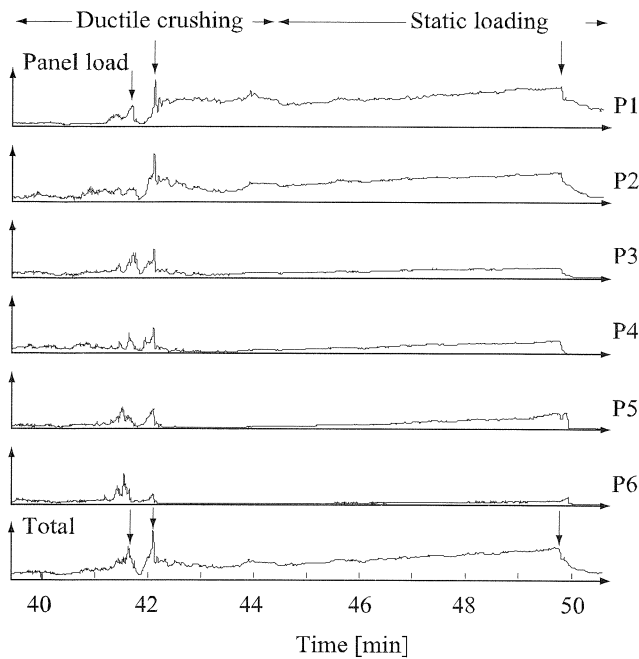
Fig. 8 Loads from 10 min of simultaneous ice contact with Norströmsgrund lighthouse from 09:40 on 31 March 2002. Drift speed = 0.05 m/s, rafted ice thickness = 1.2 m ($v/h = 4.16 \cdot 10^{-2}$ l/s). P1 to P6: adjacent panels 1.2 m wide × 1.5 m high.

The nonsimultaneous failure can be seen when comparing the total load signal with the separate panel load signals from events with brittle crushing. In Fig. 7, four discrete events are pointed out with arrows. In these events the load drops in the total load are caused by simultaneous load drops on 2 or more panels. As many as 4 panels indicate simultaneous failure in this event. Four panels give an aspect ratio D/h close to 9 for the present ice thickness ($h = 0.58$ m), which indicates that the zones are wider than assumed theoretically (Fig. 4). As noted above, events with this kind of mixing between nonsimultaneous and simultaneous failure are renamed quasi-simultaneous failure. Quasi-simultaneous failure will not fit into the ideas by Kry (1978) about independent zonal action. Vibrations of the structure during the quasi-simultaneous crushing failure were usually minor.

The event in Fig. 8 shows a scenario with initially ductile crushing and then static loading. A relatively thick rafted ice sheet on $h = 1.2$ m interacts with the lighthouse. The first hit causes simultaneously occurring peaks on all 6 active panels. Then a smooth buildup with ductile/creep of ice takes place. The failure mode goes from ductile crushing to static loading over 10 min. This is a typical example of the simultaneous failure mode observed during events with v/h in the range of 0 to 0.063 l/s. The effective contact width in Fig. 8, D_{eff}, is assumed to be in the same range as the nominal width D. The vibrations of the structure were minor during these 10 min, and the failure mode was observed as ductile crushing and static loading.

DISCUSSION

The scenarios presented above show that the mode of failure changes significantly due to the ratio v/h. With the ratio $v/h = 0.35$ l/s and $v/h = 0.042$ l/s, we get, respectively, brittle/quasi-simultaneous and ductile/simultaneous failure.

For events with high speed and thin ice, brittle and nonsimultaneous failures usually occur, and the global nominal pressure is stationary and relatively low due to nonsimultaneous peak loads. The effective contact width D_{eff} is always less than the nominal width D. The effective width in the case of load prediction has to be reduced, and the factor m in Eq. 2 is well below zero (Table 1). This is a common scenario for wide structures and frequently reported in the literature, among others by Sanderson (1988) and Blanchet and Kennedy (1996).

On the other hand, from the Norströmsgrund lighthouse, quasi-simultaneous failure has been observed in events with high drift speed and thin ice. This is not in line with the theoretical zonal approach by Kry (1978) that proposes independent failure in zones with the size of aspect ratio D/h equal unity. One explanation for the quasi-simultaneous failure could be the size of the high-pressure zones and the fact that in reality they are much wider than $D/h = 1$. Further studies have to be conducted here.

Based on full-scale measurements on relatively stiff structures, most of the ice-structure interactions consist of nonsimultaneously occurring contact forces. Nevertheless, from this study it has been realized once more that a so-called quasi-simultaneous failure mode can occur during brittle crushing. In a limited amount of events, quasi-simultaneous failure has been observed on approximately 40% of the entire structural width.

From earlier studies it is known that simultaneous loading can occur due to phase-locked ice crushing if the possibility exists for the structure to start shaking. Severe vibrations that indicate phase locking have been observed several times both during the LOLEIF/STRICE measurements and earlier programs by Engelbrektson (1977), among others. Thorough analyses of events with phase-locked vibrations will be addressed in later studies. So far, the phase-locked events described by Engelbrektson (1977) are assumed to give simultaneous ice failure along the entire width of the structure. In the present study, simultaneous loading was observed due to ductile crushing, initial hit and static loading.

It has been known for decades that high drift speed gives brittle crushing, and that very low speeds give creep failure. These findings have indicated that the effective width can be reduced due to prediction of design ice loads, because nonsimultaneous crushing will reduce the nominal pressure when the structure width increases (Sanderson, 1988). Findings by Jefferies and Wright (1988), Engelbrektson (1977) and the present study have indicated that care should be taken in reducing the effective structural width when predicting design ice loads on offshore structures.

CONCLUSIONS

This paper addresses the effective structural width during ice-load prediction. Two discrete periods divided into 14 sub-events are analysed to find out how the effective width should be taken into account for estimating ice forces.

1. Simultaneous failure is found during ductile crushing and static loading with the drift speed/ice thickness (v/h) ratio from 0 to 0.063 l/s.

2. Brittle crushing of level ice is found in events with v/h in the range of 0.33 to 0.5 l/s.

3. During brittle crushing of level ice, both nonsimultaneous and a quasi-simultaneous failure modes occur.

4. This work indicates once more that care should be taken in reducing the effective width when global ice loads need to be predicted.

Further work should focus on the dynamic effects of ice loads and further understanding of the quasi-simultaneous failure mode, which is poorly described in the literature.

REFERENCES

Afanasyev, VP, Dolgopolov, IV, and Shvashteyn, ZI (1972). "Ice Pressure on Separate Supporting Structures," *Draft Translation 346*, U.S. Army Cold Regions Res and Eng Lab, Hanover, New Hampshire.

Ashby, MF, Palmer, AC, Trouless, M, Goodman, DJ, Howard, MW, Hallam, SD, Murrell, SAF, Jones, N, Sanderson, TJO, and Ponter, ARS (1986). "Non-simultaneous Failure and Ice Loads on Structures," *Proc Offshore Tech Conf*, Houston, pp 399–404.

Bjerkås, M, Bonnemaire, B, Sodhi, DS, Gerisch, S, and Jochmann, P (2003). "Extended Observations of Ice-structure Interactions at the Lighthouse Norströmsgrund, Winter 2003," *Deliv. D-3.1_C*, 46 pp.

Blanchet, D (1990), "Design Criteria for Wide Offshore Structures," *13th Canadian Geotechnical Colloquium, Canadian Geotech J*, Vol 27, No 6, pp 701–725.

Blanchet, D, and DeFranco, SJ (1996). "Global First-year Ice Loads: Scale Effects and Non-simultaneous Failure," *Proc IAHR Ice Symp*, Beijing, pp 203–213.

Blanchet, D, and Kennedy, KP (1996). "Global First-year Ice Load Measurements in the Arctic," *Proc Conf Offshore Mech and Arctic Eng*, Italy, Vol 4, pp 103–113.

Engelbrektson, A (1977). "Dynamic Ice Loads on a Lighthouse," *Proc POAC*, Canada, pp 654–663.

Eranti, E (1992). "Dynamic Ice-structure Interaction, Theory and Applications," *PhD thesis*, 81 pp.

Fransson, LÅ, and Nyström, M (1994). "Non-simultaneous Ice Failure on Wide and Narrow Offshore Structures," *Proc IAHR Ice Symp*, Norway, Vol 2, pp 774–783.

Fransson, LÅ (2004). "Mechanical Properties of Ice at Norströmsgrund," *Interim rept to STRICE group*, Luleå Univ of Tech, 20 pp.

Frederking, RMW, Timco, GW, and Wright, B (1999). "Ice Pressure Distribution from First-year Sea Ice Features Interacting with the Molikpaq in the Beaufort Sea," *Proc Int Offshore and Polar Eng Conf*, Brest, France, ISOPE, pp 541–548.

Jefferies, M, and Wright, WH (1988). "Dynamic Response of Molikpaq to Ice-structure Interaction," *Proc Conf Offshore Mech and Arc Eng*, pp 201–220.

Jochmann, P, and Schwarz, J (2000). "Ice Force Measurements at Lighthouse Norströmsgrund, Winter 2000," *LOLEIF Rept 9*, Germany, 64 pp and Appendix.

Jochmann, P, and Schwarz, J (1999). "Ice Force Measurements at Lighthouse Norströmsgrund, Winter 1999," *LOLEIF Rept 5*, Germany, 48 pp and Appendix.

Kärnä, T, Qu, Y, and Kühnlein, W (2004). "A New Spectral Method for Modeling Dynamic Ice Actions,", *Proc Conf Offshore Mech and Arc Eng*, Canada (in press).

Kärnä, T, Kolari, K, Jochmanna, P, Gehrisch, S, Fransson, L, and Bjerkas, M (2003). "Observed Ice-structure Interactions in Winter 2002," *STRICE – Deliv. D-3.1-A2.*

Kärnä, T, and Qu, Y (2003). "Peak Forces in Continuous Brittle Crushing," *Internal Rept STRICE/NEST Deliverable*, Finland, 40 pp.

Korzhavin, KN (1962). "Action of Ice on Engineering Structures," *CRREL Rept 262.*

Kry, PR (1978). "A Statistical Prediction of Effective Ice Crushing Stresses on Wide Structures—Part I," *Proc IAHR Ice Symp*, Sweden, pp 33-47.

Løset, S, Shkhinek, KN, and Uvarova, E (1999a). "Evaluation of Existing Ice Force Prediction Methods," *LOLEIF Rept 3*, 8 pp.

Løset, S, Shkhinek, KN, and Uvarova, E (1999b). "An Overview of the Influence of Structure Width and Ice Thickness on the Global Ice Load," *Proc POAC*, Finland, Vol 1, pp 425–434.

Løset, S, Shkhinek, KN, and Kärnä, T (2003). "Global Ice Load Dependency on Structure Width and Ice Thickness," *Proc POAC*, Trondheim, Vol 2, pp 857–868.

Määttänen, MP (2001). "Numerical Simulation of Ice-Induced Vibrations in Offshore Structures—Keynote Lecture," *Proc Nordic Sem Comput Mech*, Lund Univ, pp 13–28.

Masterson, DM, Spencer, PA, Nevel, DE, and Nordgren, RP (1999). "Velocity Effects from Multi-year Ice Tests," *Proc Conf Offshore Mech and Arc Eng*, Canada, 29 pp.

Masterson, DM, and Frederking, RMW (1993). "Local Contact Pressure in Ship and Structure/ice Interactions," *Cold Regions Sci and Tech*, Vol 21, pp 169–185.

Muhonen, A, Kärnä, T, Järvinen, E, and Riska, K (1992). "Laboratory Indentation Tests with Thick Freshwater Ice," *Lab Naval Arch and Marine Eng Otaniemi, M-122*, 397 pp.

Nordlund, OP, Kärnä, T, and Järvinen, E (1988). "Measurements of Ice-induced Vibrations of Channel Markers," *Proc IAHR Ice Symp*, Japan. pp 537–548.

Runeberg, R (1888). "On Steamers for Winter Navigation and Ice-breaking—Part III," *Proc Inst of Civil Eng*, Vol 97, pp 277–301.

Sanderson, TJO (1988). *Ice Mechanics Risks to Offshore Structures*, Graham and Trotman Ltd, 100 pp.

Sanderson, TJO (1991). "Statistical Analysis of Ice Forces," *Ice-structure Interaction, IUATM Symp*, Canada, pp 439–457.

SKY 2000. "Strategie der Bundesregierung," *www.sky2000.info* (in German).

Sodhi, DS (1988). "Ice-induced Vibrations of Structures," *Proc IAHR Ice Symp*, Japan, pp 625–657.

Sodhi, DS, and Haehnel, RB (2003). "Crushing Ice Forces on Structures," *J Cold Regions Sci and Tech*, Vol 17, pp 153–170.

Sodhi, DS (1998). "Non-simultaneous Crushing During Edge Indentation of Freshwater Ice Sheets," *J Cold Regions Sci and Tech*, Vol 27, pp 179–195.

Sodhi, DS, Takeuchi, T, Nakazawa, N, Akagawa, S, and Saeki, S (1998). "Medium-scale Indentation Tests on Sea Ice at Various Speeds," *Cold Regions Sci and Tech*, Vol 28, pp 161–182.

Sodhi, DS (2001). "Crushing Failure During Ice-structure Inter-action," *Eng Fract Mech*, Vol 68, pp 1889–1921.

Thukuri, J (1995). "Experimental Observations of the Brittle Fail-ure Process of Ice and Ice-structure Contact," *J Cold Regions Sci and Tech*, Vol 23, pp 265–278.

Takeuchi, T, Sakai, M, Akagawa, S, Nakazawa, N, and Saeki, H (2000). "On the Factors Influencing the Scaling of Ice

Forces," *Scaling Laws in Ice Mech and Ice Dyn, IUATM Symp*, pp 149–160.

Uvarova, EV (1999). "Results of Parametric Studies on Ice Loads Acting on Arctic Offshore Structures," *summary of work toward degree of candidate of technical sciences*, St. Petersburg State Tech Univ, 16 pp. (in Russian).

Proceedings of the 6th (2004) ISOPE Pacific/Asia Offshore Mechanics Symposium

Vladivostok, Russia, September 12–16, 2004

Sakhalin Offshore, Ice Engineering, Hydrodynamics and Coastal Engineering, Offshore Systems, Energy and Environment, Underwater Vehicles and Control

The Proceedings (ISBN 1-880653-63-X, 350 pp. est.: $100 (ISOPE Member; $80) in a single volume CD-ROM) is available from ISOPE, P.O. Box 189, Cupertino, California 95015-0189, USA (Fax +1-650-254-2038; orders@isope.org)

Chapter 5, Paper II

Applications of Continuous Wavelet Transforms on Ice Load Signals

By Morten Bjerkås, Asle Skiple and Ola Iver Røe

Engineering Structures

Submitted February 2005

(In review)

Applications of Continuous Wavelet Transforms on Ice Load Signals

Morten Bjerkås[1], Asle Skiple[1], Ola Iver Røe[2]

[1] Department of Civil and Transport Engineering, Norwegian University of Science and Technology, Høgskoleringen 7a, 7491 Trondheim, Norway
[2] Department of Mathematical Sciences, Norwegian University of Science and Technology, Alfred Getz vei 1, 7034 Trondheim, Norway

Abstract

This paper gives an introduction to how Continuous Wavelet Transform (CWT) can be applied in analyzing ice load time series to gain more information about the distribution of power in the time domain. The aim of the study was to localize short intervals of intermittent crushing in initially long time series. Intermittent crushing was supposed to occur with dominant frequencies in the range of the fundamental frequencies of the structure and to give resonance-like response histories of the structure. To ensure that the localization of periods of intermittent crushing was realistic, corresponding time signals of normalized acceleration was plotted together with selected CWT coefficients. Five different time records were selected for analyses. The length of intervals was calculated from the up and down crossing of chosen threshold values for both normalized CWT coefficients and normalized acceleration signals. The presented method seems to be suitable for analyzing signals in time and frequency domains simultaneously, however the threshold values have to be tuned in the case of new structures and/or new loading situations. Together with already existing tools for analyzes, CWT will give more information from ice load time series than traditional methods. More work is needed on significance testing of wavelet coefficients and development of a proper background spectrum for such testing.

Keywords: Ice load, Frequency, Full-scale measurements, Fourier, Wavelets, CWT

Corresponding author:
Email: morten.bjerkaas@ntnu.no
Fax: +47 73 59 70 21
Phone: +47 73 59 46 40

1 Introduction

Dynamic ice loads due to crushing failure of infinite floating ice sheets have been thoroughly analyzed by numerous authors since Peyton [11] published his results from measurements on platforms in the Cook Inlet, Alaska. The ice pressure and the corresponding structural response have usually been analyzed separately in the time and frequency domains. Analyses in the time domain have been proposed by e.g. Engelbrektson [3] and Jefferies and Wright [6] who reported severe steady-state vibrations on a lighthouse structure and a caisson structure, respectively. Laboratory investigations by e.g. Sodhi [15] detected three different types of ice crushing in dynamic ice structure interaction; namely, brittle crushing, intermittent crushing and ductile crushing which included creep failure. Intermittent crushing failure was reported to be the reason for severe steady-state vibrations during ice actions.

Reddy et al. [13] studied how the response spectrum method could be applied in the analysis of ice forces, which can be defined both for a stationary and non-stationary excitation process. The response spectrum method is nowadays widely used in, for instance, seismic analysis of structures. Sundararajan and Reddy [16] initiated the application of stochastic processes and random vibrations in the analyses of dynamic ice actions. Määttänen et al. [10] applied both the response spectrum method and the stochastic approach to study the behaviour of the Kemi I lighthouse under ice actions. Recently, Kärnä et al. [8] followed up the idea of ice loads as stationary random processes and proposed a new spectral method based on measurements from the Norströmsgrund lighthouse in Sweden (Fig. 1). The popularity of the methods initiated by Sundararajan and Reddy [16] are limited because they do not cover situations with steady state vibrations and ice loads of lock-in type.
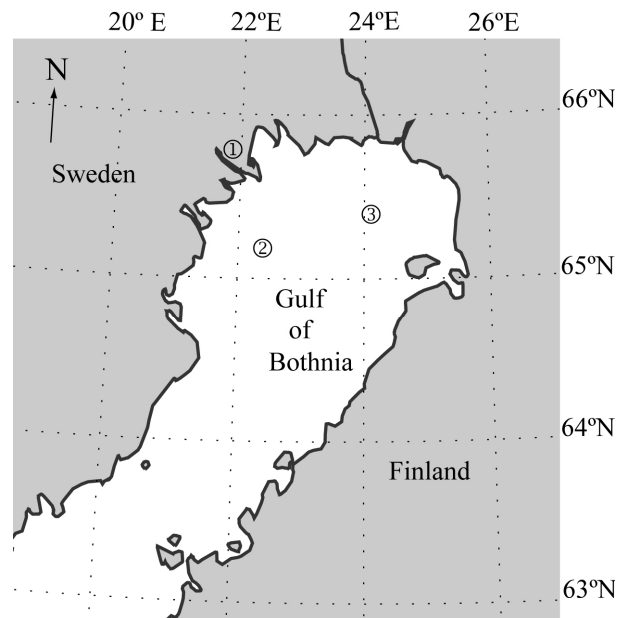

Figure 1. Map of the Gulf of Bothnia with locations of ① Luleå city, ② Norströmsgrund and ③ Kemi.

Spectral methods have been used extensively for analyses of environmental loads on structures for decades. Due to time averaging, short periods with dominant frequencies in long signals can be difficult to detect. For example, the response of a linear system to a unit amplitude stationary white noise or an impulse excitation will have identical spectral descriptions but different time histories.

At least three methods are available to meet the problems with detecting dominant frequencies in non-stationary signals. Two of those methods are the Wigner-Ville distribution and the Short Time Fourier Transform (STFT) [2]. This study contains applications of the third of these methods, the Wavelet Transform (WT).

The WT has been proven to be applicable in several engineering disciplines. Gurley and Kareem [4] show several examples of application of continuous and discrete wavelet transforms to data from wind, ocean and earthquake engineering, Jakobsen et al. [5] show the Continuous Wavelet Transform (CWT) applicability to detection of freak waves in wave records.

The detection of ice induced vibration is relatively straightforward if data describing the structural response are available (see Fig. 2), measured accelerations will most probably give high amplitudes during resonance events. As shown in Fig. 2, the occurrence of resonance vibrations is not directly connected to the magnitude of ice loads. For that reason it was decided that the frequency information from load signals have to be used in addition to the magnitude of ice loads. The main motivation behind this work was to come up with a method that could handle detection of ice induced resonance vibrations with use of measured ice loads or ice pressure.
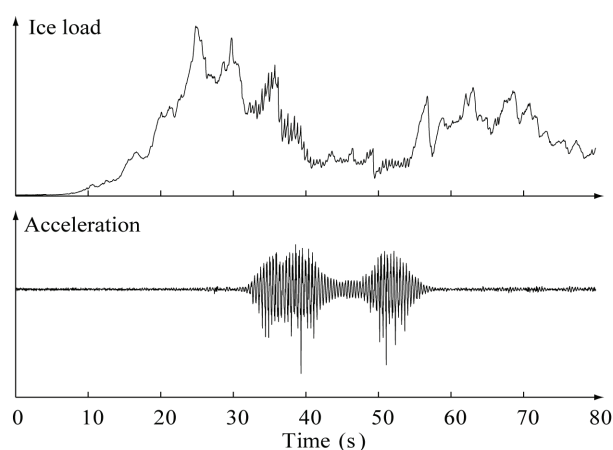

Figure 2. Ice load with its corresponding acceleration signal from an event with ice thickness $h = 0.68$ m and drift speed $v = 0.1$ m/s, occurring 22:37:10, 9 April 2003 at the Norströmsgrund lighthouse.

The objective of the paper is to present a new application of CWT on ice loads and figure out if it is suitable for detection and localization of periods with intermittent ice crushing. The paper goes briefly through the

experimental setup. A description of the observed ice load time records is then presented before a brief introduction of the theory CWT is offered. Examples of applications of the CWT is then presented as a method to detect intermittent crushing in ice load signals and how these intervals correspond with measured strong accelerations.

2 Experimental setup

Extensive ice load measurements were conducted in the period 1999 to 2003 at Norströmsgrund lighthouse in the Gulf of Bothnia (Sweden), by the LOLEIF and STRICE teams [14]. Norströmsgrund lighthouse is located approximately 60 km offshore Luleå in Sweden (Fig. 1). The structure is a 42 meter high gravity based cylindrical structure resting on moraine masses at a water depth of 15 m + tidal changes (Fig. 3). Its water line diameter is 7.6 m. The lighthouse was instrumented in 1998 with nine load panels measuring normal forces with 167 degrees coverage from North. Biaxial accelerometers and inclinometers were installed in 2001 to record the structural response. Measurements of the ice thickness, air temperature, wind speed and air pressure have been conducted as well. Loads and responses were recorded at a varying sampling rate between 1 and 100 Hz, depending on the category of interaction. All selected events in this study were sampled at 30 Hz. Due to a confidentiality agreement within the STRICE project, no numerical values of ice loads could be printed in this paper.
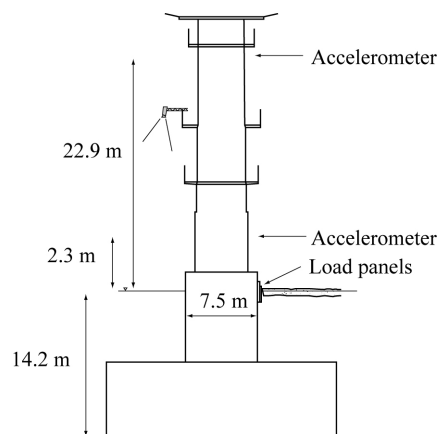

Figure 3. Location of some of the measuring devices at the lighthouse Norströmsgrund winter 2001, 2002 and 2003.

3 Ice load signals

Ice loads from crushing sea ice on vertical structures give signals which are random by nature. These signals can occasionally be characterized as stationary if a homogenous level ice sheet is continuously crushing at a sufficient high drift speed. During the actions from inhomogeneous ice sheets, pressure ridges, open leads and low drift speeds with structural feedback, load signals tend to be of a non-stationary character. Laboratory investigations have distinguished the crushing failure mode of ice sheets into three categories,

ductile, intermittent and brittle crushing mainly dependent on the drift speed of the ice floe, the aspect ratio (exposed width/ice thickness) and ice temperature. Events studied in this project are limited to contain only intermittent and ductile ice crushing.

Ductile crushing is described as loads gradually increasing until attaining a peak value, and then gradual reduction until reaching a steady state value of 50 to 60 % (see ❶ in Fig. 4) of the peak force with minor structural vibration [9,15] Two methods have been proposed to estimate loads from ductile crushing, one empirical method by Michel and Toussaint [9] and one method based on reference stresses by Ponter et al. [12]. Neither of these methods have been compared to full-scale data as far as the authors are aware.

Intermittent crushing is characterized as a failure mode linked to heavy structural vibrations caused by alternation between brittle and ductile failure. The changes in failure mode between brittle and ductile ties in with the compliance of the structure. Due to the rate-dependency of the ice strength, the limit resistance is changing, dependent on the relative speed between the ice edge and the structure. When the load signal has a smoothly increasing trend, as shown Fig. 4, the ice sheet fails in a ductile mode with gradually increasing ice resistance. When a certain stress limit has been reached, the ice cover fails and the structure swing-back phase starts. During the swing-back phase, the relative velocity between the arriving ice edge and the swinging structure is high and the failure mode changes from ductile to brittle. The ice strength is supposed to be lower in the brittle failure mode than in the ductile failure mode, so energy is released and the steady-state vibration of the structure is maintained. To predict the loads generated from intermittent crushing ice, Kärnä [7] among others proposed a method with time-integration, and Engelbrektson [3] presented a deterministic model based on summation of harmonic functions. No general agreement has been reached on this topic so far.

Fig. 4 shows an example of a time series recorded during continuous crushing of a level ice sheet at relatively low drift speed ($v = 0.1$ m/s). Judging from visual observations, the signal could be characterized as non-stationary during the selected 80 seconds. For further elucidation, two sub-samples of four and nine seconds respectively were selected, these samples are labeled ❶ and ❷ in Fig. 4. During period ❷, the structure had significant vibrations and the load signal had dominant frequencies in the range of 2.3 to 2.4 Hz. The failure mode was characterized as intermittent crushing. In the period labeled ❶, the load signal had a more random pattern dominated by lower frequencies, mostly less than 1 Hz. This failure mode was characterized as ductile crushing. Further, it is supposed that the occurrence of intermittent crushing as shown in Fig. 4 has a strong link to structural vibrations and synchronized ice loads along the water line of the structure. The aim of the present work is to figure out if CWT can be applied on ice load signals of this type to localize events of intermittent crushing within periods of ductile crushing.
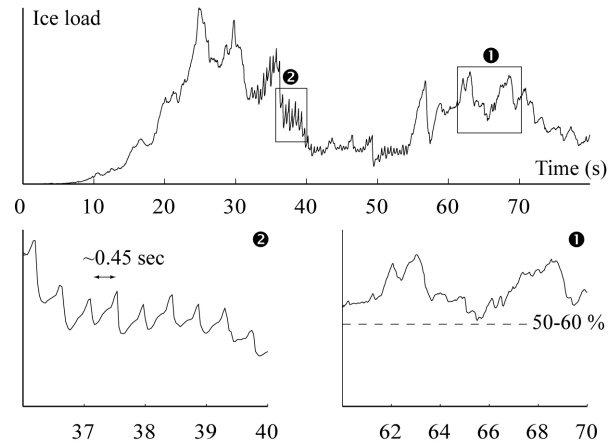
Figure 4. Ice loads (linear relative scale) versus time with selected periods of ductile crushing ❶ and intermittent crushing ❷. The sample was recorded 9 April 2001, 22:37:10 at the Norströmsgrund lighthouse. The ice thickness and drift speed were 0.68 m and 0.1 m/s, respectively.

4 The Continuous Wavelet Transform

The WT is a tool for decomposing a signal into its time and frequency-dependent components. Based on a special way of implementing WT presented by Torrence and Compo [17], the CWT has been applied to full-scale data from the Norströmsgrund lighthouse in the Gulf of Bothnia.

There are two principal ways to perform a WT, a continuous wavelet transform (CWT) and a discrete wavelet transform (DWT). The CWT is performed on a non-orthogonal basis which means that scaling coefficients of a chosen wavelet function are used in every time step of the signal, independent of the period (or scale). Otherwise, the DWT is performed on an orthogonal basis which means that the number of scaling coefficients is increased where short periodic information is required. The CWT generates smooth pictures of how periods develop in time but is more time consuming due to higher degree of redundancy at longer periods. The DWT is more suited for simulation of signals than CWT, due to no redundancy and a fixed number period (or scale) levels.

Given a signal (x_n) $n = 0,…,N\text{-}1$ with sampling interval δt and length N. A wavelet function is defined by $\psi(\eta)$ where $\eta = t/s$ is a non-dimensional time parameter and t and s are time and scale respectively. The scale parameter has a link to Fourier periods and is chosen to cover a range of Fourier periods from 0.03 to $2\delta t$ seconds.

Numerous wavelet functions are available in the literature. To be admissible as a wavelet, $\psi(\eta)$ should have zero mean and be localized in both time and frequency space. The choice of wavelet function should be evaluated on the basis of shape of the signal to be transformed. Due to the choice of the CWT with a non-orthogonal basis for the wavelet transform and because it is well known and widely applied in other

engineering fields, the Morlet wavelet was chosen in this study. The Morlet wavelet reads in the non-dimensional time domain

$$\psi_0(\eta) = \pi^{-\frac{1}{4}} e^{-i\omega_0\eta} e^{-\frac{\eta^2}{2}} \tag{1}$$

where $\omega_0 = 6$. The corresponding expression in the frequency domain reads

$$\hat{\psi}_0(\omega) = \pi^{-\frac{1}{4}} e^{-\frac{(\omega-\omega_0)^2}{2}} \tag{2}$$

The real part of the Morlet wavelet is plotted in Fig. 5 in non-dimensional time (η) and frequency ($s\omega$) domains. Other wavelet functions might be better suited to the task of describing ice load signals, therefore it is an assignment for further work to compare different wavelet functions and to develop new wavelets for ice load transformations.
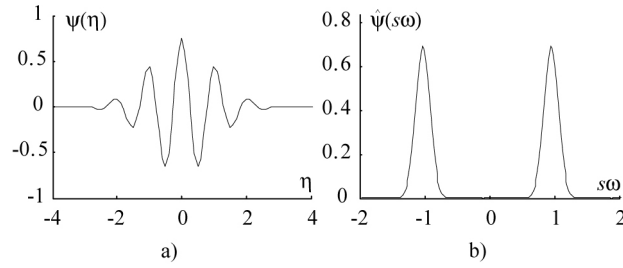

Figure 5. The Morlet wavelet as used in the present analyses together with its Fourier spectral representation.

The idea behind CWT is to apply the wavelet function in Eq. (1) as a bandpass filter on the time series x_n. The CWT of a discrete signal x_n is defined as the convolution of x_n with a scaled and translated version of the complex conjugate of $\psi(\eta)$. This convolution reads

$$W_n(s) = \sum_{n'=0}^{N-1} x_{n'} \psi^* \left[(n'-n) \frac{\delta t}{s} \right] \tag{3}$$

where * means the complex conjugate and n' means the current location. In practice it is faster to do the convolution in the Fourier space (for details see [17]). Because the wavelet function $\psi(\eta)$ is complex (Eq. 1), the W_n is also complex. The wavelet coefficients can then be divided into a real part $W_{n\,R}$ and a complex part $W_{n\,I}$. The amplitude reads then $|W_n|$ and we can define the wavelet power as $|W_n|^2$. To make it easier to compare different transforms, wavelet coefficients are normalized by the variance of the time series before plotting.

The normalized wavelet coefficients are usually displayed with scalograms. A scalogram has time and scale (or period) along horizontal and vertical axis respectively. Color intensity or contour lines make high energy intervals and frequencies distinguishable from a chosen background spectrum. To make the values of scales observed in scalograms accessible and comparable to what can be seen in a Fourier spectrum, scales can be translated to Fourier periods. In the case of the Morlet wavelet, the Fourier period T_F is almost equal to the

scale for $\omega_0 = 6$, namely $T_F = 1.03 \cdot s$. This may be different for other choices of $\psi(\eta)$, therefore T_F have to be calculated in each separate case.

When the coefficients in the scalogram are obtained and outlined we still do not know the significance of the distinct areas in the scalogram. To do a test of significance, a background spectrum is calculated based on a synthetic red-noise signal [17]. Red noise is well known as an approximation to different geophysical processes. A simple model for the red noise approximation is the univariant lag-1 autoregressive process (AR1 or Markov process). If we suppose that the ice crushing phenomena can be estimated as an AR1 process, the wavelet spectrum of this approximation can be used as a background spectrum of the CWT gained from the real signal. The discrete Fourier power spectrum of an AR1 process after normalizing is given by

$$P_k = \frac{1-\alpha^2}{|1-\alpha\,e^{-2i\pi k}|^2} \tag{4}$$

where α is the lag-1 autocorrelation coefficient and k is the Fourier frequency. In this study $\alpha = 0.72$ has been used because it has been reported to fit well into observed time series of several other geophysical processes [1]. When the value α approaches zero, P_k goes to one and describes white noise. Eq. (4) can then be applied to model the red-noise spectrum. More work is necessary to predict values of α which describe the ductile ice crushing phenomena better than 0.72. Torrence and Compo [17] describe how the red noise estimate can be implemented as a background of wavelet scalograms.

Due to the fact that a chosen time series has finite length, the wavelet is not completely localized in time for all n. For that reason the signal was padded with zeros in both ends before applying Eq. (3). To distinguish the real coefficients from the artificially obtained coefficients in the padded signal, the cone of influence (COI) was introduced. The COI is the region of the wavelet spectrum in which edge effects become important and is defined as the e-folding time for the autocorrelation of wavelet power at each scale (see [17]). The e-folding time for the Morlet wavelet equals $\sqrt{2} \cdot s$ and is displayed as white areas in both ends of the scalogram in Fig. 8.

5 Applications of CWT on ice load time series
Five samples of ice loads were selected from time records with continuous crushing. The ice drift speeds of the selected time records were in the range 0.02 to 0.1 m/s. Corresponding acceleration signals indicated that resonance-like events could have occurred in the selected time records. Fig. 6 shows one of the selected ice load time series with two distinguishable periods with changes in the loading frequencies labelled ❶ and ❷. Fast Fourier Transforms (FFT) were obtained from the time series and a Power Spectral Density (PSD) was calculated as shown in Fig. 7a. The frequency content of the selected ice load time record seems to be of a red-noise character dominated by frequencies in the lower range.
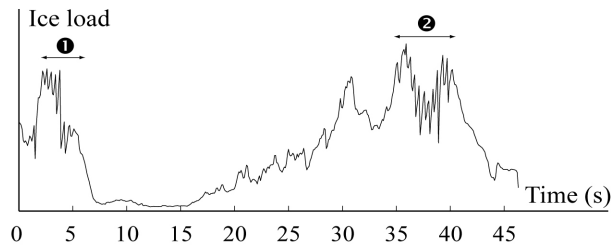
Figure 6. Panel ice load (linear relative scale) versus time during 50 seconds of ice crushing with average ice thickness h = 0.38 m and average drift speed v = 0.03 m/s, sampling frequency f_s = 30 Hz, measured 13:23:00, 4 April, 2002.

To get more information out of the frequency content in the labelled periods ❶ and ❷, the signal was cropped. New FFT were obtained from periods ❶ and ❷ with PSD functions as shown for period ❷ in Fig. 7b. Dominant frequencies were distinguishable at 2.3-2.4 Hz and 4.4-4.8 Hz. From that information it was believed that the ice load signal was forced by the vibrations of the structure due to the intermittent ice crushing phenomena as described above. The spectra in Fig. 7 illustrate the uncertainty principle, which says that one has to choose between resolution in time or frequency.
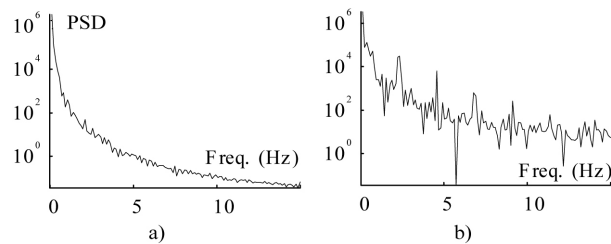

Figure 7. Power spectral density (PSD) of the measured panel ice load signal presented in Fig. 6. a) whole length, b) selected period ❷ in Fig. 6.

To handle the problems with localization of periods with dominant frequencies, the CWT was applied to the ice load signals. CWT coefficients were calculated as shown in Eq. (3) and normalized to the variance of the selected time records. Coefficients were then plotted together with a red-noise spectrum as contour plots (Fig. 8). Wavelet scales are transformed to Fourier periods T_F before plotting. The 95% confidence level against red noise is shown as a thick black contour line in the scalogram. Clusters of significant energy can be observed in the range $T_F < 1$ s. From this it could be assured that the lag-1 value of 0.72 in the AR1 process could be tuned even more to fit into the nature of ice crushing.
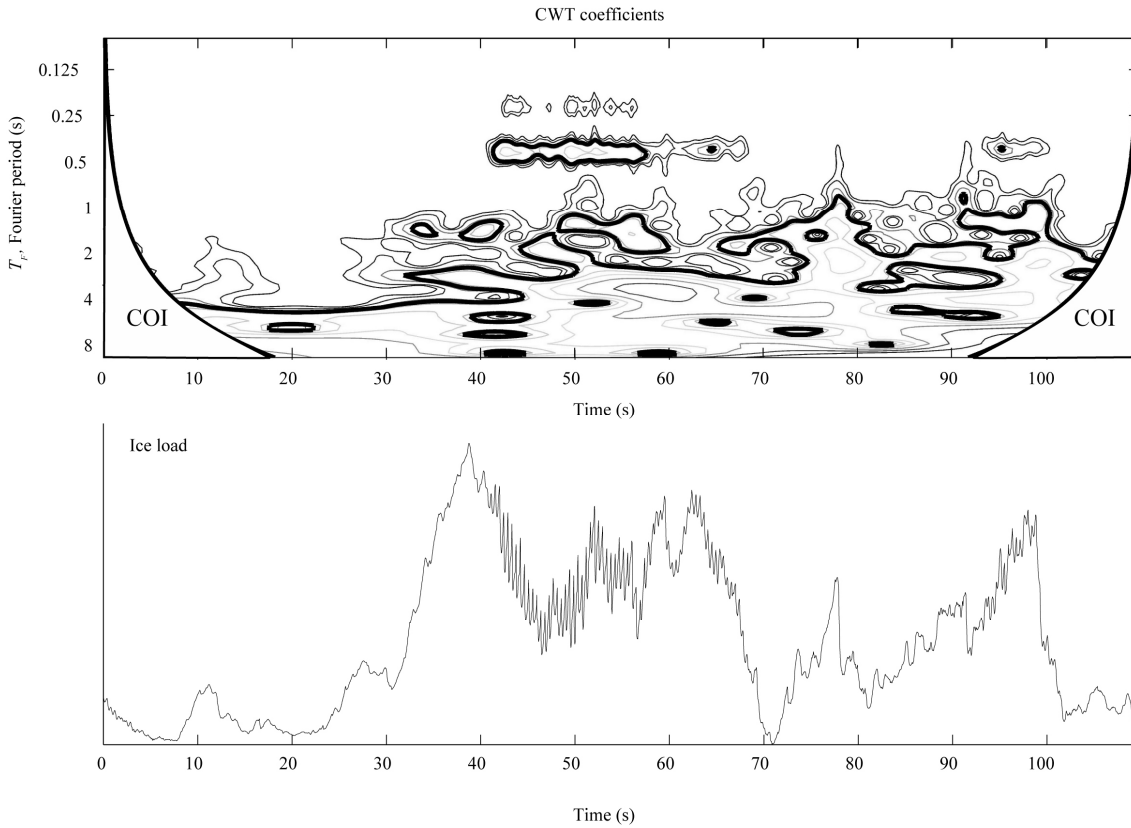
Figure 8. Upper plot shows CWT coefficients as a contour plot with 95 % confidence against red noise shown as a thick black contour line. Ice load (linear relative scale) versus time is shown below from 22:38:40, 9 April 2001.

Two Fourier period ranges T_{F1} and T_{F2} are defined in the range T_{F1} = [0.40 → 0.45 s] and T_{F2} = [0.21 → 0.23 s]. For T_{F1}, two intervals with high energy can be localized in Fig. 8. An interval between 40 and 68 seconds, together with an interval between 92 and 100 seconds can be seen. The interval between 40 and 68 s reach the 95 % limit of confidence against red noise in the interval 42 to 58 seconds and in a short interval around 66 sencods. The interval between 92 to 100 sencons reach the 95 % confidence level against red noise only in a short period around 93 seconds. For T_{F2} two intervals were detected which both are in the range of the first interval detected for T_{F1} (42 to 68 s). The two intervals detected for T_{F2} are located between 44 and 45 s and between 49 and 59 s, Neither of those intervals reach the 95 % confidence against red noise. From the wavelet scalogram in Fig. 8 we recognized that the high energy intervals can be localized in the time domain with relative ease, even though it is difficult to determine the accurate length of the detected intervals.

To quantify the observations in the scalograms, discrete vectors of wavelet coefficients were selected at fixed Fourier periods. In Fig. 9, T_F is fixed at 0.45 s and the corresponding vector of normalized CWT coefficients is plotted against time. The intermittent crushing was then supposed to start when the normalized CWT coefficients reached 0.01. This level was chosen by visual observations and further work is needed to figure out a method to establish this level with better certainty. The crossing rate of the fixed level

was then counted and the length of the period of intermittent crushing was calculated as the time length between up and down crossing of the 0.01 level as reported in Table 1.

To prove if the calculated duration of the intermittent crushing corresponds to high magnitude of measured response of the structure, matching acceleration signals were selected. The acceleration measured 16.5 m above seabed was normalized by its peak value and plotted against time as shown in Fig. 9. A significant event was defined to start and stop when the line between local acceleration peaks crossed 0.1. The duration of the event was then calculated as the time between up and down crossing of the 0.1 level as indicated in Fig. 9.

Five events were analysed as described above and shown in Fig. 9. The selected periods with intermittent crushing and corresponding vibrations of the structure are reported in Table. 1. The up-crossings of the 0.01 level by the CWT coefficients reported in Table 1 are on average 0.2 s earlier than the corresponding up-crossings of the level 0.1 of the acceleration signal. The difference between down-crossing time of the CWT coefficients and the normalized acceleration signals is slightly larger than the difference in up-crossing time. On average the CWT down-crossing is 1.2 seconds prior the corresponding down-crossing of the acceleration. The reason why the down-crossing time of the CWT is earlier than the acceleration could be because the CWT coefficients are obtained from the ice load signal which in this case, most probably is the dominant reason for the measured structural response. The total length of the significant period was calculated to be 1.1 seconds longer by the accelerometer signals than by the CWT coefficients.

It should be pointed out that the threshold value of 0.01 for the CWT coefficients and 0.1 for the normalized acceleration signals have to be adjusted in case of different structures and/or loading situations.
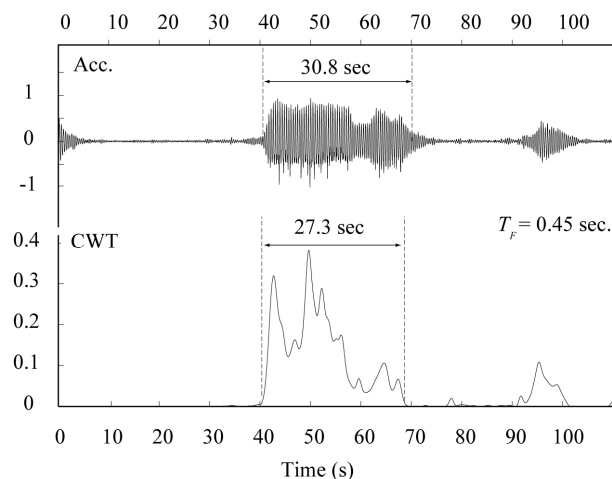

Figure 9. Normalized acceleration and CWT coefficients versus time from an event with resonance like vibrations due to ice crushing at Norströmsgrund lighthouse 22:38:00, 9 April 2001.

Table 1. Characteristics of five selected ice load and acceleration time records from the lighthouse Norströmsgrund in the Gulf of Bothnia. Numbers addressed to the up and down crossings are in seconds.

Time of event	Ice		CWT		Acceleration		Length	
	v	h	Start	Stop	Start	Stop	CWT	Acc
	(m/s)	(m)	(s)	(s)	(s)	(s)	(s)	(s)
223800-0904-01	0.10	0.7	40.7	68.3	40.6	71.4	27.3	30.8
121430-3003-03	0.02	0.2	29.9	39.9	30.5	41.4	10.0	11.4
153600-2503-03	0.05	1.1	18.3	25.1	18.5	24.2	6.8	5.7
224140-0904-01	0.10	0.7	17.4	48.0	17.4	47.6	30.6	30.2
223900-0904-01	0.10	0.7	20.4	48.6	20.6	51.4	28.2	30.8

(v = drift speed, h = ice thickness)

6 Conclusions

This paper gives an introduction to how the Continuous Wavelet Transform (CWT) can be applied to ice load signals to gain more information from ice load time series. The aim of the study was to localize short intervals of intermittent crushing in long time series.

CWT was applied to detect possible intervals of intermittent crushing which was supposed to be linked to resonance-like vibrations of the structure. The identification of intervals with intermittent crushing was compared and showed a good match with corresponding steady state vibrations measured by accelerometers. Five different time records were selected for analyses. The detected duration of intermittent crushing predicted by the CWT coefficients was on average 1.1 seconds shorter than resonance-like events revealed by the accelerometer.

The presented method appears to be well suited to analyze signals in time and frequency domains simultaneously. Together with existing analyzing tools, CWT will distill more information from ice load time series. More work is needed on the significance testing of wavelet coefficients and the development of a proper background spectrum for such tests.

References

[1] Allan MR, Smith LA. Monte Carlo SSA: Detecting irregular oscillations in the presence of coloured noise, J Clim 1996; 9: 3373-404.

[2] Daubechies I. Ten Lectures on Wavelets, CBMS-NSF conference series in applied mathematics, SIAM Ed, 1992.

[3] Engelbrektson A. A Refined Ice/Structure Interaction Model Based on Observations in the Gulf of Bothnia, Proc Int Conf Offs Mech Arctic Eng (OMAE) 1997; 4: 373-76.

[4] Gurley K, Kareem A. Applications of wavelet transform in earthquake, wind and ocean engineering, Eng Struc 1992; 21: 149-67.

[5] Jakobsen JB, Haver S, Ødegård JE. Study of Freak wave by Use of Wavelet Transform, Proc Int Offs Polar Eng Conf (ISOPE) 2001; 3: 58-64.

[6] Jefferies M, Wright WH. Dynamic response of Molikpaq to ice-structure interaction, Proc Int Conf Offs Mech Arctic Eng (OMAE) 1988, 201–20.

[7] Kärnä T. A Procedure For Dynamic Soil-Structure-Ice Interaction, Proc Int Offs Polar Eng Conf (ISOPE) 1992: 764-71.

[8] Kärnä T, Qu Y, Kühnlein W. A New Spectral Method for Modeling Dynamic Ice Actions, Proc Int Conf Offs Mech Arctic Eng (OMAE) 2004; OMAE2004-51360.

[9] Michel B, Toussaint N. Mechanisms and theory of indentation of ice plates. J Glac 1977; 19: 81 285–300.

[10] Määttänen MP, Reddy D, Arockiasamy M, Cheema P. Ice-structure interaction studied on a lighthouse in the Gulf of Bothnia using response spectrum and power spectral density function analyses. Proc Int Conf Port and Ocean Eng under Arctic Cond (POAC) 1977: 321-34.

[11] Peyton HR. Sea ice strength, University of Alaska, Geophysical Institute, Final Report for the Navy Office of Naval Research 1966, Contract Nr. 2601 (01).

[12] Ponter ARS, Palmer AC, Goodman DJ, Ashby MF, Evans AG, Hutchinson JW. The force exerted by a moving ice sheet on an offshore structure. Cold Reg Sci Tech 1983; 8: 109–18.

[13] Reddy DV, Cheema PS, Swamidas ASJ. Ice Force Response Spectrum Modal Analysis of Offshore Towers, Proc Int Conf Port and Ocean Eng under Arctic Cond (POAC) 1975: 305-14.

[14] Schwarz J. Validation of Low Level Ice Forces on Coastal Structures, Proc Int Offs Polar Eng Conf (ISOPE) 2001: 749-53.

[15] Sodhi DS. Ice-structure interaction during indentation tests. In Ice-Structure Interaction: Proc. of IUTAM-IAHR Symposium 1991: 619–640.

[16] Sundararajan C, Reddy DV. Stochastic analysis of ice-structure interaction. Proc Int Conf Port and Ocean Eng under Arctic Cond (POAC) 1973: 345-53.

[17] Torrence C, Compo GP. A Practical Guide to Wavelet Analysis, Bulletin of the American Meteorological Society 1997; 79: 1: 61-78.

Chapter 6, Paper III

Wavelet transforms and ice actions on structures

By Morten Bjerkås

Cold Regions Science and Technology

Vol. 44, pp. 159-169

ELSEVIER

Wavelet transforms and ice actions on structures

Morten Bjerkås *

Department of Civil and Transport Engineering, Norwegian University of Science and Technology (NTNU), Norway

Abstract

A wavelet cross-correlation analysis was applied to ice loads and corresponding acceleration signals measured at the Norströmsgrund lighthouse in the Gulf of Bothnia, Sweden. It was shown that the excitations of the lighthouse by actions from ice floes are influenced by structural responses with dominant excitation frequencies in the same range as the frequencies of the responses. The lengths of intervals with synchronized excitations and responses are predicted to be from 1.9 to 8.6 s. Local ice loads were found to be synchronized in the same intervals and for the same frequencies, but for a slightly shorter time. This synchronization causes simultaneous ice actions which can trigger higher global ice loads on the structure than has been obtained during brittle non-simultaneous crushing.
© 2005 Elsevier B.V. All rights reserved.

Keywords: Cross-wavelets; Fourier; Ice load; Acceleration; Offshore

1. Introduction

First-year ice actions on a fixed offshore structure are studied to investigate further details about ice–structure interaction. Such a structure could be a platform for hydrocarbon production or a windmill foundation. Because the stability and integrity of an offshore structure in ice-infested waters have to be satisfied, engineers have to estimate the magnitudes of stresses in the structure due to ice actions. State-of-the-art load predicting methods are scattered by a factor of 10–15 according to Croasdale and Kennedy (1996). Hence, increasing activity in ice-infested areas such as the eastern Barents Sea, the Caspian Sea and offshore Sakhalin Island may require more work to find reliable methods for the estimation of applied loads caused by actions from first-year ice features on offshore structures.

Full-scale data may be the most valuable source of information that is obtainable for the estimation of ice actions on structures. Due to the large data storage and computer capacities available today, scientists conducting measurements are able to generate more raw data from their investigations than in the past. Previously, with limited storage capacities, dynamic ice action events often had to be filtered out at the measurement site (Engelbrektson, 1983). The latest data sources such as the projects Measurements on Structures in Ice (STRICE), Low Level Ice Forces (LOLEIF) (Schwarz, 2001) and the Canadian Confederation Bridge (Brown, 2001) consist of a large amount of unfiltered time records. In order to analyze such data, there is a need for a data management tool to show the occurrence of characteristic frequencies in the time domain together with the applied global ice forces. This issue has been addressed by, wavelet transform methods which have been applied to raw data to get information about the distribution of energy at different frequencies in the time domain.

_____

* Fax: +47 73 59 70 21.
  E-mail address: morten.bjerkaas@ntnu.no.

The main contribution of this paper is to illustrate further applications of the wavelet technique by applying the cross-wavelet spectra on time records measured during ice actions on an offshore structure. The application of the cross-wavelet spectra detects coherence by highlighting intervals with common high power at specific frequencies in two signals measured simultaneously.

The wavelet transform, first introduced by Grossmann and Morlet (1984), is based on the theory of square integrable functions, and allows a signal to be unfolded into time and scales (frequencies). The theory of both continuous and discrete wavelet transforms, has been thoroughly developed in recent years by researchers such as Daubechies (1992), and applied in several fields of physics and engineering, particularly for the processing, filtering and compression of time series and images.

The application of cross-correlation techniques based on the continuous complex-wavelet transform (CWT) was first introduced by Hudgins et al. (1993), but as far as the author is aware has never previously been applied to direct or indirect measurements of ice actions on fixed offshore structures.

The dynamic response phenomenon from ice actions on offshore structures has been extensively depicted since Peyton (1966) reported harsh ice-induced vibrations on oil drilling platforms in Cook Inlet, Alaska. In spite of this, there have been no full-scale data showing both the ice loads and responses of a structure with high resolution in space and time. The data in the present work are obtained from nine different load panels in the water-line covering $167°$ of the perimeter from the North. The load panels are working in parallel with two accelerometers and two inclinometers, which together give higher resolution than has been reported in earlier full-scale programs.

The present work is a further extension of the application of CWT in analyzing ice loads and ice-induced dynamic response. The proper use of the wavelet cross-correlation analysis on ice load and ice-induced response allows a physical description of the dynamic ice–structure interaction phenomenon. This approach differs from the traditional Fourier cross-correlation analyses as described by Bendat and Piersol (2000) because it is possible to localize relevant information in time-frequency space and compute local or global functions of the wavelet scalograms on the basis of the time-resolved information. The aim of the present work is twofold. First, to find out whether the fluctuations in the ice load signals are governed by the vibrations of the structure or not. Second, prove whether local ice

loads in the waterline are synchronized during intermittent crushing or not. Definitions of different kinds of ice crushing by Sodhi (1991) are applied in this work.

The paper has the following structure. Section 2 gives a brief introduction to the wavelet theory and an extension to the cross-wavelet transform. Section 3 provides an overview of the data collection methods and how the data are interpreted in the presented analyses. Section 4 presents the results of the wavelet analyses with a following discussion. Section 5 summarizes and concludes.

2. Wavelet transforms

A brief introduction to wavelet transforms and cross-wavelet analysis is presented in this section. For more details about wavelet theory and engineering applications, Daubechies (1992) and Gurley and Kareem (1999) should be studied.

2.1. Fundamentals

Mathematical transforms are usually applied to measured data to extract information which cannot be read from time series in a straightforward manner. The most common of such analyses is the Fourier transform, which decomposes a measured signal into harmonic components. The limitations of the Fourier transform is that it is only valid for stationary signals, which means that distinct changes within the chosen time interval cannot be distinguished from a Fourier transform. The so-called Short Time Fourier Transform (STFT) or Gabor-transform could be applied to deal with such non-stationary signals using Fourier techniques. The STFT is applied to time series by splitting the time series up in narrow and overlapping windows, where the Fourier spectrum could be obtained from the time series inside each of the windows. According to the Heisenberg uncertainty principle, the main limitation of the STFT method is that if the window is narrow, the frequency resolution will be poor and if the window is wider the time resolution will be less precise. Such limitations become evident when different frequency levels are dominant at different times in the signal. Seismic engineers introduced the wavelet transform to overcome these problems in analyzing data from earthquakes (Grossmann and Morlet, 1984). The main advantage of the wavelet transform is the varying window size with frequencies. For low frequencies, a wide window is applied and vice versa. This leads to optimal time-frequency resolution at all frequencies. On the other hand, Fourier analyses are still a suitable tool

to reveal information from stationary processes during the signal, whereas the wavelet transform can be used to detect the time evolution of non-stationary processes in the time and frequency spaces simultaneously.

There are two different ways to perform a wavelet analysis: a discrete wavelet transform which deals with wavelets on an orthogonal basis (Farge, 1992) and CWT which applies a non-orthogonal basis (Torrence and Compo, 1998). Following the latter approach, a time series x_n is defined for $n = 0, \ldots, N-1$ with sampling interval δt and length N. A wavelet function is then defined as $\psi(\eta)$ where $\eta = t/s$ is a non-dimensional time parameter and t and s are the time and scale, respectively. The scale parameter is linked to Fourier periods with the choice of wavelet function ψ.

Numerous wavelet functions are available in the literature and to be admissible as a wavelet, a function ψ should verify the following admissibility condition:

$$C_\psi = \int_{-\infty}^{+\infty} |\hat{\psi}(\omega)|^2 |\psi|^{-1} d\omega < \infty \qquad (1)$$

where, C_ψ and $\psi(\omega)$ are the admissibility constant and the Fourier transform of the wavelet function, respectively. The choice of a wavelet function should be evaluated based on the shape of the signal to be transformed. Due to the choice of the CWT with a non-orthogonal basis for the wavelet transform and as is well known and applied in other engineering fields (Jakobsen et al., 2001), the Morlet wavelet developed by Grossmann and Morlet (1984) was chosen for the application of the wavelet transform on ice loads and their responses. In the non-dimensional time domain, the Morlet wavelet reads:

$$\psi_0(\eta) = \pi^{-\frac{1}{4}} e^{-i\omega_0 \eta} e^{-\frac{\eta^2}{2}} \qquad (2)$$

where $\omega_0 = 6$. The corresponding expression in the frequency domain reads

$$\hat{\psi}_0(\omega) = \pi^{-\frac{1}{4}} e^{-\frac{(\omega - \omega_0)^2}{2}} \qquad (3)$$

The real part of the Morlet wavelet is plotted in Fig. 1 in the non-dimensional time (η) and frequency ($s\omega$) domains. Other wavelet functions might be better suited to the task of representing ice load signals, thus it is an assignment for further work to compare various wavelet functions and to develop new wavelets for the specialized use of the wavelet transform on ice load signals.

The idea regarding CWT is to apply the wavelet function ψ as a bandpass filter on the time series x_n. The CWT of a discrete signal x_n is defined as the convolution of x_n with a scaled and translated version
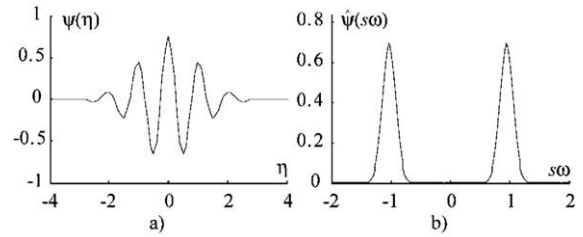

Fig. 1. Real part of the Morlet wavelet as used in the present work (a), with its Fourier spectral representation (b).

of the complex conjugate of $\psi(\eta)$. This convolution reads

$$W_n(s) = \sum_{n'=0}^{N-1} x_{n'} \psi^*[(n' - n)\delta t / s] \qquad (4)$$

where ψ^* means the complex conjugate and n' means the current location. The parameters s and n imply the scale factor and the time shift parameter, respectively. In practice it is more time efficient to do the convolution in Fourier space (for details see Torrence and Compo, 1998). Further, because the wavelet function $\psi(\eta)$ is complex, as shown in Eq. (2), the W_n is also complex. The wavelet coefficients can then be divided into a real part W_{nR} and a complex part W_{nI} while the amplitude then reads $|W_n|$ and the wavelet power $|W_n|^2$. Wavelet coefficients are normalized by the variance of the time series before plotting to make it easier to compare different transforms.

Wavelet coefficients are usually displayed with scalograms (Fig. 3c) which have the time and scale (or period) along horizontal and vertical axes, correspondingly. The variability in the color intensity makes an interval with high power that is distinguishable from a specific chosen background spectrum. In order to make the magnitudes of scales observed in scalograms accessible and comparable to a Fourier spectrum, scales might be translated to Fourier periods. In the case of the Morlet wavelet, the Fourier period (T_F) is almost equal to the scale for $\omega_0 = 6$, namely $T_F = 1.03 \cdot s$. This varies between different choices of $\psi(\eta)$, hence T_F has to be calculated with new choices of ψ.

If a vertical slice of the scalogram in Fig. 3c is chosen with a width n_a, a local wavelet spectrum can be defined by time integration of the coefficients inside the selected slice. If the borders of the vertical slice along the time axis are equal to n_1 and n_2, the local time integrated spectrum can be defined as

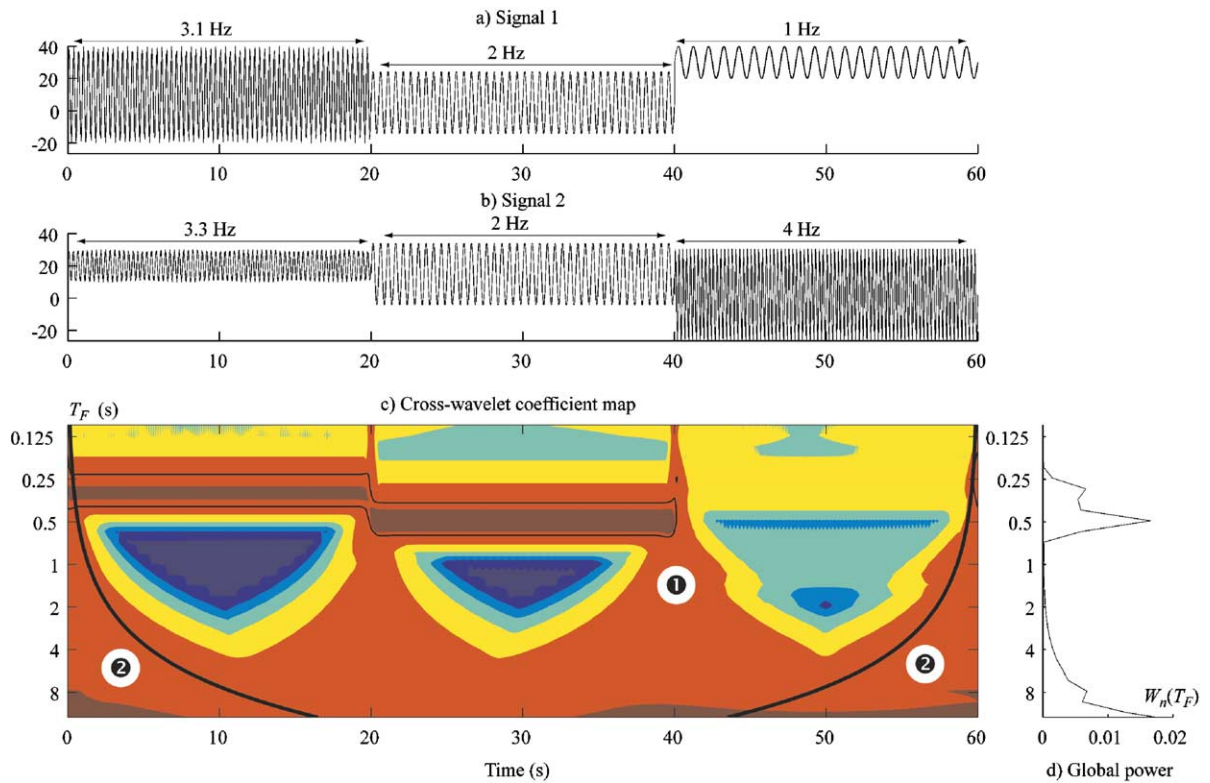$$\bar{W}_n^2(s) = \frac{1}{n_a} \sum_{n=n_1}^{n_2} |W_n(s)|^2 \qquad (5)$$

Fig. 2. Two test signals (a)–(b) with their corresponding cross-wavelet coefficient map (c) and global cross-wavelet spectrum (d). Symbols ❶ and ❷ in (c) denote the 95% significance level and the cone of influence (COI), respectively.

where n is the midpoint of the span n_1 to n_2 and $n_a = n_2 - n_1 + 1$ is the number of points inside the selected vertical slice. When choosing n_1 and n_2 to be located at the start and at the end of the time series, respectively, the global wavelet spectrum can be obtained as

$$\bar{W}_n^2(s) = \frac{1}{N} \sum_{n=0}^{N-1} |W_n(s)|^2 \qquad (6)$$

where the global wavelet spectrum can be displayed in Fig. 2d. The global wavelet spectrum can be handled as a smoothed version of the Fourier spectrum, hence it can be used as a first approximation to isolate dominant frequencies in the signal as well as to compare coefficients from FFT and CWT on the same basis. A theoretical description of the linkage between the global wavelet spectra and the classical Fourier spectra is given by Perrier et al. (1995). The global wavelet spectrum is shown in Fig. 2d where it can be seen that the Fourier period with the highest common power is 0.5 s (2 Hz) in the two harmonic test signals.

2.2. Cross-wavelet analyses

The wavelet cross-correlation analyses allow an extension of standard Fourier correlation analyses to non-stationary signals with power spectral characteristics that are variable in time. In the case of ice excitation of an offshore structure, the connection between the applied load and measured response might be studied in greater detail when the characteristic load and response frequencies could be studied both in the time and frequencies and not only in time or frequency domains. Another way to apply the wavelet cross-correlation is on ice load signals measured at different locations on the structure. In such cases, intervals with synchronized loading and simultaneous crushing could be detected both with respect to time and frequency.

Given two signals x_n and y_n measured at two different locations on a structure (Fig. 2a–b), the aim is to determine whether the signals are coherent at some time instances in the selected interval or not. A CWT is conducted on each of the time series x_n and y_n by applying Eq. (4). Similar to classical Fourier cross-

spectra procedures, it can be defined a cross-wavelet spectrum W_n^{xy} as the expectation value of the product of the two corresponding wavelet spectra W_n^x and W_n^y as

$$W_n^{xy}(s) = W_n^x(s) \cdot W_n^{y*}(s) \tag{7}$$

where the asterisk (*) means the complex conjugate of the matrix W_n^y. By using a complex mother wavelet as the Morlet wavelet, the cross-spectrum reads $W_n^{xy} = W_{n\,\mathrm{R}}^{xy} - iW_{n\,\mathrm{I}}^{xy}$, where R and I means the co and quadrature spectra, correspondingly. It should be noted that the amplitudes of the average cross-wavelet spectrum would be relatively small if there is no consistent phase relationship between a pair of signals. This is because cross-spectra with opposite phases cancel each other out through summation in the complex plane.

A global wavelet spectrum is obtained from the CWT of a single time series as expressed in Eq. (6) while a similar procedure can be applied to obtain a global wavelet spectrum from the matrix calculated in Eq. (7). Fig. 2 shows an example of two harmonic and non-stationary test signals with their corresponding wavelet cross-spectrum (Fig. 2c). The global wavelet spectrum (Fig. 2d) shows that the two signals have large common power at $T_F = 0.5$ s (2 Hz) and slightly less around $T_F = 0.3$ s (3 Hz). The wavelet cross-spectrum in Fig. 2c shows that the intervals with high common power are present between the start and 40 s after the start, with a changing period of oscillation around 20 s from the start. Between 40 and 60 s from the start, the two signals oscillate with 1 Hz and 4 Hz, respectively, which results in significantly less common power. Analyses of the phase angle of the signals, which can be calculated by the complex part of Eq. (7) are not a part of the present study.

2.3. Cone of influence

Given that a time series has a finite length, the wavelet is not completely localized in all choices of n. For that reason the signal must be padded with zeros at both ends before applying the convolution in Eq. (4). A cone of influence (COI) has to be defined to distinguish the real coefficients from the artificially created coefficients in the padded signal. The COI is the region of the wavelet spectrum where edge effects become important. The COI is defined by Torrence and Compo (1998) with an e-folding time, which equals $\sqrt{2} \cdot s$ for the Morlet wavelet. Calculated for each choice of s, the COI is indicated by a thick continuous black line in Figs. 2c, 5d and 7c).

2.4. Significance testing

When the coefficients in the scalogram are obtained, the significance of the distinct areas in the scalogram is still unknown. In order to carry out a test of significance, a background spectrum is calculated based on a synthetic signal. Such a synthetic signal could be red or white noise, which is well known as an approximation to different geophysical processes (Dyer, 1971). A simple model for the red noise approximation is the univariant lag − 1 autoregressive process (AR1). If the ice crushing time series can be estimated as such an AR1 process, the Fourier spectrum of this approximation can be used as a background spectrum of the CWT gained from a real signal. The discrete Fourier power spectrum of an AR1 process after normalization is given by

$$P_k = \frac{1 - \alpha^2}{|1 - \alpha e^{-2i\pi k}|^2} \tag{8}$$

where α is the lag − 1 autocorrelation coefficient and k is the Fourier frequency. In this study, $\alpha = 0.72$ has been used because it has been reported to fit well into the observed time series of several other geophysical processes (Dyer, 1971). When $\alpha = 0$, P_k goes to one and describes white noise. Eq. (8) can then be applied to model the red-noise spectrum. Further work is necessary to predict values of α which describe the ice crushing phenomena more accurately than $\alpha = 0.72$ that is used in this study.

Eq. (8) is initially suited as a background spectrum of one single time series, hence modifications are needed to apply a similar approach to the scalogram obtained from a cross-wavelet transform. More work is needed on significance testing of wavelet spectra in general and especially on background spectra used for significance testing of wavelet cross-spectra. The current study applies a method proposed by Torrence and Compo (1998) which assumes a confidence level p which can be derived from the square root of the product of two chi-square distributions. Applying the Morlet wavelet and a significance level of 95%, the theoretical background spectrum reads

$$D\left(\frac{|W_n^x(s)W_n^{y*}(s)|}{\sigma_x \sigma_y} < p \right) = \frac{Z_v(p)}{v} \sqrt{P_k^x P_k^y} \tag{9}$$

where, $Z_v(p)$ is the confidence level associated with the probability p to reach a certain level. $Z_v(p)$ equals 3.99 for the complex Morlet wavelet with two degrees of freedom ($v = 2$). P_k^x and P_k^y are the theoretical red-noise Fourier spectra of each of the time series, x_n and y_n.
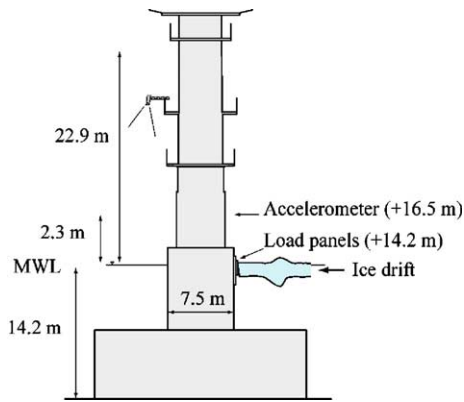
Fig. 3. Location of some of the measuring devices at the Norströmsgrund lighthouse winters 2001, 2002 and 2003.

The value of $Z_v(p)$ must be recalculated for other choices of mother wavelet and confidence levels.

2.5. Scale averaging

A scale averaging method can be used to obtain more detailed information on the distribution of energy at specific frequency bands. Scale averaged wavelet power is defined as the weighted sum of the wavelet power spectrum over scales s_1 to s_2:

$$\bar{W}_n^2 = \frac{\delta j \delta t}{C_\delta} \sum_{j=j_1}^{j_2} \frac{|W_n(s_j)|^2}{s_j} \tag{10}$$

where δj is a factor that dictates the scale resolution and C_δ is a reconstruction factor specific to each wavelet form which equals 0.78 for the Morlet (Torrence and

Compo, 1998). Eq. (10) describes a time series of wavelet coefficients for the chosen scales s_1 and s_2. Torrence and Compo (1998) describe how the significance of such lines could be tested in case of a single time series. However, how such tests should be conducted in the case of cross-wavelet coefficient maps is more uncertain. In the present study, a 5% level of the maximum was defined as a threshold value, which describes the start and the stop of intervals with common power in the two signals.

3. Data collection and interpretation

Ice load measurements were conducted in the period 1999 to 2003 at the Norströmsgrund Lighthouse in the Gulf of Bothnia (Sweden), by the LOLEIF and STRICE projects (Schwarz, 2001). The Norströmsgrund lighthouse is located approximately 60 km southeast and offshore Luleå in Sweden. The lighthouse is a 42.0-m-high gravity-based cylindrical concrete structure resting on moraine masses at a mean water depth of 14.2 m (Fig. 3). The waterline diameter of the lighthouse is about 7.5 m. The fundamental frequency of the lighthouse was calculated by Engelbrektson (1997) to be 2.3 Hz while Björk (1981) reported 2.8 Hz.

Norströmsgrund was instrumented in 1998 with nine load panels measuring normal forces 167 degrees from the North. Biaxial accelerometers and inclinometers were installed in 2001 to record the structural response. Additionally, measurements of the ice thickness, air temperature, wind speed and air pressure have been computed. Ice loads (F) and responses ($\ddot{u}$) were sampled at 1, 10, 30 or 100 Hz rate, depending on the
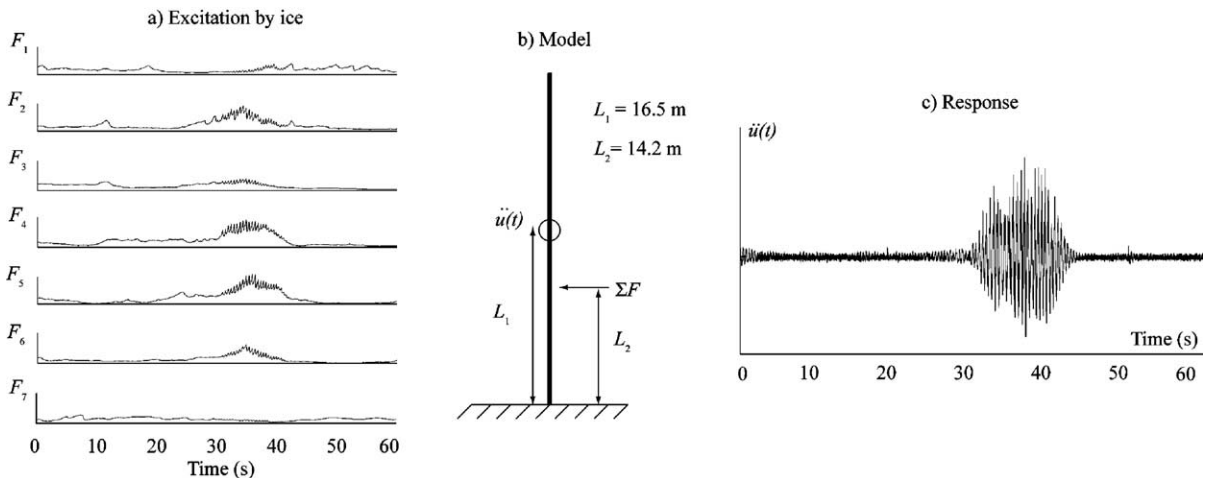

Fig. 4. (a) Time series of ice loads on seven active panels during 60 s, (b) principle model of the Norströmsgrund lighthouse with some of its measuring devices, (c) corresponding time trace of acceleration to the ice load time series measured 16.5 m above seabed.

category of interaction. Due to confidentiality agreements, no numerical values of ice loads could be included in this paper.

Fig. 4 shows a situation with 60 s of a continuously crushing level ice sheet including about 10 s with significant dynamic response. Fig. 4a shows time series of seven panel ice forces while Fig. 4b is a principle model of the structure. Fig. 4c shows $\ddot{u}$ corresponding to F in Fig. 4a. Lengths L_1 and L_2 indicate the distance from seabed to the waterline and from seabed to the lowest accelerometer, respectively. The global ice load F_G is the sum of the local ice forces acting in the waterline. During brittle ice crushing, local forces F_i reach their peak values non-simultaneously while with intermittent crushing the local ice forces F_i tend to reach their highest values at the same time, controlled by the fundamental frequencies of the structure. The global ice pressure p_G is defined as the sum of the local forces divided in the contact area as $p_G = F_G / Dh$, where D is the width of the structure and h is the ice thickness. One might think that during intermittent crushing p_G must exceed p_G during brittle crushing because the local load components reach their peaks at the same time in intermittent and not in brittle crushing.

4. CWT conducted on data from ice actions

The present analyses reveal information on the distribution of energy on specific frequencies in the time domain. Using this information, it might be possible to determine if the measured $\ddot{u}$ has high power at the same frequencies as the excitation F at the same time. This information could provide new inputs for the physical explanation of dynamic ice–structure interaction. Another element in this study is to use the wavelet approach to prove whether the local F_i becomes synchronized during an interval of dynamic ice–structure interaction. The localization of intervals with synchronized F_i is important because ice is a brittle material which usually fails in a non-simultaneous manner (Ashby et al., 1986; Bjerkås, 2004).

4.1. Ice loads and acceleration response

A first application of the wavelet cross-correlation technique was conducted to highlight possible correlation between measured $F_i(t)$, and its corresponding $\ddot{u}(t)$. Five different time traces were selected for the analyses, all lasting from one to two minutes. For example, a 60-s interval was selected from a long interval with continuously crushing level ice with estimated drift speed 0.03 m/s and mean ice thickness

about $h = 0.9$ m. It was a typical feature within the selected events that the ice thickness had little variation as indicated in Fig. 5c. Video record analyses were conducted to observe the variation in drift speed during the selected events. Generally, intervals with ice-induced vibrations were frequently observed when the ice drift speed went from a significant speed down to rest. The intervals with decaying drift speeds always lasted longer than the interval with significant vibrations, hence it was not possible to observe a change in drift speed before and after a detected interval. Fig. 5d shows a map of cross-wavelet coefficients as calculated by Eq. (4). Fig. 5a–b show the time series as they were measured in situ (F normalized). The horizontal axis displays time in seconds and the vertical axis displays F and $\ddot{u}(t)$ as indicated in the plot. The wavelet map has time in seconds on the horizontal axis and an equivalent Fourier period on the vertical axis. To the right of the wavelet map, the global cross-wavelet power is plotted as calculated by Eq. (6).

The first impression of Fig. 5 is that F as well as $\ddot{u}$ seem to change significantly around 30 s and 42 s from start. The whole interval starts with an almost constant F for about 20 s. The structural response during this almost constant load level is supposed to be of a static character and no correlation is to be seen between F and $\ddot{u}$. Then an increase in the load level is triggered by some process around 30 s with a distinct drop followed by an interval with almost steady state vibrations. The ice load signal consists of a static contribution in the range of 50–60% of the maximum load, with an additional fluctuating part. Going to the cross-wavelet coefficient map (Fig. 5c), it can be observed that high correlation is to be seen for T_F slightly faster than 0.5 s. One should recall that the fundamental frequency of the structure has been calculated as 2.3 Hz and 2.8 Hz, which means that the ice load most likely is locked-in to a frequency in this range by the response of the structure. The global wavelet spectrum indicates that the most common energy is present at T_F slightly faster than 0.5 s.

Coefficient lines are selected which correspond to the fundamental frequencies of the structure to obtain further details about periods with common high power in the two signals displayed by Fig. 5a–b. Määttänen (1983) shows that several of the fundamental modes of a structure can possibly control the ice crushing process if the modes themselves are excitable in the waterline. As a first approach, this study aims to investigate the first fundamental mode of the structure, with its abilities to control the ice crushing process. The fundamental frequency of the Norströmsgrund lighthouse has been reported as both 2.3 Hz and 2.8 Hz, hence all scales
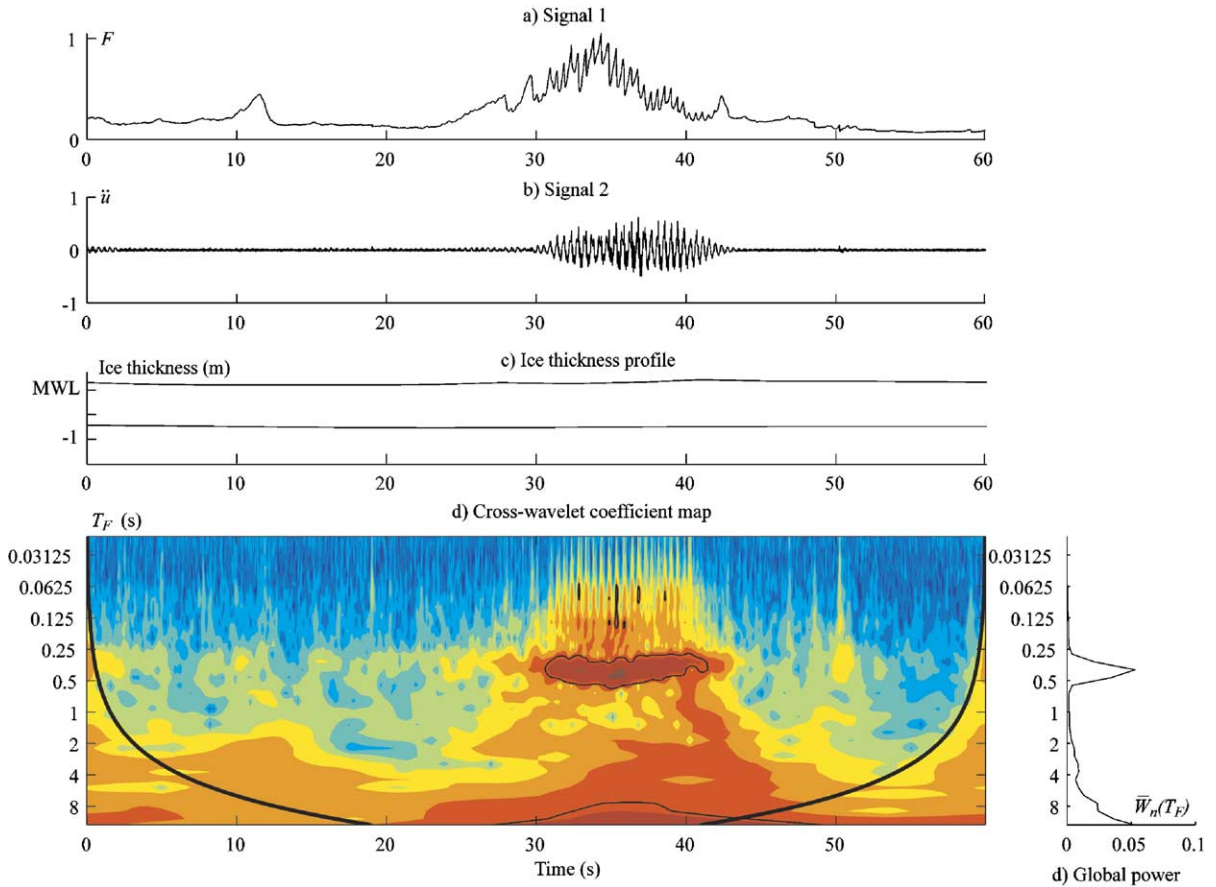
Fig. 5. (a) Normalized ice load (F_i); (b) acceleration ($\ddot{u}$); (c) ice thickness; (d) cross-wavelet coefficient map; (e) global wavelet cross-spectrum obtained for Event no. 1.

corresponding to the frequencies between 2.3 Hz and 2.8 Hz were averaged as indicated in Eq. (10) and displayed in Fig. 6. Using a threshold value of 5% of the normalized maximum value of the coefficient line at the chosen scales, a length of an interval L_R is selected which describes the time span of synchronization between F and $\ddot{u}$.

Table 1 lists five intervals analyzed as described in the current section. Intervals with synchronization be-

tween the load and the response have lengths from 1.9 s to 8.7 s with corresponding ice thickness from $h = 0.2$ m to $h = 0.8$ m and drift speeds from 0.03 m/s to 0.06 m/s, respectively. Due to high stiffness and significant damping of the Norströmsgrund lighthouse, intervals with synchronization might have been of shorter length than observed on other offshore structures such as multi-legged structures (Yue and Bi, 2000) and steel lighthouses (Määttänen, 1987). However, Bjerkås and
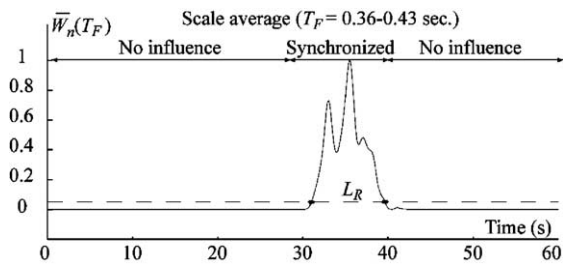
Fig. 6. Averaged and normalized cross-wavelet coefficient line referring to Fourier period 0.36–0.43 s (continuous line) and 5% threshold line (dashed line), Event no. 1.

Table 1
Calculated length of intervals with assumed synchronization between acceleration and ice load and intervals with assumed simultaneous ice crushing with their corresponding ice thicknesses and drift speeds

Event	h (m)	v (m/s)	$F_i - \ddot{u}$		$F_i - F_j$ $(i \neq j)$	
			L_R (s)	Separation (m)	L_S (s)	Separation (°)
1	0.2	0.03	8.6	+2.3	7.1	72
2	0.8	0.06	4.8	+2.3	4.7	18
3	0.2	0.03	3.8	+2.3	3.4	36
4	0.2	0.03	3.0	+2.3	2.0	18
5	0.5	0.05	1.9	+2.3	1.8	36

Skiple (submitted for publication) reported on the occurrence of intervals with steady state vibrations from the same structure where they found vibrations which lasted for 80 s.

4.2. Correlation of local ice forces

The next application of wavelet cross-correlation analyses is between time series F_i and F_j measured at different locations on the structure ($i \neq j$). The global ice load on a structure decreases if local forces F_i reach their peak values at different times during a sequence of ice crushing. Due to this, it is interesting to know if initially independent time series of F_i can be synchronized during an interval of ice crushing. If such synchronization can be identified, structures have to be designed for higher global pressure than what can be seen during intervals where all series of F_i reach their peaks at different times. Cross-correlation analyses that use wavelet transforms have been applied to predict length, L_S, i.e., the length of the interval with synchronized loading. Table 1 shows the results from the current analyses.

Cross-wavelet analyses were performed on time traces measured by ice load panels on the Norströms-grund lighthouse. Two time traces of ice loads were selected (F_2 and F_6) measured $+18°$ and $+90°$ from the north, separated by about 9 m along the perimeter of the structure. The normalized time traces and results from the cross-wavelet analyses are shown in Fig. 7.

At first sight, the time series in Fig. 7a–b appear to contain two typical characteristics. The first characteristic is an almost constant load level with some peaks occurring non-simultaneously in the two signals as shown by the interval from the start to about 25 s. The second characteristic is the interval between 30 s and 40 s from the start, which contains an almost constant static load contribution of about 50% to 60% of the maximum load magnitude together with a fluctuating part with a characteristic frequency. It can be observed from the cross-wavelet coefficient map (Fig. 7c) that high common power is present in long Fourier periods exceeding 4 s during the whole interval. A distinct change takes place between 30 s and 40 s where the fluctuating part of the load signal is present. High common power is present at a period between 0.50 s and 0.25 s together with lower Fourier periods between 0.25 s and 0.125 s. The global power spectrum cannot identify any details of periods in the range of the fundamental period of the structure, simply because the
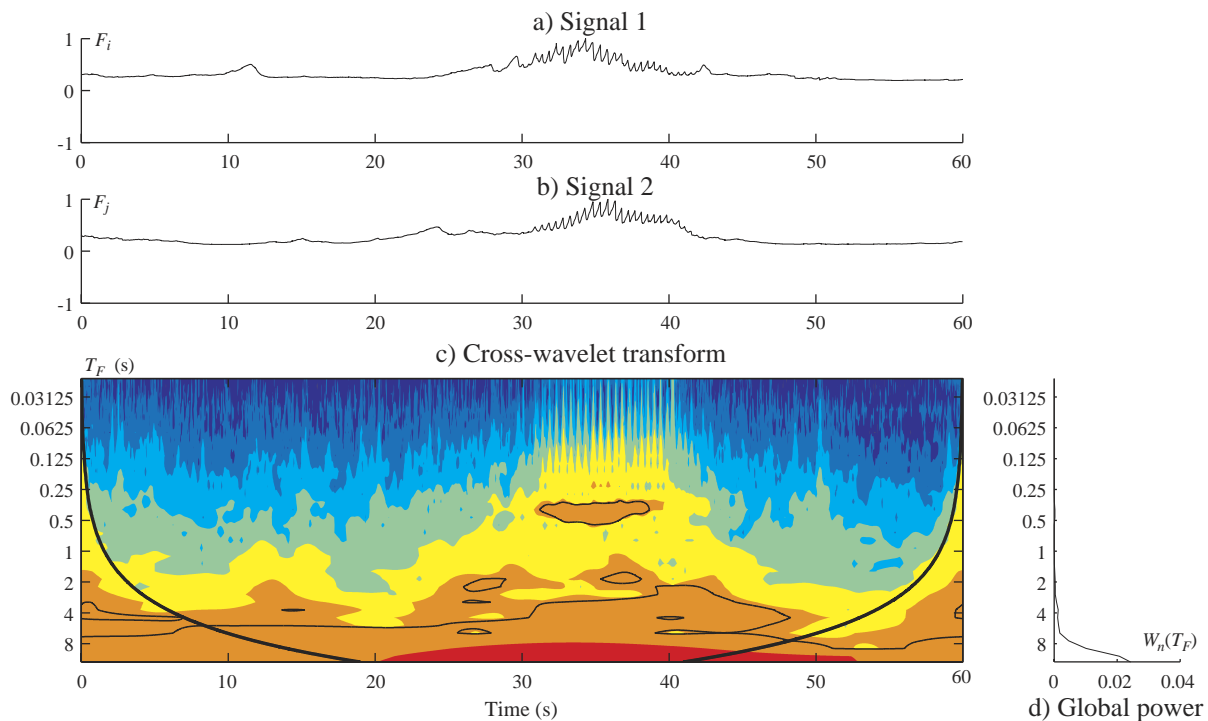

Fig. 7. (a) Normalized ice load time series; (b) acceleration time series; (c) cross-wavelet coefficient map; (d) global wavelet cross-spectrum, obtained signals in panels (a) and (b), Event no. 1.
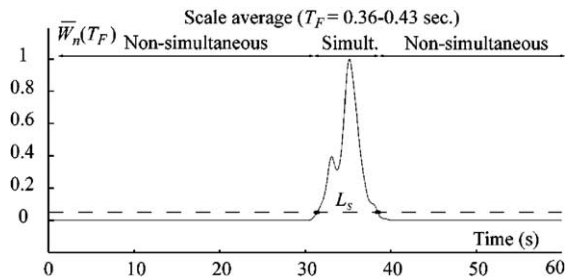
Fig. 8. Scale averaged and normalized cross-wavelet coefficients referring to Fourier period 0.36–0.43 s (continuous line), Event no. 1.

low-frequency periods have too much power. Additionally, the 95% confidence line shows that there is an interval with high common power in the two signals between 30 s and 40 s from the start.

Scale averaging of the coefficient lines connected to frequencies between 2.3 Hz and 2.8 Hz gives the continuous line shown in Fig. 8. From the start to about 30 s, and from 40 s to 60 s, there is practically no common power at the chosen Fourier periods and the two load signals can be characterized as uncorrelated, which were assumed to be caused by non-simultaneous ice crushing. Between 30 s and 40 s from the start, there is a clear peak that means that the common power at the chosen period is high and the signals most likely to be synchronized in this interval. The ice loading type can be described as synchronized loading with simultaneous ice failure.

Altogether, five load samples were studied with respect to simultaneous loading in this work, all of them are reported in Table 1. The lengths of the intervals with simultaneous loading were 1.8 s to 7.1 s, slightly shorter than the intervals which were characterized by synchronization between the load and the response. On the other hand, all intervals with simultaneous ice failure were within the same time intervals, as the intervals with synchronization between the load and the response. Hence, it was supposed that lengths L_R and L_S are physically coupled, which leads to the presumption that the load signals are locked-in to the fundamental frequency of the structure.

5. Summary and conclusions

This work describes applications of the cross-wavelet spectrum based on continuous wavelet transforms. Cross-wavelet analyses seem to be well suited to an analyzing Morlet wavelet for the prediction of the length of intervals with synchronization between the applied ice load and the measured ice-induced response. Additionally, cross-wavelet spectra were ap-

plied to detect whether local ice forces were correlated within the ice-structure contact area.

From analyses of five selected time traces lasting for one to two minutes, intervals with measured ice loads and acceleration measured 2.3 m above the waterline seem to be synchronized in time and frequency. The intervals have lengths between 1.9 and 8.6 s and are synchronized around frequencies in the range 2.3 Hz to 2.8 Hz.

Intervals with synchronized local ice loads were assumed to be caused by simultaneous ice failure. Local ice loads measured by panels separated by about nine meters were found to be synchronized in intervals lasting from 1.8 s to 7.1 at frequencies in the range 2.3 Hz to 2.8 Hz.

From the present application of cross-wavelet analyses on ice load signals and ice-induced response, it was reasonable to assume that ice load signals can be locked-in to the fundamental frequency of the structure for intervals in the range of 2 s to 10 s. Further, it was observed that simultaneous ice failure seems to be possible and has to be taken into account in the design of offshore structures that are vulnerable to ice-induced vibrations.

Further applications of correlation analyses with the use of cross-wavelet transforms on ice loads and their corresponding response are required. A short list is offered to give ideas about further applications:

– Calculation of Fourier spectra from time series of load and response measured simultaneously with the isolation of dominant frequencies.
– Application of the convolution in Eq. (4) on the chosen time series with a contour plot of the coefficient matrices. Dominant frequencies can be isolated from the time integrated global wavelet spectrum.
– Application of the cross-wavelet spectrum as shown in Eq. (7) with the location of intervals with high common power.
– Further details can be obtained by selecting scales of special interest as indicated in Eq. (10).

References

Ashby, M.F., Palmer, A.C., Trouless, M., Goodman, D.J., Howard, M.W., Hallam, S.D., Murrell, S.A.F., Jones, N., Sanderson, T.J.O., Ponter, A.R.S., 1986. Non-simultaneous failure and ice loads on structures. Proceedings of Offshore Technology Conference, Houston, TX, pp. 399–404.

Bendat, J.S., Piersol, A.G., 2000. Random Data, Analysis and Measurement Procedures. Wiley, p. 594.

Bjerkås, M., 2004. Global design ice loads' dependence on failure mode. International Journal of Offshore and Polar Engineers (IJOPE) 14 (3), 189–195.

Bjerkås, M., Skiple, A., submitted for publication. Occurrence of continuous and intermittent crushing during ice–structure interaction, Proceedings of the 18th International Conference of Port and Ocean Engineering under Arctic Conditions (POAC), Potsdam, USA, vol. 3.

Björk, B., 1981. Ice induced vibrations of fixed offshore structures: Part 2. Experiences with Baltic Lighthouses. In: Carstens, T. (Ed.), Marine Structures and Ships in Ice, p. 100. Rep. 81-06/2.

Brown, T., 2001. Four years of ice force observations on the confederation bridge. Proceedings of the 16th International Conference of Port and Ocean Engineering under Arctic Conditions (POAC), Ottawa, Canada, vol. 1, pp. 285–298.

Croasdale, K.R., Kennedy, K., 1996. Ice loads consensus study update. Proceedings of the International Offshore Mechanics and Arctic Engineering Conference (OMAE), Firence, Italy, vol. 4, pp. 115–118.

Daubechies, I., 1992. Ten lectures on wavelets. CBMS-NSF Conference Series in Applied Mathematics, SIAM Ed, 1992, p. 358.

Dyer, R.M., 1971. Method for filtering meteorological data. Monthly Weather Review 99 (5), 435–438.

Engelbrektson, A., 1983. Observations on a resonance vibrating lighthouse structure in moving ice. Proceedings of the International Conference on Port and Ocean Engineering under Arctic Conditions (POAC), Helsinki, Finland, vol. 2, pp. 855–864.

Engelbrektson, A., 1997. A refined ice/structure interaction model based on observations in the Gulf of Bothnia. Proc. of Offshore Mechanics and Arctic Engineering Conference (OMAE), Yokohama, Japan, vol. 4, pp. 373–376.

Farge, M., 1992. Wavelet transforms and their applications to turbulence. Annual Review of Fluid Mechanics 24, 395–457.

Grossmann, A., Morlet, J., 1984. Decomposition of Hardy functions into square integrable wavelets of constant shape. SIAM Journal of Mathematical Annals 15, 723–736.

Gurley, K., Kareem, A., 1999. Applications of wavelet transform in earthquake, wind and ocean engineering. Engineering Structures vol. 21. , pp. 149–167.

Hudgins, L., Friehe, C.A., Mayer, M.E., 1993. Wavelet transforms and atmospheric turbulence. Physical Review Letters 71 (20), 3279–3283.

Jakobsen, J.B., Haver, S., Ødegård, J.E., 2001. Study of freak waves by use of wavelet transform. Proceedings of the International Offshore Polar Engineering Conference (ISOPE) 2001, vol. 3, pp. 58–64.

Määttänen, M.P., 1983. Dynamic ice–structure interaction during continuous crushing. CRREL Report 83-5. 49pp.

Määttänen, M.P., 1987. Ten years of ice-induced vibration isolation in lighthouses. OMAE 1987, Houston, TX, USA, vol. 4, pp. 261–266.

Perrier, V., Philipovitch, T., Basdevant, C., 1995. Wavelet spectra compared to Fourier spectra. Journal of Mathematical Physics 36 (3), 1506–1519.

Peyton, H.R., 1966. Sea ice strength, University of Alaska, Geophysical Institute. Final Report for the Navy Office of Naval Research, Contract No. 2601 (01).

Schwarz, J., 2001. Validation of low level ice forces on coastal structures. Proceedings of the International Offshore Polar Engineering Conference (ISOPE) 2001, Stavanger, Norway, pp. 749–753.

Sodhi, D.S., 1991. Ice–structure interaction during indentation tests. In Ice–Structure Interaction: Proc. of IUTAM-IAHR Symposium, St. Johns, Canada. , pp. 619–640.

Torrence, C., Compo, G.P., 1998. A practical guide to wavelet analysis. Bulletin of the American Meteorological Society 79 (1), 61–78.

Yue, Q., Bi, X., 2000. Ice-induced jacket structure vibrations in Bohai Sea. Journal of Cold Regions Engineering 14 (2), 81–92.

Chapter 7, Paper IV

Occurrence of intermittent and continuous crushing during ice-structure interaction

By Morten Bjerkås and Asle Skiple

Proceedings of the 18'th International Conference on Port and Ocean Engineering under Arctic Conditions (POAC), Vol. 3, Potsdam, NY, USA, June 2005.

(In review)

OCCURRENCE OF CONTINUOUS AND INTERMITTENT CRUSHING DURING ICE-STRUCTURE INTERACTION

Morten Bjerkås and Asle Skiple
Department of Civil and Transport Engineering,
Norwegian University of Science and Technology (NTNU), Trondheim, Norway

ABSTRACT
This paper presents an interpretation of full-scale data from the Norströmsgrund lighthouse in the Gulf of Bothnia. From analyses of load and response patterns, periods with ice crushing were decided to be either intermittent or continuously crushing. Details of the initialization of intermittent crushing were studied and two different types of triggering were discovered, namely triggering with a circumferential crack and triggering with internal cracking. Another issue of the analyses was to figure out a range of drift speeds where intermittent crushing was more likely to occur. From all the selected intervals, intermittent crushing seemed to occur between 0.02 m/s and 0.08 m/s. Further studies revealed that the transition speed between continuous and intermittent crushing was slightly increasing both with increasing ice thickness and a 24 hour averaged air temperature. The reason for the increasing transition speed with increasing temperature seem to be that both speed and temperature can cause either brittle or ductile failure of the ice. The increasing transition speed with increasing ice thickness was addressed to the failure of independent zones during continuous crushing. It was believed that because the number of zones is decreasing for increasing ice thickness, the zones synchronize easier when the ice gets thicker, simply because there are fewer zones.

INTRODUCTION
With a high focus on activities in ice-infested waters, structures for offshore oil drilling and production as well as offshore wind mill foundations have to withstand highly dynamic actions from floating ice sheets in the sea.

Extensive work on ice induced vibrations was first conducted in Cook Inlet, Alaska (Peyton, 1968). These studies gave rise to theoretical models, that assumed the structure to be self-excited and explained the sustained vibrations with the rate dependency of sea ice strength. This model was extended by Määttänen (1978) for multi-degree-of-freedom systems and was applied to design of structures in e.g. the Gulf of Bothnia (GOB). Another approach was presented by Sodhi (1988) which shed new light on the idea of ice-induced vibrations as

forced oscillations with a characteristic ice failure frequency. Several laboratory programmes have been completed to increase the knowledge about ice induced vibrations (Muhonen et al., 1992; Sodhi, 1989; Timco et al., 1992; Izumiyama et al., 1994; Kärnä et al., 2003; Gravesen et al., 2005). Extensive field programmes have been completed as well (Jefferies and Wright, 1988; Nordlund et al., 1988; Schwarz and Jochmann, 2001; Yue and Bi, 2003).

Despite already extensive work, it has not been successfully presented a commonly acceptable explanation for the dynamic ice-structure interaction phenomenon. Sodhi (1991) introduced the concept of ductile (DC), intermittent (IC) and brittle (CC) crushing mainly controlled by the relative speed and the aspect ratio (D/h) where D is the structural width and h is the ice thickness. The borders between DC, IC and CC were supposed to be separated by transition speeds (v_1 and v_2 in Fig. 1), which recently Sodhi and Haehnel, (2003) indicated could be influenced by ice temperature. Several methods have been presented to mitigate ice-induced vibrations. Such methods are installation of a cone in the water line and the increasing of modal damping of the structure (Määttänen, 1987) where the latter was the only way that have been proven successful.
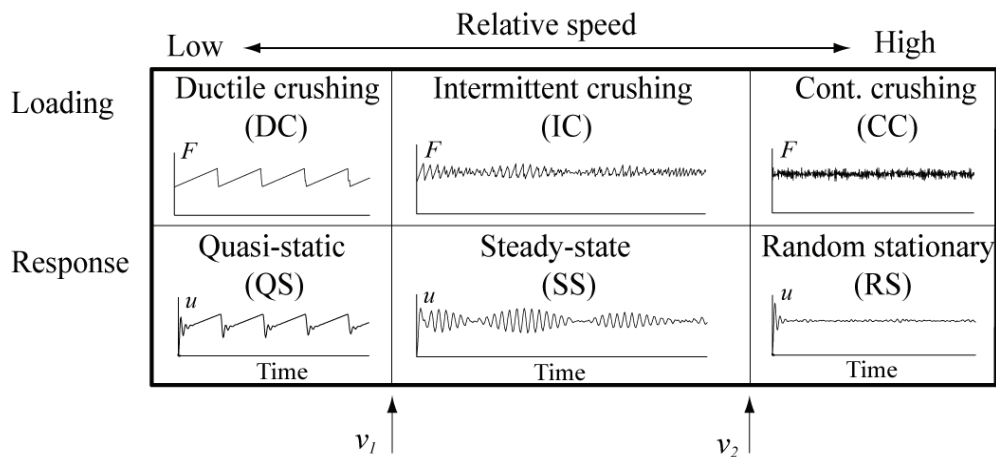

Figure 1. Transition between DC and CC during ice-structure interaction with their corresponding load (F) and response (u) signals obtained by simulations.

The present study is based on the hypothesis that the v_2 could be influenced by both ice thickness and temperature since thickness and temperature earlier have been shown to influence on the failure mode during indentation tests. The aim of the present study was to make a quantitative and qualitative analyses of the transition between continuous crushing (CC) and intermittent crushing (IC) based on measured structural response and visual observations.

EXPERIMENTAL METHODS

Data obtained at the lighthouse Norströmsgrund in the GOB during the STRICE project (Measurements on Structures in Ice) have been interpreted in this work. Norströmsgrund is located at about 14 m water depth, in the drifting ice zone about 60 km offshore Luleå in the northernmost Sweden. Loads were measured direct in the water line by nine stiff load panels and indirect by two biaxial accelerometers (16.5 m and 37.0 m) and two biaxial inclinometers (22.0 m and 37.0 m) where the heights refer to the distance from the seabed. Due to a confidentiality agreement within the STRICE project, all ice loads in this study are normalized against its highest measured load within the selected interval. All load traces refer to signals from single panels. Acceleration signals which are used in this study are permanently from the accelerometer 16.5 m above seabed.

A description of the experimental setup in the actual period (2001-2003) is given by Schwarz and Jochmann (2001). The ice thickness has been estimated from video records together with available data from an electromagnetic induction device (Haas, 1998) and an Upward Looking Sonar (Vinje and Berge, 1989). The ice drift speed was estimated by means of frame-by-frame studies of video records. Snow fields or large air-bubbles in the ice cover were followed during a certain distance on the screen. In the case of long events with CC, the speed was calculated several times and averaged.

Failure modes during the selected intervals were first evaluated with emphasis on response signals. DC was eliminated because a lower cut-off on drift speed was set to 0.02 m/s. IC was decided to occur when the accelerations 16.5 m above the seabed exceeded 0.3 m/s^2 for more than 10 seconds. It has earlier been observed that the fundamental frequencies of the structure can clearly be seen in the load signal during IC (Määttänen, 1983). Hence, IC was decided to occur if the fundamental frequencies of the structure could be seen in the same period as the significant response was observed. To implement such analyses, continuous wavelet transforms (Torrence and Compo, 1998) together with classical fast Fourier transforms were applied on the ice load signals. Fig. 2a shows an ice load signal with its corresponding acceleration signal from an interval which was defined as IC.
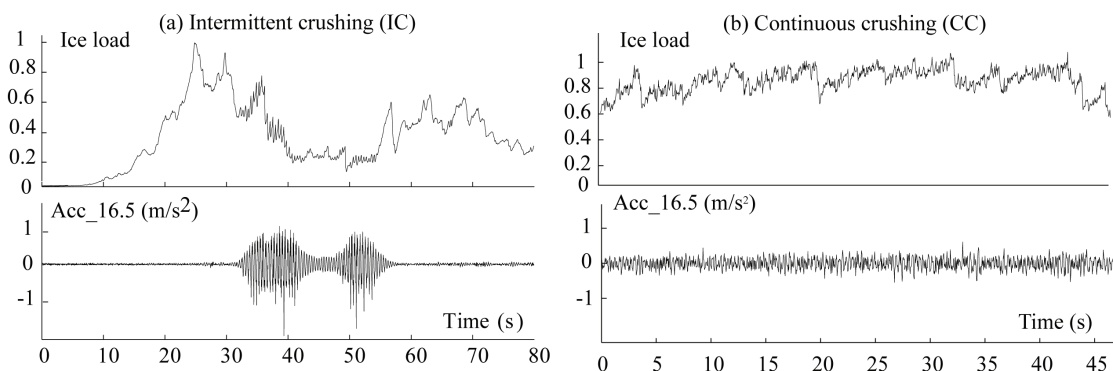

Figure 2. Load-time traces: (a) Intermittent crushing (IC), $h = 0.3$ m, drift speed $v = 0.05$ m/s; (b) Continuous brittle crushing (CC), ice thickness $h = 0.3$ m and drift speed $v = 0.3$ m/s.

CC was decided to occur where the response was seen as a broad band stochastic process around a defined mean level of ice load. Dominance of the fundamental frequencies of the structure could not be observed if the interval should be defined as CC. The ice load signal was usually seen as a random stochastic process defined with a static mean value and a variance. Frequency analyses show that the fluctuating part of the ice load from CC could be

131

approximated by a Monte-Carlo process, which means that the energy in the signal are linearly decreasing to zero from the lowest frequencies (Allan and Smith, 1996). Fig. 2b shows an example of an ice load signal with its corresponding response during a period which was defined as CC with RS response.

RESULTS AND ANALYSES
Altogether 99 intervals were selected for further analyses, 50 were decided to contain IC and 49 as CC. Typical situations from IC and CC are shown in Figs. 2a and b, respectively. The corresponding data as video records, ice drift speed, ice thickness and air temperature was obtained for the selected intervals. For more careful visual studies of the transition between CC and IC, two samples were selected, one from 30 March 2003 (Fig. 4) and one from 25 March 2003 (Fig. 5).

By studying video records and time series from ice crushing with its response simultaneously, one can get some ideas about why IC occurs. First, two typical cases were selected which contained IC (Fig. 3a) and CC (Fig. 3b), respectively. Fig. 3a shows that the rubble pile ❷ contains pulverized ice with size up to about 50 % of the ice thickness ($h = 0.2$ m). With no snow on the ice, it can be assumed a relatively low friction coefficient ice-on-ice. Thus the crushed ice pieces are able to slide on the intact ice surface ❶. Fig. 3b shows a situation where all crushed ice in the rubble pile ❷ seems to be pulverized and it is hard to find any ice pieces of a measurable size. The ice thickness here was about 0.5-0.6 m. The intact ice ❶ is here slightly covered by snow and the sliding of rubble seems to be limited by the ice-snow friction.
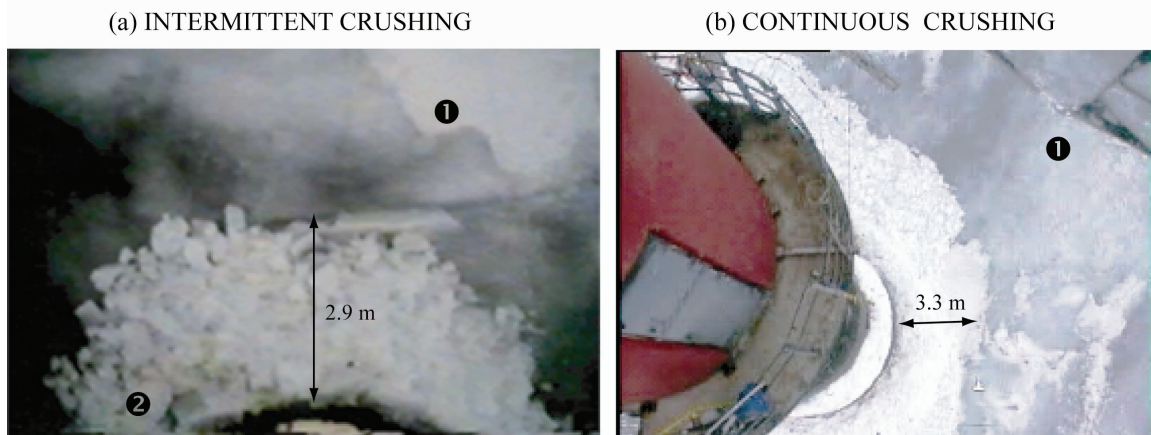

Figure 3. (a) Intermittent crushing with ice thickness 0.2 m and drift speed 0.05 m/s occurring 12:06:39, 30 March 2003, (b) Continuous crushing with ice thickness 0.5-0.6 m and drift speed 0.35 m/s occurring 21:23:02, 19 March 2003.

Transition between CC and IC
A closer study was conducted on a selected interval from 30 March 2003. This interval contains one of the most extensive intervals (80 sec.) with IC observed during this study. The main focus was on mechanisms which trigger IC; hence only the first transition period from CC to IC was studied. Fig. 4 shows a sample with a window labelled ❶, which highlights the beginning of the period with IC.

From label ① we can observe steady loading with a low magnitude due to the circumferential crack which are highlighted with a dashed line on the corresponding snapshot. Free floating rubble can be seen through the transparent ice cover as a white shade

on the photo. The circumferential cracking process has produced blocks with sizes up to about an ice thickness, ($h = 0.65$ m).
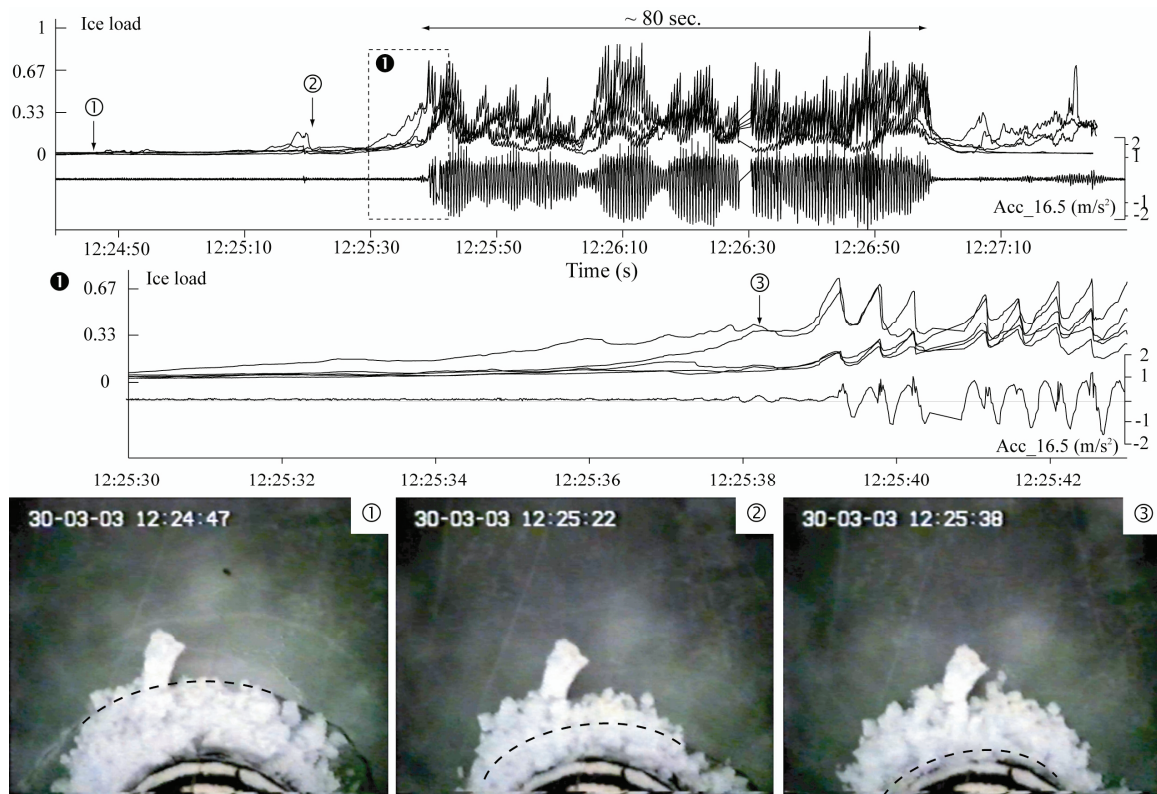

Figure 4. An interval with SS vibrations occurring 30 March 2003, $h = 0.65$ m, $v = 0.02$ m/s.

Then 35 sec. later (label ②), the circumferential crack has moved closer to the structure and are almost completely hidden by the debris from the crushing. The position of the circumferential crack is indicated by the dashed line. Most of the crushed ice is going downwards between position ① and ②.

The position with label ③ is located less than a second before the large amplitude vibrations and the synchronization of ice loads starts. The circumferential crack has now almost reached the vertical structure and the ice loads synchronize on all active panels immediately after this point. A period of 80 seconds is starting with heavy vibrations and simultaneous ice crushing on the panel. The main reason for triggering this period with IC loading was supposed to be the smooth ice edge caused by the circumferential fracture highlighted by a dashed line on the snapshots in Fig. 4. This triggering procedure was frequently observed for ice floes with thicknesses thinner than $h = 0.8$ m.

For the thicker ice sheets ($h > 0.7$ m) it was in many cases not possible to see any physical change of the failure mode on the topside of the ice cover during transition between IC and CC. An example of such an interval is shown in Fig. 5. The load signals show a non-simultaneous pattern during the first 30 seconds of the interval. A high load is building up at label ① followed by about 11 seconds of synchronized loads with corresponding strong vibrations of the structure. Mechanisms which feed the SS vibrations with energy after the initialization are not studied in this work.
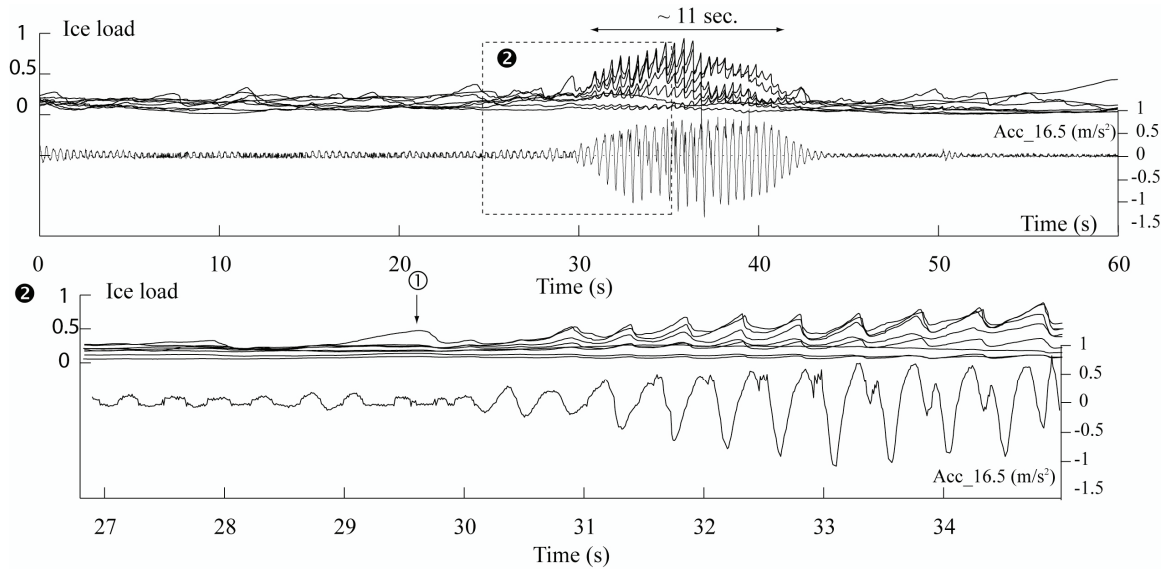
Figure 5. An interval with SS vibrations occurring 30 March 2003, 12:14:30, $h = 0.72$, $v = 0.03$ m/s.

Dependence on ice thickness

A quantitative study was obtained on all the observed intervals. Fig. 6 shows that IC occurs for v from 0.02 m/s to 0.08 m/s and CC for speeds from 0.10 m/s and higher. Intervals containing CC with drift speeds higher than 0.15 m/s are not displayed in Figs. 6 and 7. An upper bound linear trend line was fitted to all the observed occurrences of IC. A general but weak trend is that v_2 (Fig. 1) is increasing with increasing ice thickness.
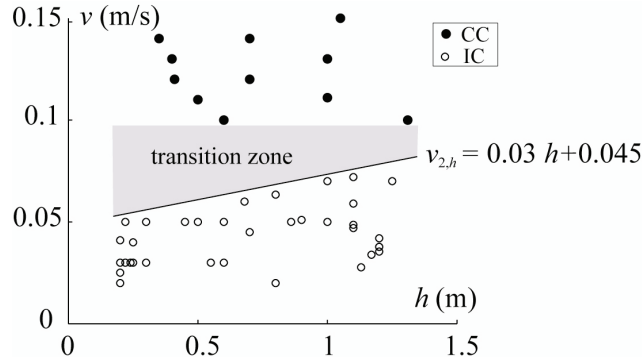
Figure 6. Distribution of CC and IC with respect to drift speed versus ice thickness.

However, there is a lack of observations of CC with thin ice and lower speeds at the same time. The shaded area is therefore an unclear transition zone which should be studied in further detail by interpretation of more data. The linear trend of v_2 versus ice thickness reads:

$$v_{2,h} = 0.03 \cdot h + 0.045 \text{ (m/s)} \quad 0.2 \text{ m} < h < 1.2 \text{ m} \tag{1}$$

Dependence on temperature

It was supposed to be a time delay between the current ice temperature and the measured air temperature. Hence, to have an indication of the corresponding ice temperature, a 24 hour time average of the air temperature was calculated for each of the selected intervals. The linear trend line fitted as an upper bound to the observations of IC in Fig. 7 indicates a weak

increasing trend of speeds with the average air temperature. Note that the number of observations of IC for temperatures below -1°C is only three. The linear trend line reads:

$$v_{2,T} = 0.004 \cdot T_a + 0.071 \text{ (m/s)} \quad -12°\text{C} < T_a < 5°\text{C} \tag{2}$$

More data is needed to establish any qualitative analyses on the transition speeds dependence on temperature.

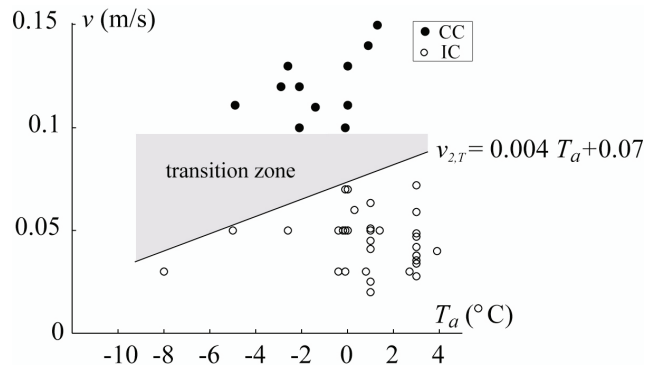Figure 7. Distribution CC and IC with respect to ice drift speed versus 24 hour average air temperature.

DISCUSSION
Ice crushing on a vertical structure can be divided into three categories, DC, IC and CC. From interpretation of full-scale data we have studied the transition between CC and IC and how the periods with IC are triggered. The main results from these studies were that periods with SS vibrations were initiated in two different ways, namely: 1) Synchronized loads due to a smooth ice edge because of a existing circumferential crack, and 2) high loads on one or two panels, which cause a loading process where all the other panels are synchronized after a few cycles. The other findings were that IC occurs for drift speeds between 0.02 m/s and 0.08 m/s and that CC occurs for speeds higher than 0.1 m/s. The transition speed tends to increase for both increasing ice thickness and temperature.

The reason why the circumferential cracking, which could cause the initialisation of IC, takes place could be addressed to upward-downward motions of the ice floe (Kärnä and Jochmann, 2003). These vertical motions occur due to changing equilibrium between buoyancy forces from rubble underneath the ice floe and the weight of the extruded rubble on the top of the level ice surface. Another way to trigger IC, which was observed could be connected to high loads on one or two panels before synchronization. Several reasons could be connected to this starting procedure. It has been assumed that IC occurs when a dominant frequency of the load is close to one of the fundamental frequencies of the structure. These data show that the frequency of the load is very much lower than the fundamental frequency of the structure until one critical load build-up occurs and starts the whole event. A reasonable explanation is therefore that in-plane cracks are developing in the crushing zone which can cause wide horizontal cleavages of the ice sheet (Hirayama, 1974).

The overall reason for the transition between CC and IC could be addressed to differences in ice drift speed, which have been indicated since Peyton (1968) presented his results. The intuitive reason for synchronization of loads is changing failure mode from brittle to ductile. This study highlights three of the aspects of synchronization due to brittle to ductile

transition, namely; changing drift speed, changing temperature and changing aspect ratio (D/h). The borders v_1 and v_2 were found in this study to be 0.02 m/s and 0.08 m/s respectively. On the other hand, they have been indicated to change both with an average temperature and changing ice thickness. It is known that the brittleness of ice (as most other solids) is increasing with decreasing temperature. Hence one can think that an ice sheet is more likely to fail in ductile mode for higher drift speeds when it gets warmer, simply because ice is more ductile when it is warmer. Higher drift speeds makes ice more brittle, thus ice temperature has to compensate for the increased brittleness by making it warmer and more ductile. In that way, warmer ice sheets get into IC with SS vibrations for a broader range of drift speeds than colder ice floes because the temperature compensate for the increased brittleness. Conversely, it has been observed that it tends to be lower wind speeds when the lowest temperatures are occurring. If this is true and we know that an ice sheet must have driving forces to cause both CC and IC, this might explain the few occurrences of IC for low temperatures.

Kry (1978) proposed an idea about independent zones in the waterline of a structure during ice crushing. He assumed that the width of these zones could be approximately as wide as an ice thickness. Using Kry's assumptions and further suppose that ice loads act as non-simultaneous processes in the zones denoted F_i in Fig. 8 during CC and as synchronized loads during IC, it is clear that the zones have to synchronize at some time during the transition from CC to IC. When the ice thickness increases, the number of independent zones decreases. Hence the reason why the ice sheet gets into IC for higher drift speeds when it gets thicker could be that the number of zones that have to synchronize is fewer when the ice sheet is thicker. On the other hand, the triggering of IC from CC will most probably change due to changing ice thickness as indicated in the section above. IC will be introduced by circumferential cracks when the ice sheet gets thinner and probably more due to internal fractures for thicker ice sheets.
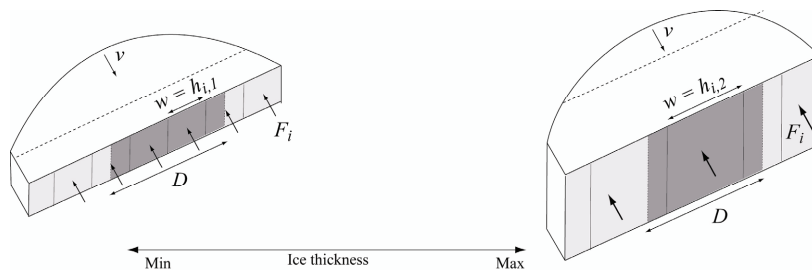

Figure 8. Two ice sheets with thickness h_1 and h_2 are drifting with speed v against a structure of width D with a decreasing number of independent failure zones F_i for increasing ice thickness. Dark shaded area indicates the contact area between the structure and the ice.

CONCLUSIONS
Analyses were conducted on 99 selected intervals of ice crushing on a vertical structure during these studies. The intervals were divided into intermittent and continuous crushing. The intermittent crushing was known to cause the harshest loading situations to the structure because of synchronized loading in the water line. The triggering of intermittent crushing was discovered to be caused by two different phenomena, which were:
- Circumferential cracking which produces a smooth ice edge with following simultaneous contact between the ice edge and the structure.
- High loads on one or two panels simultaneously without any visible changes in physical failure mode.

The next topic of the study was transition speeds between continuous crushing and intermittent crushing. The results of these studies were that:

- Continuous crushing was found for drift speeds higher than 0.1 m/s.
- Intermittent crushing was found for speeds between 0.02 m/s and 0.08 m/s.
- The upper transition speed seems to increase slightly for both increasing ice thickness and increasing temperatures.

ACKNOWLEDGEMENTS

REFERENCES

Allan, M.R. and Smith, L.A. (1996), Monte Carlo SSA: Detecting irregular oscillations in the presence of coloured noise, J. Clim. 9, pp. 3373-3404.

Fransson, L.Å. (2001), Some observations of Continuous and Intermittent Crushing Failure of Ice, Proc. of the POAC conference, Ottawa, Canada, pp. 393-402.

Gravesen, H., Sørensen, S., Vølund, P., Barker, A. and Timco, G.W. (2005), Ice loading on Danish wind turbines: Part 2. Analyses of dynamic model test results, Cold Regions Science and Technology, Vol. 41, pp. 25-27.

Haas, C. (1998), Evaluation of ship-based electromagnetic-inductive thickness measurements of summer sea-ice in the Bellingshausen and Amundsen Seas, Antarctica, Cold Regions Science and Technology Vol. 27, pp. 1-16.

Hirayama, K. (1974), An Investigation of Ice Forces on Vertical Structures, Phd-Thesis, The University of Iowa, 151 p.

Izumiyama, K., Irani, M.B. and Timco, G.W. (1994), Ice loading on a compliant indentor, Proc. of the IAHR, Ice Symposium, Trondheim, Norway, Vol 1, pp. 229-238.

Jefferies, M and Wright, W.H. (1988), Dynamic response of Molikpaq to ice-structure interaction, Proc. of the OMAE Conference, Houston, U.S.A., pp. 201–220.

Kärnä, T., Kolari, K., Jochmann, P., Evers, K.U., Xiangjun, B., Määttänen, M. and Martonen, P. (2003), Tests on dynamic ice-structure interaction, Proc. of the OMAE conference, Cancun, Mexico 7 p.

Kry, P.R. (1978), A statistical prediction of effective ice crushing stresses on wide structures, Proc. of the IAHR, Ice Symposium, Luleå, Sweden, Vol 1, pp. 33–47.

Muhonen, A., Kärnä, T, Järvinen, E. and Riska, K. (1992), Laboratory indentation tests with thick freshwater ice, Laboratory of Naval Architecture and Marine Engineering, Otaniemi, M-122. 397 p.

Määttänen, M. (1978), On conditions or the rise of self-excited ice-induced autonomous oscillations in slender marine structures, Finnish-Swedish Winter Navigation Board, Finland, Research Report 25, 98 p.

Määttänen, M. (1983), Dynamic ice-structure interaction during continuous crushing, CRREL report 83-5, 49 p.

Määttänen, M. (1987), Ten years of ice-induced vibration isolation in lighthouses. OMAE 1987, Houston, TX, USA, Vol IV, pp. 261-266.

Nordlund, O.P., Kärnä, T and Järvinen E (1988), Measurements of ice-induced vibrations of channel markers, Proc. of the IAHR, Ice Symposium, Sapporo, Japan. pp. 537–548.

Timco, G.W., Irani, M.B., Tseng, J., Liu, L.K. and Zheng, C.B. (1992), Model tests of dynamic ice loading on the Chinese JZ-20-2 jacket platform, Canadian Journal of Civil Engineering, Vol. 19, pp. 819-832.

Torrence, C. and Compo, G.P. (1998), A Practical Guide to Wavelet Analysis, Bulletin of the American Meteorological Society, Vol. 79, No.1, pp. 61-78.

Schwarz, J. and Jochmann, P. (2001), Ice Force measurements within the LOLEIF, Proc. of the POAC conference, Ottawa, Canada, pp. 669-680.

Sodhi, D.S. (1988), Ice-induced vibrations of structures, Proc. of the IAHR, Ice Symposium, Sapporo, Japan, pp. 625–657.

Sodhi, D.S. (1991), Ice – Structure Interaction During Indentation Tests, In Ice-Structure interaction (Eds. S. Jones, R.F.McKenna, J. Tillotson and I. Jordaan), St. Johns, New Foundland, pp. 619-640.

Sodhi, D.S. and Haehnel, R.B. (2003), Crushing Ice Forces on Structures, Journal of Cold Regions Engineering, Vol. 17, pp. 153–170.

Vinje, T. and Berge, T. (1989), Upward Looking Sonar Recordings at 75 N-12 W from 22 June 1987 to 20 June 1988 (Data Report Nr. 51), Norsk Polarinstitutt, Oslo, Norway.

Peyton H. (1968), Sea ice forces. Ice pressure against structures, National Research Council of Canada, Ottawa, Canada, Technical Memorandum 92, pp. 117-123.

Yue, Q. and Bi, X. (2003), Ice-induced jacket structure vibrations in Bohai sea, Cold Regions Engineering, Vol. 14, No. 2, pp. 81-92.

Chapter 8, Paper V

Ice actions from ridged ice on the Norströmsgrund lighthouse

By Morten Bjerkås and Basile Bonnemaire

(To be submitted)

Ice actions from ridged ice on the Norströmsgrund lighthouse

Morten Bjerkås[1] and Basile Bonnemaire[2]

[1] *Department of Civil and Transport Engineering, Norwegian University of Science and Technology*

[2] *Barlindhaug Consult, Tromsø, Norway*

Abstract

This paper addresses the analyses of 14 interactions between first-year ice ridges and the Norströmsgrund lighthouse in the Gulf of Bothnia, Sweden. An electromagnetic device and a laser device were used to predict the sub and top surface of the ridges, respectively. Loads from the ice ridges to the structure were recorded by load panels in the water line. The keel to sail ratio was higher than reported previously while the keel depth itself was found to decrease faster in time than reported earlier. Four failure modes were detected among which failure on a rubble wedge and splitting were dominant for deeper ridges and crushing and bending were seen for smaller ridges. The keel depth was found to have a minor influence on the magnitude of the highest ridge loads, oppositely to the thickness of the consolidated layer, which seemed to have larger influence. From examination of one single ridge interaction, a peak load was detected during transition between local crushing and global splitting of the ridge.

Keywords: First-year ice ridge, actions, full-scale, Gulf of Bothnia, gravity based structure

Corresponding author: Morten Bjerkås,

E-mail: morten.bjerkaas@ntnu.no

Fax: +47 73 59 70 21

1 Introduction

Actions from ridged sea ice are one of the major threats to the integrity of structures in ice infested waters. In general, loads on structures from ice ridges are challenging to record, hence very little information from full-scale ice actions including ridged ice exists. To contribute on the knowledge about actions from ice ridges to vertical structures, this work offers new analyses of the geometry and loads exerted by ice ridges on the Norströmsgrund lighthouse. Norströmsgrund is located in an area where drifting sea ice regularly includes a large number of drifting ice ridges with a typical cross section such as shown in Fig. 1.
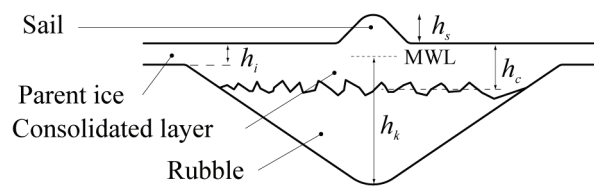

Figure 1. Typical composition of a first-year ice ridge where h_s, h_c, h_k, and h_i are the sail height, thickness of consolidated layer, keel depth and parent ice sheet thickness, respectively.

Studies on the geometry of ice ridges in general were summarized by Timco and Burden (1997). Data on the shape of ice ridges in Gulf of Bothnia were first presented by Palosuo (1975). Later, the geometry of pressure ridges in the Baltic has been reported in studies by Kankaanpää (1997), Leppäranta and Hakala (1992), Veitch et al. (1991) and Høyland et al. (2000).

Earlier investigations of full-scale ice ridge loads on structures were summarized by Timco et al. (2000). Engelbrektson (1983) has reported that several lighthouses in the Gulf of Bothnia were damaged by actions from pressure ridges while the primary sources of information about loads from ice ridges in the Gulf of Bothnia are Määttänen (1977), Hoikkanen (1984), Krankkala and Määttänen (1984) and Eranti et al. (1992).

This particular study contains analyses of selected data from measurements conducted during the joint project "Measurements on structures in ice" (STRICE) performed in the period 2001-2003. First analyses of the present data were presented by Bonnemaire and Bjerkås (2004) and Bjerkås and Bonnemaire (2004). Topics that are of concern in the present study are the geometry of ice ridges with its evolution in time in addition to failure modes of ridges occurring during interactions with a vertical structure. Attention was paid to the recorded loads from selected ridges with special emphasis on contributions from consolidated and unconsolidated ice in the ridge keel. Ice load data from the STRICE project are still confidential, hence normalised load values of loads are presented.

2 Methods

2.1 General

Norströmsgrund lighthouse is located 60 km southeast of Luleå (Fig. 2), in an area with active drift of sea ice during an average time span from December to late April (FMIR, 2005).
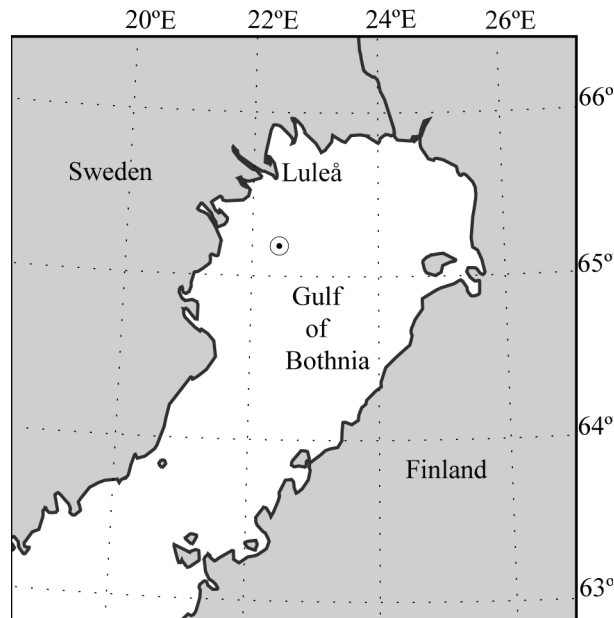

Figure 2. Map of the Gulf of Bothnia with location of Norströmsgrund lighthouse (⊙).

The Norströmsgrund lighthouse is a 42.5 m high gravity based concrete structure that has a surface piercing breadth of 7.6 m (including load panels). The structure is founded on an underwater caisson that is 23 m in diameter, resting on dense moraine masses. The experimental setup at Norströmsgrund is shown in Fig. 3a, while the coverage of video cameras situated 17 m above mean water line (MWL) is shown in Fig. 3b. A downward looking laser (DLL), electromagnetic device (EM) and upward looking sonar (ULS) devices were installed to profile the ice features that interacted with the lighthouse. However, the ULS device was damaged by ice interaction and worked properly only during the measurements in 2000 and a few days in 2001.
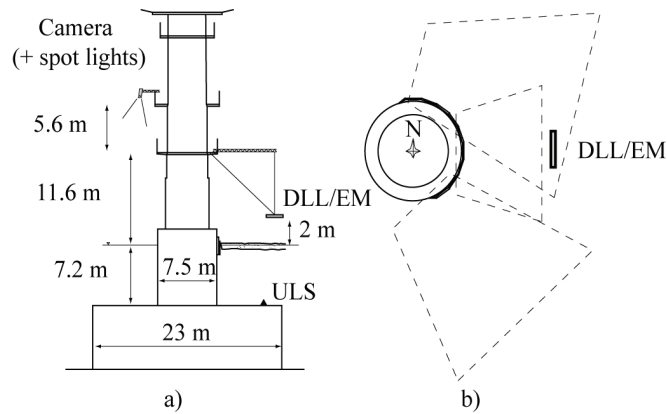
Figure 3. Experimental setup at Norströmsgrund lighthouse (1999-2003) with downward looking laser (DLL), electromagnetic (EM) induction device located approximately 10 m from the lighthouse, b) Footprint of the cameras recording the ice-structure interaction zone.

Nine load panels were installed in the water line, which were organized from north to south via east, covering altogether 167° of the surface piercing perimeter as indicated in Fig. 4. The size of the load panels was 1.2 m × 1.5 m, and one panel facing straight towards east was segmented into a matrix of eight segments 0.4 m × 0.5 m. The top of the panels were aimed to be located in the MWL.
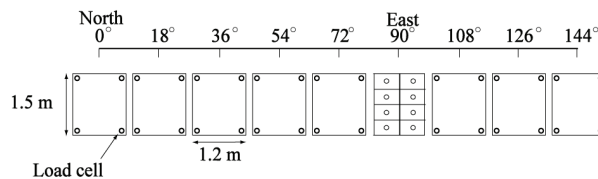

Figure 4. Ice load panel arrangement on the Norströmsgrund lighthouse, winter 2002.

2.2 Ridge geometry prediction

Three different geometrical quantities were studied, keel depth, sail height and a thickness of the consolidated layer. The profiling of the ice features interacting with the structure was limited to 2D recording with dimensions time and magnitude. As an ice ridge is a 3D body drifting in the sea, any of the three parameters mentioned are challenging to predict using 2D signals only. However, time series (see example of DLL, EM and ULS profiling in Fig. 5) are in this work assumed to give a representative characterization of an ice ridge.
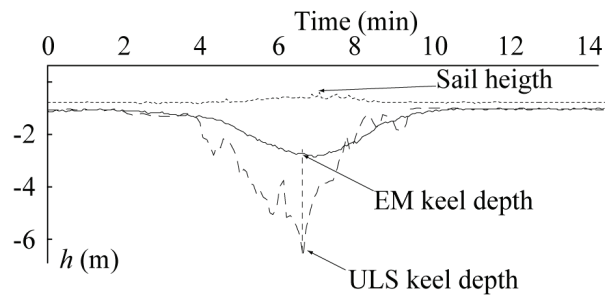
Figure 5. Example of an ice ridge passage with the cross-section profiled by DLL (Top surface), EM and ULS (Sub surface). The significant difference between the sub surfaces predicted by EM and ULS devices should be noted.

The sail height was predicted by DLL and chosen as the maximum height in the unfiltered DLL raw data during each of the ridge interactions (for example see Fig. 5). The subsurface of the ice features were estimated simultaneously by EM and ULS during a period of 6 days in 2001. However, during the interval 3 March to 4 April 2002 (period of the present ice ridge observations), measurements were conducted by the EM device only. As shown in Fig. 5 as well as in previous studies by Haas (1999), EM measurements seem to under predict keel depths of first-year ice ridges. The profile provided by ULS was assumed to give the most realistic keel depth available, hence ten ridges with simultaneously measured keels by ULS and EM were collected from the period 3 March to 9 March 2001 (not among the 14 mentioned above). The maximum keel depths were measured from the sub-surface profile by ULS and the corresponding EM signal as indicated in Fig. 5. Regression analyses were conducted on the ten ridge keel depths to determine a factor that could transform keel depths measured by EM to realistic keel depths (Fig. 6). The best linear fit was found by multiplying the EM keel depth with 3.16 to obtain a value that was as close as possible to the keel depths measured by ULS. However, it should be recalled that the scatter is notable and it is highly recommended to conduct more research on the transformation of keel depths measured by EM to realistic keel depths. When keel depths are denoted h_k later in this work, it means the keel depth recorded by EM multiplied with 3.16.
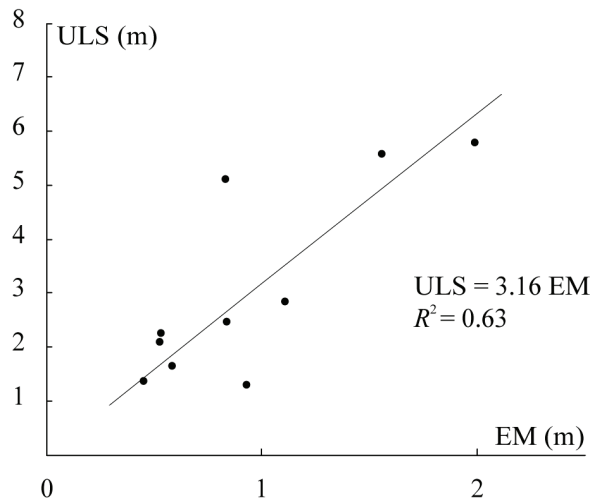
Figure 6. Ten ridge keels measured by ULS and EM during the period
3 March to 9 March 2001 with a linear regression line.

The thickness of the consolidated layer was predicted using the segmented load panel shown in Fig. 4. A situation with crushing failure of a level ice sheet that covered one row of segments was selected as a benchmark situation. Then during a ridge interaction, the consolidated layer was assumed to cover a segment if the highest loads on this segment reached 20 % of the highest load measured during the benchmark test. Even tough the failure mode differs between level ice floes and ice ridges, this procedure should be regarded as a first try to determine the amount of consolidated ice in an ice ridge from load time records on a segmented panel. The sensitivity of the 20 % limit needs further research, hence refinements might present more realistic results than presented herein. Fig. 7 shows three examples of how the consolidated layer has been predicted with the benchmark situation and the 20 % limit. Fig. 7a-c shows examples on how the segment loads F_S are applied to predict the thickness h_c for different water stages where Fig. 7d shows the benchmark situation.
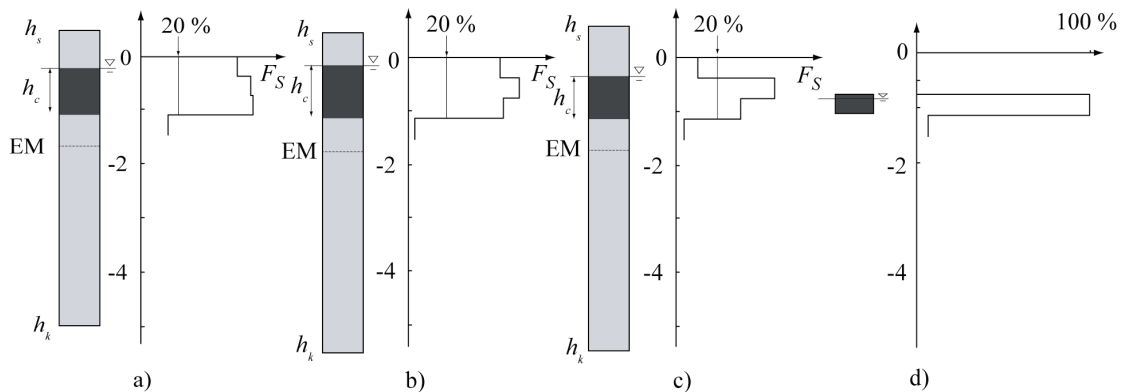

Figure 7. Ice loads from three ridges on a segmented panel (a - c) and from a level ice sheet (d); h_s, EM and h_k mean the sail height, EM measured keel depth and the scaled keel depth respectively.

3 Results

3.1 General

This work contains interpretations and analyses of data from 14 interactions between first-year ice ridges and the Norströmsgrund lighthouse during the period 3 March to 4 April 2002. All ridges in the study had a defined sail and keel, consisting of ice rubble and with a maximum keel depth limited to 7.2 m by the underwater caisson (see Fig. 3). Table 1 lists in its first column the event-names that contain the date and the time of occurrence following the format "day month_hour minute". Then the sail height and the keel depth are listed together with the thickness of the consolidated layer (h_c) and the parent ice sheet (h_i). In the cases where values of h_c are missing, the ice was drifting from a direction that did not caused loads on the segmented panel. The ice ridge load F_R and the load from the parent ice sheet F_{pi} follow in column six and seven, and the drift speed and the occurrence of snow on the parent ice sheet are listed in column eight and nine. Information about the parent ice sheet and the occurrence of snow is provided for further analyses and will not be mentioned further.

Table 1. Key information about interactions between 14 first-year ice ridges and the Norströmsgrund lighthouse between 3 March and 4 April, 2002. F_R and F_{pi} means the highest loads measured from the ridge and the parent ice sheet, respectively. Both loads are divided on a load F_{norm}. (RW = failure on a rubble wedge, B = bending failure, S = splitting, C = crushing)

Event no.	h_s (m)	h_k (m)	h_c (m)	h_i (m)	F_R /F_{norm}	F_{pi} /F_{norm}	v (m/s)	Failure mode	Snow
0303_0904	0.8	6.9	-	0.4	0.25	0.08	0.08	RW	Yes
0403_0053	1.0	6.0	0.4	0.3	0.25	0.12	0.09	B	Yes
0403_0320	0.9	6.7	0.8	0.8	0.22	0.11	0.09	RW	Yes
1903_2023	0.7	5.1	1.1	0.6	0.53	0.33	0.03	B	Yes
2003_0150	0.8	6.0	0.8	0.6	0.38	0.23	0.10	B	Yes
2103_1225	0.6	6.0	1.1	0.8	0.58	0.43	0.07	C	No
2103_1400	0.6	6.8	1.1	0.7	0.38	0.16	0.11	RW	No
2103_1450	0.5	5.5	1.5	0.4	0.45	0.19	0.11	C	No
2103_1530	1.0	7.0	0.8	0.6	0.29	0.28	0.11	S	No
3103_1450	0.3	3.5	0.4	0.4	0.23	0.14	0.05	C	No
0204_1015	0.6	5.5	0.8	0.2	0.35	0.05	0.10	C	No
0304_0045	0.7	6.0	-	0.6	0.34	0.19	0.12	B	No
0304_1730	0.5	6.1	1.1	0.3	0.75	0.14	0.05	C	No
0404_0530	0.4	4.9	0.4	0.4	0.29	0.11	0.05	B	No

3.2 Geometry of ice ridges

Two aspects of the geometry of the studied ridges are reported here; first the keel-to-sail ratio and secondly the average evolution of keel depths with respect to time. Fig. 8 shows the keel versus sail height including a linear trend line which follows the relation $h_k = 8.2\ h_s$. Two other trend lines from

ridge surveys are displayed in Fig. 8 as $h_k = 6.3\ h_s$ (from Kankaanpää, 1997) and $h_k = 4.5\ h_s$ from Timco and Burden (1997).
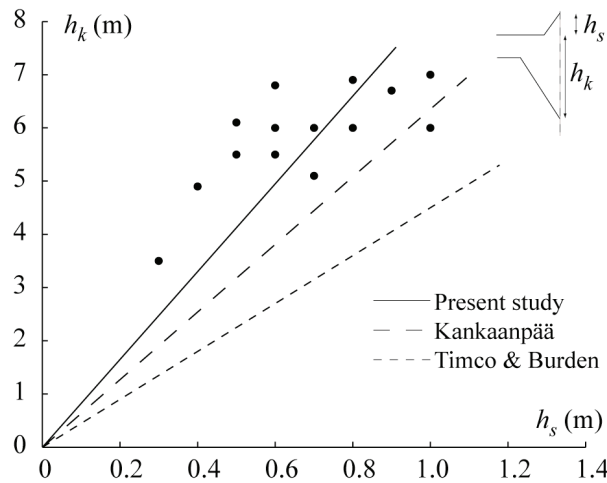

Figure 8. Keel vs. sail height for 14 ridges interacting with the

Norströmsgrund lighthouse 3 March to 4 April, 2002.

The trend of keel depths with respect to time is illustrated in Fig. 9. A linear trend line is fitted to the data, which has a negative slope of 0.04 m/day in the current period. Additionally, the ridge incidents during the period 3 March to 4 April were concentrated in three intervals, first three ridges were selected early in March, then six ridges in late March and at last five ridges in early April.
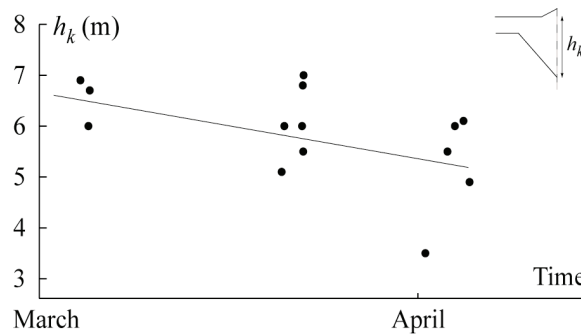

Figure 9. Keel depth of 14 ridges with respect to time in the period

3 March to 4 April 2002.

3.3 Failure modes during ridge-structure interactions

Failure modes of first-year ice ridges were investigated by studies of video films showing the ice-structure interaction zone. The failure modes were thus determined based on those visual studies. Fig. 10 shows a typical scenario with an ice ridge failing on a rubble wedge, a failure mode that occurred among three of the 14 selected ridges. The rubble wedge established in those cases when debris could not be cleared sufficiently fast from the upstream side of the lighthouse. The current failure mode occurred for keel depths deeper than 6.3 m and drift speeds between 0.08 m/s and 0.12 m/s.

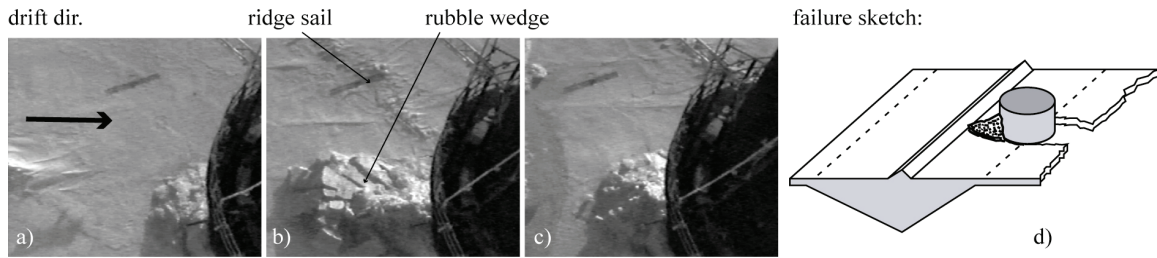drift dir.   ridge sail   rubble wedge   failure sketch:

Figure 10. Ice-ridge failure on a floating rubble wedge to the lighthouse Norströmsgrund occurring 09:15, 3 March 2002, a-c) picture sequence, d) principle sketch.

Fig. 11 shows bending failure of a ridge, a failure mode that occurred in five of the 14 selected incidents. Bending failure was frequently combined with other failure modes where the typical scenario was for example that initial crushing failure produced rubble that accumulated on the top surface of the ice (Fig. 11) while after some time of accumulation, the ice sheet bended downward. Bending failure occurred with keel depths from 4.9 m to 6.0 m while drift speeds ranged from 0.03 m/s to 0.12 m/s.

drift dir.   ridge sail   bending crack   failure sketch:
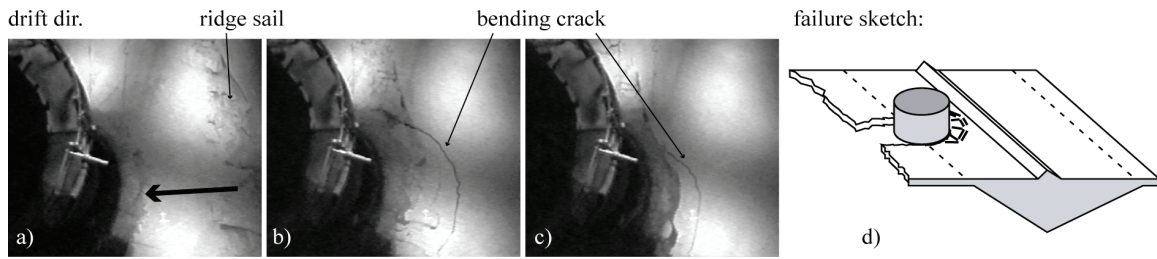
Figure 11. Ice ridge bending failure to Norströmsgrund lighthouse occurring 00:55, 4 March 2002, a-c) picture sequence, d) principle sketch.

The crushing failure mode is illustrated by Fig. 12, a failure mode that appeared in four of the 14 selected ice ridge-structure interactions, frequently combined with the other failures modes. Crushing failure occurred for keel depths from 3.5 m down to 6.1 m and for drift speeds from 0.05 m/s to 0.11 m/s and was only appearing in cases where the debris could be transported quickly from the ice-structure interaction zone.

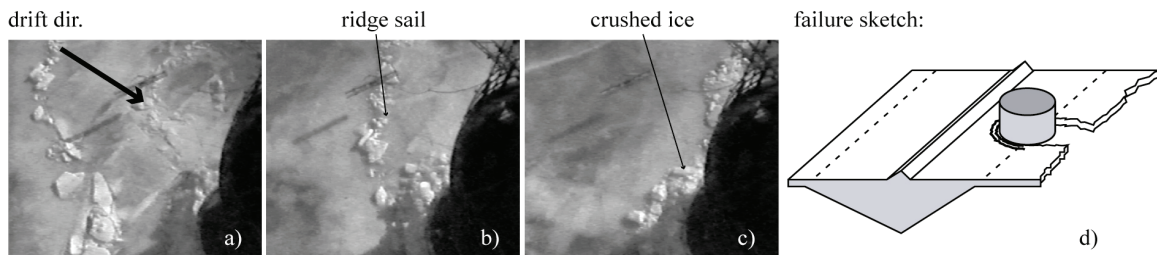drift dir.   ridge sail   crushed ice   failure sketch:

Figure 12. Crushing of an ice ridge to Norströmsgrund lighthouse 12:10, 31 March 2002, a-c) picture sequence, d) principle sketch.

Splitting failure occurred only once among the 14 ridges as shown in Fig. 13. The drift speed during this incident was 0.11 m/s and the keel depth was 7.0 m.
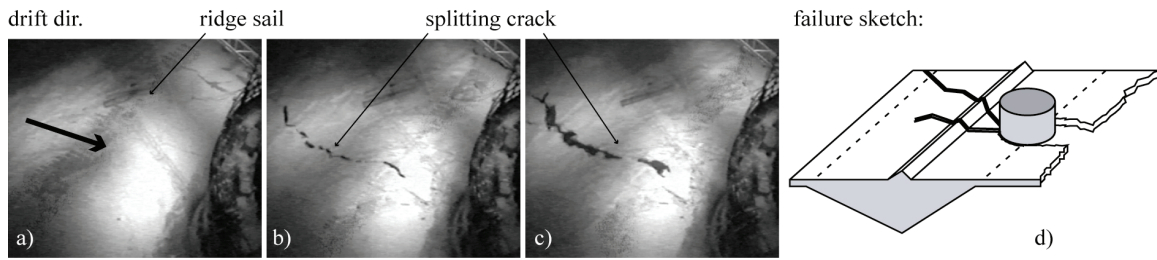
Figure 13. Ice-ridge with splitting failure to the lighthouse Norströmsgrund 18:50, 27 February 2002, a-c) picture sequence, d) principle sketch.

To summarize the observed failure modes with respect to keel depths and drift speeds, Fig. 14 shows a map where failure modes are displayed with symbols. The failure mode map illustrates that ridge failure on a rubble wedge are frequent for keels deeper than 6.3 m. Bending failure occurs for keel depths between 4.9 m and 6.0 m and crushing failure is observed for keel depths from 3.5 m to 6.1 m. Global splitting of an ice ridge occurred for a keel depth of 7.0 m.
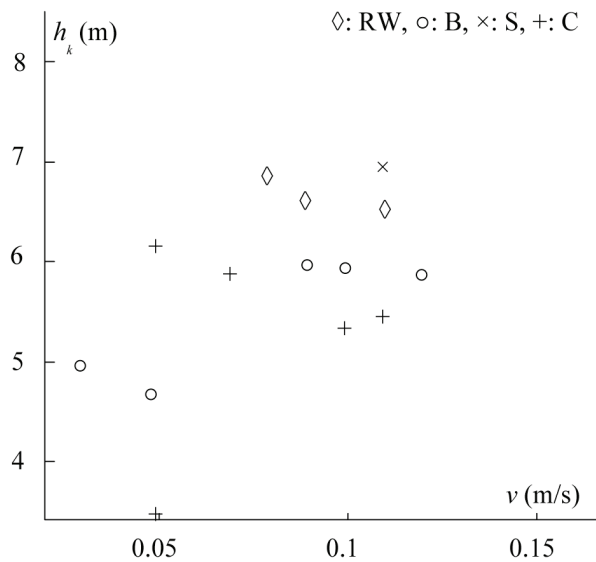

Figure 14. Observed failure mode from video records with respect to keel depth and drift speed.

3.4 Loads from pressure ridges to a vertical structure

This section presents measured loads caused by the ice ridges with respect to the ridge geometry and failure mode during these ice actions. Fig. 15 displays the measured loads from the selected ridges as a function of keel depth. Although a load panel covers only 1.5 meter of the keel depth and the data scatters considerably, the regression line reads

$$F_R = 0.003h_k + K \qquad (1)$$

where K is a constant that will be presented when all data are public. Eq. (1) indicates a minor influence of the keel depth on the highest measured loads from ridges.
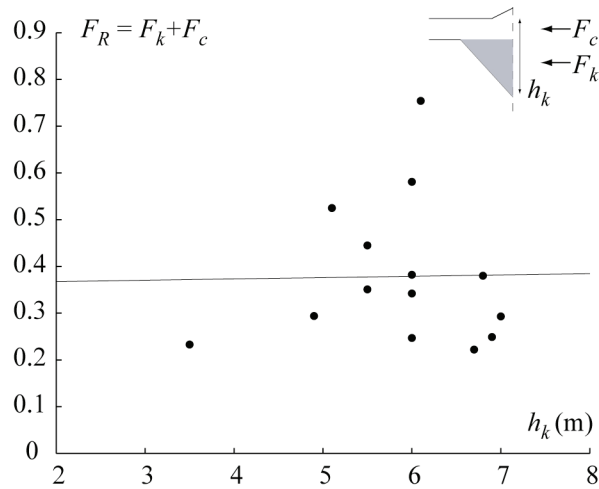
150

Figure 15. The highest ridge normalised ridge loads versus keel depth from 14 ridge interactions with Norströmsgrund lighthouse.

Further investigations were conducted to reveal more details about the influence of the keel depth on the ridge loads. Two failure modes were selected, first an event with failure on a rubble wedge and secondly an event with continuous crushing. Then, time records from the segmented panel were displayed as shown in Fig. 16 where Fig. 16a shows that during ridge failure on a rubble wedge, the most significant loads are transmitted to the structure through the uppermost segments in an area close to MWL. The magnitude of loads acting on segments deeper than 0.5 m below MWL is less than 10 % of the loads acting on the upper segments during failure on the rubble wedge. On the other hand, during continuous crushing, loads that are more significant can be seen deeper in the keel as displayed in Fig. 16b. However, the spikes seems to last shorter in time deeper down in the keel during this failure mode.
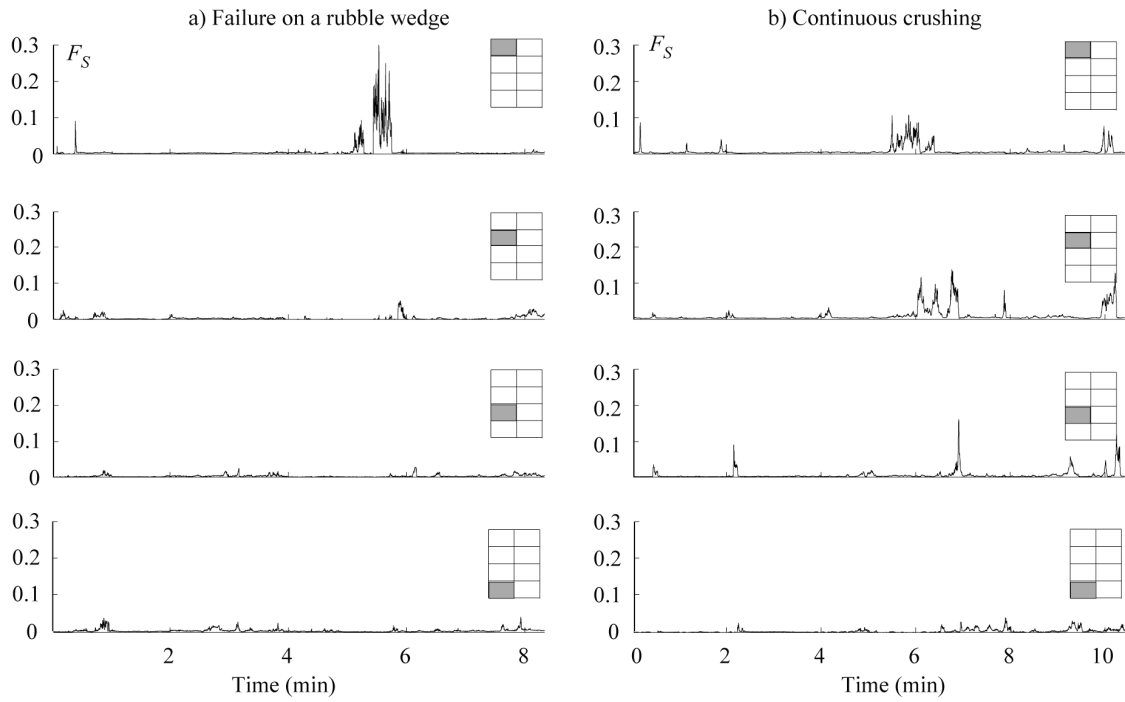
Figure 16. Vertical distribution of loads from a ridge keel during two interactions with equal water level, a) ridge failure on a rubble wedge and b) Continuous crushing.

To investigate an influence of the consolidated layer in ridges, loads were displayed as a function of consolidated layer thickness as shown in Fig. 17. Even though the data in Fig. 17 scatters, the line

$$F_R = 0.310 h_c + C \tag{2}$$

where C is a constant that will be revealed when all data are public. Eq. (2) describes the trend of increasing ridge load with an increasing thickness of the consolidated layer.
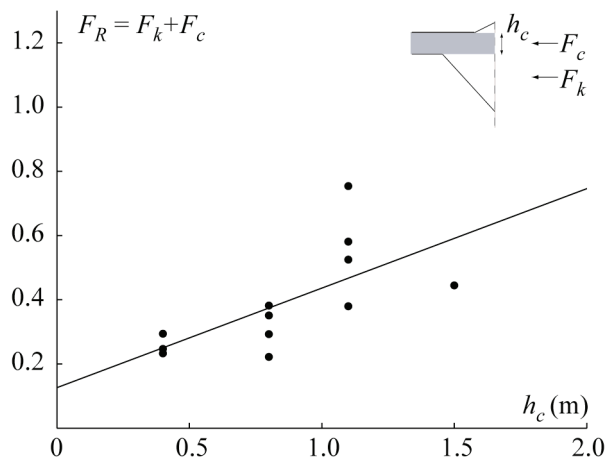

Figure 17. Maximum panel load as a function the amount of consolidated ice.

Time series from one event (not among the 14 mentioned above) are examined more thoroughly to reveal details about the ridge-structure interaction scenario. Fig. 18a shows the summation of loads

152

measured by the ice load panels (Fig. 4) and Fig. 18b displays the measured profile of the ridge along the same time axis. The sequence is the following:

①: Level ice is crushing against the structure and the forces are relatively low and of a stochastic nature.

②: The consolidated layer of the ridge fails in crushing while the load presents a saw tooth profile. α: The load in the interaction zone reaches a maximum and the force necessary to develop splitting failure is reached; there is a change in failure mode.

③: The fragments from the splitting failure cannot be evacuated and a wedge builds up in front of the structure. The incoming ice fails on the wedge where the load level on the structure is low. The rubble wedge usually builds up to a maximum length approximately two times the diameter of the lighthouse. The wedge length varies in time while it usually increases until some collapse appears within the wedge that causes its partial reduction. β: The wedge builds up in height and ice accumulates on the lighthouse balcony. The increase in keel depth after the 15 second instant might very well be interference of the rubble wedge under the EM device. γ: Some higher forces are recorded on a panel almost perpendicular to the drift direction, the incoming ice at that point did not meet the wedge and fails directly on the structure.

④: The wedge collapses under the pressure of the incoming ice and the fragments can be cleared around the structure, the ridge event is almost finished. δ: The virgin level ice impacts the structure. ①: Level ice crushing with some local bending failure restarts.
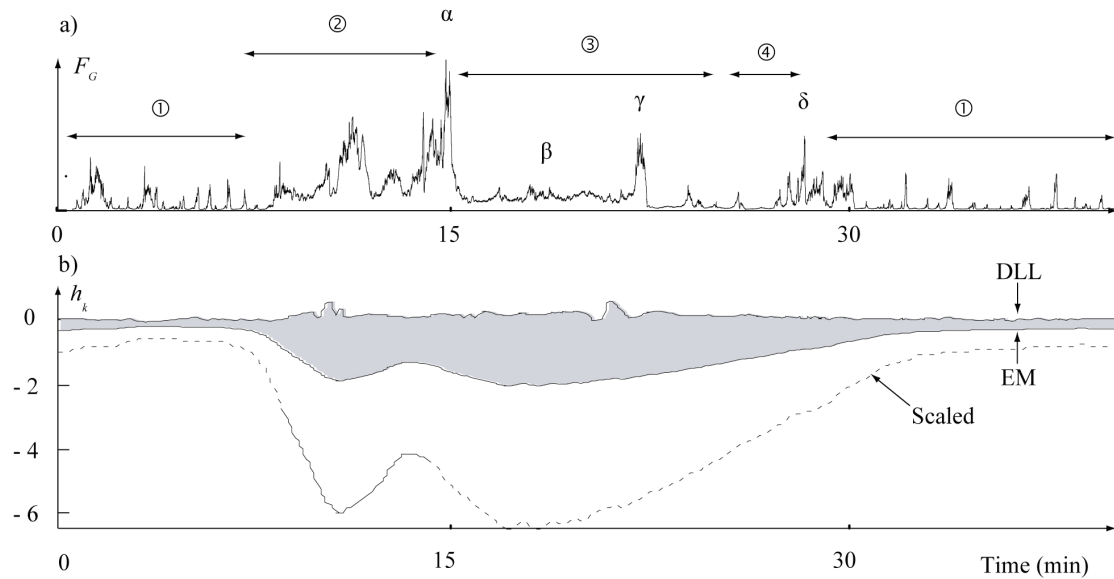
Figure 18. Ridge loading event start 11:00, 2 April 2002 at the lighthouse Norströmsgrund, $h_i = 0.4$ m, $h_s = 0.7$ m, $h_k = 6.0$ m, $v = 0.1$ m/s (event 0204_1100), a) the total load versus time with failure mode intervals indicated, b) top surface and sub surface measured by DLL and EM, respectively. The corresponding scaled subsurface profile indicated below the EM.

4 Summary and discussions

4.1 Geometry of ridges

The present study shows a survey of 14 interactions between first-year ice ridges and the Norströmsgrund lighthouse. Concerning the geometry of ridges, the ratios between the ridge sail height and ridge keel depth were found to be 8.2 (Fig. 8), which is higher than presented in earlier studies on Arctic ridges (Timco and Burden, 1997) and Baltic ridges (Kankaanpää, 1997). The reason for the higher keel to sail ratios on temperate Baltic ridges compared to Arctic ridges might be more melting of the sail in the temperate regions. Another effect might be higher temperatures and more moderate temperature gradients, which might cause higher porosity of ridges and larger buoyancy of the keel. The slightly higher keel to sail ratios in the present study than reported by Kankaanpää (1997) might be addressed by the different keel depth prediction procedures used in the two studies.

The trend of decreasing ridge keel depths was found to be in average 0.04 m/day in the current study (Fig. 9). Leppäranta et al. (1995) reported on the life story of a single first year ice ridge in the land fast ice offshore Oulo in Finland where they investigated that the keel depth decreased 0.03 m/day. Even though the situations in the study by Leppäranta et al. (1995) and the present are different, comparable decreasing rates were found. The higher rate investigated in the current study might be caused by mechanical erosion of the ridge keels during ice drift, an effect which is not present on a ridge in land fast ice.

4.2 Loads and failure modes of ridges

Four different failure modes were detected among the selected ridges. Failure on a rubble wedge occurred for ridges with the deepest keels, which were between six and seven meter in depth (Fig. 14). Bending and crushing failure were about evenly frequent for more shallow keels between 3.5 m and 6.5 m. The presence of a rubble wedge during failure of deeper ridges might occur because the amount of rubble in the keel is larger in deeper ridges and hence needs more energy to be removed from the upstream side of the structure during failure. It was not detected any clear trend with respect to the failure mode and drift speed.

The highest ridge load as defined in this study seemed to be very little influenced by the keel depth (Fig. 15). This is an effect also recently detected by Lemme and Brown (2005) from ridge actions on the Confederation Bridge in Canada. However, one should recall that their studies were conducted on records from a structure that had a complex geometry in the water line, while the present study shows data from interactions with a vertical structure. The weak influence on the current ridge load from the increasing keel depth might be elucidated in two ways. First, unconsolidated ice rubble is a material which has relatively low resistance against horizontal penetration compared to consolidated ice in ridges. Second and maybe most important, the load panels are covering only the uppermost 1.5 meter of the ridge keel independent of depth, hence loads from the increasing part of the keel depth are not covered by any panel. On the other hand, comparisons of time series recorded during failure of a ridge on a rubble wedge and continuous crushing, respectively, showed that loads deeper in the ridge keel tended to be higher during continuous crushing than during failure on a rubble wedge, an effect that could be addressed to shading of loads from the floating rubble wedge.

A trend of increasing ridge loads with increasing thickness of the consolidated layer was detected (Fig. 15). A similar effect was proposed from analyses of loads on the Molikpaq, where ice loads seemed to increase with increasing thickness of level ice (Timco and Johnston, 2004). On the other hand, how the horizontal resistance of the consolidated layer in ridges differs from that of level ice is unclear and must be studied more before conclusions can be drawn.

From a specific study of the interaction between one of the 14 ridges and the vertical lighthouse it was detected that the highest ridge load occurred just before splitting of the ridge and in the end of an interval with crushing of the consolidated layer (Fig. 18). Other episodes that seemed to cause high loads were when ice floes were crushing directly to the structure just after an accumulated amount rubble had cleared.

5 Conclusions

From the present survey, which has revealed details about 14 ice ridges interactions with the Norströmsgrund lighthouse, the following conclusions can be drawn:

1. The keel to sail height ratio was measured to be 8.2, which is higher than two other comparable surveys

2. The ridge keels seems to decrease with 0.04 m/day, which is faster than shown in an earlier study

3. Four failure modes were detected where ridges with keels deeper than 6.3 m failed either on a rubble wedge or by splitting while ridges with keels in the range 3.5 m to 6.1 m failed in bending or crushing

4. The keel depth of ridges was found to have a minor influence on the peak ridge loads, however, loads from deeper parts in the ridge keel were more significant during crushing failure than during failure on a rubble wedge

5. Ridge loads were found to increase with increasing thickness of the consolidated layer

6. The highest ice ridge loads to a structure might occur in the final stage of the failure of the consolidated layer

References

Bjerkås, M. and Bonnemaire, B. (2004), Ice ridge-structure interaction, part II: loads from ice ridges and their surrounding ice sheets, Proceedings of the International Association of Hydraulic Engineering and Research (IAHR), Ice Symposium, Saint Petersburg, Russia, pp. 122-129.

Bonnemaire, B. and Bjerkås, M. (2004), Ice ridge-structure interaction, part I: geometry and failure modes of ice ridges, Proceedings of the International Association of Hydraulic Engineering and Research (IAHR), Ice Symposium, Saint Petersburg, Russia, pp. 114-121.

Dolgopolov, Y.V., Afanasiev, V.A., Korenkov, V.A. and Panfilov, D.F. (1975), Effect of Hummocked Ice on Piers of Marine Hydraulic Structures, Proceedings of the International Association of Hydraulic Engineering and Research (IAHR), Ice Symposium, Hanover, New Hampshire, USA, pp. 469-478.

Eranti, E., Lehmus, E. and Nortala-Hoikkanen, A. (1992), First-Year Ice Ridge Characteristics and Loads on Offshore Structures. Proceedings of the International Offshore and Polar Engineering Conference (ISOPE), San Francisco, USA, Vol. II, pp. 681-687.

Engelbrektson A. (1983), Observations on a Resonance Vibrating Lighthouse Structure in Moving Ice. Proceedings of the International conference on Port and Ocean Engineering under Arctic conditions (POAC), Helsinki, Finland, Vol II, pp. 855-864.

FMIR (2005), Finnish Maritime Administration, http://www.fma.fi.

Haas, C. (1998), Evaluation of ship-based electromagnetic-inductive thickness measurements of summer sea-ice in the Bellingshausen and Amundsen Seas, Antarctica, Cold Regions Science and Technology, Vol. 27, pp. 1-16.

Haas, C. and Jochmann, P. (2003), Continuous EM and ULS Thickness profiling in support of ice force measurements, Proceedings of the International conference on Port and Ocean Engineering under Arctic conditions (POAC'03), Trondheim, Norway, pp. 849-856.

Lemee, E. and Brown, T. (2005), Review of ridge failure against the confederation bridge, Cold Regions Science and Technology, Vol. 42, pp. 1-15.

Leppäranta, M. and Hakala, R. (1992), The structure and strength of first-year ice ridges in the Baltic Sea, Cold Regions Science and Technology, Vol 20, pp. 295-311.

Leppäranta, M., Lensu, M., Kosloff, P., and Veitch, B., (1995), The life story of a first-year sea ice ridge. Cold Regions Science and Technology, Vol. 23, pp. 279-290.

Määttänen, M. (1977), Ice-force measurements at the Gulf of Bothnia by the instrumented Kemi I Lighthouse, Proc. International conf. on port and ocean eng. under arctic cond. (POAC), St. Johns, Canada, Vol. 2, pp. 730-740.

Hoikkanen, J. (1984), Measurements and analysis of ice pressure against a structure in level ice and in pressure ridges. IAHR'84, Hamburg, Germany, pp. 151-160.

Høyland, K.V. (2000), Measurements and simulations of consolidation in first-year sea ice ridges, and some aspects of mechanical behaviour, Phd. Thesis, NTNU, Trondheim, Norway, 151 p.

Kaankanpää, P. (1997), Distribution, morphology and structure of sea ice pressure Ridges in the Baltic Sea, Fennia 175:2, pp. 139-240.

Krankkala, T. and Määttänen, M. (1984), Methods for determining the forces due to first and multi-year ridges, Proceedings of the International Association of Hydraulic Engineering and Research (IAHR), Hamburg, Germany, pp. 263-280.

Palosuo, E. (1975), Formation and structure of ice ridges in the Baltic, Winter Navigation Research Board, Rep. No. 12, Board of Navigation, Helsinki.

Timco, G.W. and Burden, R.P. (1997), An analysis of the shape of sea ice ridges. Cold Regions Science and Technology, Vol 25: pp. 65-77.

Timco, G.W., Croasdale, K. and Wright, B. (2000), An overview first year sea ice ridges. Technical report, PERD/CHC Report 5-112.

Timco, G.W. and Johnston, M. (2004), Ice loads on the caisson structures in the Canadian Beafort Sea, Cold regions Science and Technology, Vol. 38, pp. 185-209.

Veitch, B., Lensu, M., Riska, K. Kosloff, P, Keiley, P. and Kujala, P. (1991), Field observations of ridges in the Northern Baltic Sea, Proceedings of the International conference on Port and Ocean Engineering under Arctic conditions (POAC), St. Johns, Canada, pp. 381-400.

Chapter 9, Paper VI

Mechanical properties of ice ridges and level ice, in-situ and laboratory testing

By Knut V. Høyland, Morten Bjerkås and Sergey Vernyayev

Proceedings of 17th International Symposium on Ice, International Association of Hydraulic Engineering and Research (IAHR), St. Petersburg, Russian Federation

June 2004, Vol. 1, pp. 69-75.

MECHANICAL PROPERTIES OF ICE RIDGES AND LEVEL ICE, IN-SITU AND LABORATORY TESTING 2003

Knut V. Høyland[1],

Morten Bjerkås[2] and Sergey Vernyayev[1],[3]

ABSTRACT

Ice has been sampled from first-year sea ice ridges and level ice both in the Van Mijen fjord in Svalbard and in the North-western Barents Sea. In-situ drop ball test and unconfined compression tests in the laboratory were conducted on horizontal and vertical samples of ice from the consolidated layer, the rubble and the level ice. The salinity, density and the ice texture was also examined. The average unconfined strength for vertical samples was 6.0 MPa for the level ice, 5.0 MPa for the consolidated layer and 3.3 MPa for the rubble. The hardness was clearly dependent on the temperature, and it varied from 11 to 37 MPa and $H_i \approx H_c > H_r$.

INTRODUCTION

Sea ice ridges are formed by compression or shear in the ice cover. In many Arctic and sub-Arctic areas ice ridges give the design forces for marine structures. However, the forces and deformations mechanisms involved in an ice ridge-structure interaction are not clear. When estimating the forces from first-year ridges on structures one needs the thick-

---

[1]The University Centre in Svalbard, Norway

[2]Norwegian University of Science and Technology, Trondheim, Norway

[3]St.Peterburg State Polytechnical University

ness of the consolidated layer (h_c) and some mechanical properties as input (Blanchet, 1998). Mechanical properties of first-year ice ridges are not well known. The consolidated layer is often assumed to behave similar to level ice, that is crush against a vertical structure and flexure against an inclined structure. Small scale samples from the consolidated layer has been tested by Frederking and Wright (1982), Høyland et al. (2000, 2002), Høyland et al. (2003) and by Veitch et al. (1991), see Høyland et al. (2003) for a summary of the results. The strength of individual blocks of rubble may of importance when modelling the mechanical behaviour of rubble (Liferov and Høyland, 2004) but is difficult to test and poorly known.

SITE AND EXPERIMENTAL SET-UP

Ice was sampled from two artificially produced ice ridges and the surrounding level ice in the Van Mijen fjord between February and April 2003 (Liferov and Høyland, 2004), and from one ice ridge and the neighbouring level ice in the Barents Sea close to Hopen (N76°16' E23°07') in May 2003. Dynamic hardness tests were performed in-situ and ice was sampled and uniaxial compression strength, salinity, density and ice texture were examined in the cold lab at UNIS. The hardness tests were performed on vertical and horizontal surfaces as described in Bonnemaire et al. (2003) and Vatne (2003). The vertical samples were cored directly with a core drill that gives ice cores with a diameter of 70 mm, but the horizontal ones were first cored with a large core drill and then recored with the small core. All the samples for unconfined compression tests then became cylindrical, with dimensions of about 175 mm and 70 mm and they were compressed with a constant speed corresponding to a nominal strain rate of $\dot{\varepsilon} = 10^{-3}\text{s}^{-1}$, see Sinha (1981) for a discussion on real and nominal strain rates. The capacity of the compression machine is 100 kN and the ice temperature was between -15°C and -20°C for all tests except when warm ice was tested (T≈-2 and -5°C). The ice for these tests were was also kept in the freezer at UNIS and carefully heated before testing. The temperature of each sample was measured directly after each test.

RESULTS AND DISCUSSION

Main results

Table 1 sums up all the main results. The unconfined compressive strength is given as

$$\sigma = F_{max}/A_0$$

Table 1: Summary of results

	Barents Sea							Van Mijen fjord			
	Level ice		Cons. 1		Rubble		Sail	Level ice		Cons. 1	
	Vert	Hor	Vert	Hor	Vert	Hor	Vert	Vert	Hor	Vert	Hor
Unconfined compressive strength (MPa), T=(-15°C -20°C)											
σ_{av}	6.0	3.4	5.0	2.4	3.3	3.8	4.0	5.9	4.3	4.4	-
st. dev	1.5	0.9	1.6	1.0	1.3	1.4	1.7	2.8	1.3	0.9	-
n	7	8	40	22	25	7	11	83	25	12	-
Salinity (ppt)											
S_{av}	4.6	3.9	4.7	3.9	3.9	2.9	2.14	5.3	4.5	3.6	
st. dev	1.5	0.9	1.4	1.1	0.9	0.5	0.6	1.2	1.1	0.4	
n	7	8	40	22	25	7	11	83	25	12	
Density (kg/m^3)											
ρ_{av}	883			928			964	1002		-	
st. dev	49			31			74	53		-	
n	9			29			3	4		-	

Properties of the warm Van Mijen level ice, vertical cores

$\sigma_{av}/\sigma_{st.\ dev}$ (MPa)	$S_{av}/S_{st.\ dev}$ (ppt)	$T_{av}/T_{st.\ dev}/T_{range}$ (°C)	n (-)
6.2/3.4	4.6/1.6	-5.1/0.7/(-4.2, -6.4)	10
3.4/1.7	4.3/1.3	-2.0/0.2/(-1.6, -2.5)	11

The samples from the ridge were in general a bit weaker than the ones from the level ice. Firstly, the level ice was basically sampled from colder ice (earlier in the season) than the ridges, so the ridged ice may have been more porous. But no relevant differences can be found in the salinity and the density measurements. secondly, it may be that cracks and

other defects are introduced in the ice during the ridging process making the ridged ice weaker than the level ice. and thirdly, most of our level ice samples were from the landfast ice in the Van Mijen fjord, whereas most of our ridge samples were from the drift ice in the Barents Sea and this may also have contributed to the differences.

It also is seen that the strength of the horizontal samples was less than that of the vertical ones. This has also been found by Frederking and Timco (1989) for level ice and by Frederking and Wright (1982) for ridges. They both found $\sigma^{vert} \approx 3 \cdot \sigma^{hor}$, but did their tests with lower velocity. The difference for the level ice can be explained by the anisotropic nature of S2 (or S3) sea ice, but this should not apply for ridges. The lower strength of the horizontal samples may in our case be related to the sampling technique as cracks may have been created in the cold ice by the large core drill. The salinity of the horizontal samples was less than that of the vertical ones and this may also be due to the sampling technique. On the other hand there may be real effects related to the orientation of the brine channels, as these are more prone to be vertical than horizontal.

Fig 1 shows the average salinity and strength of vertical samples to the depth for ice from the Barents Sea. As can be seen the strength varies with depth. The upper part was weak, probably because the melting season had begun and the top ice was warm and porous. The consolidated layer was stronger than the ice from the rubble even if the testing was done in laboratory with the same ice temperature. So the rubble ice must have been more porous than the consolidated layer. This was also found by Høyland et al. (2000) with ice from the Gulf of Bothnia. There is a larger difference on the in-situ strength, but the authors are not aware of any published results of small scale in-situ tests of rubble strength. Warm sea ice is weaker because the temperature itself affects the behaviour of pure ice and because the temperature strongly affects the porosity of sea ice. The unconfined strength of the -2°C-ice was 57% of that of the cold ice, whereas the -6°C-ice was slightly stronger. However, we believe that our -2°C-ice was in the stronger range of what can be expected for rubble in-situ. Firstly because when ice approaches its freezing point the temperature alone is no longer sufficient to describe the internal energy of the ice as substantial phase transfer goes on. Our ice had only been at -2°C for a few hours and was not exposed to any eroding currents. Secondly, our ice had been stored in the freezer for some months

and brine had drained. Lower salinity means that less brine is created as the ice is heated and the porosity becomes less than that of in-situ rubble.
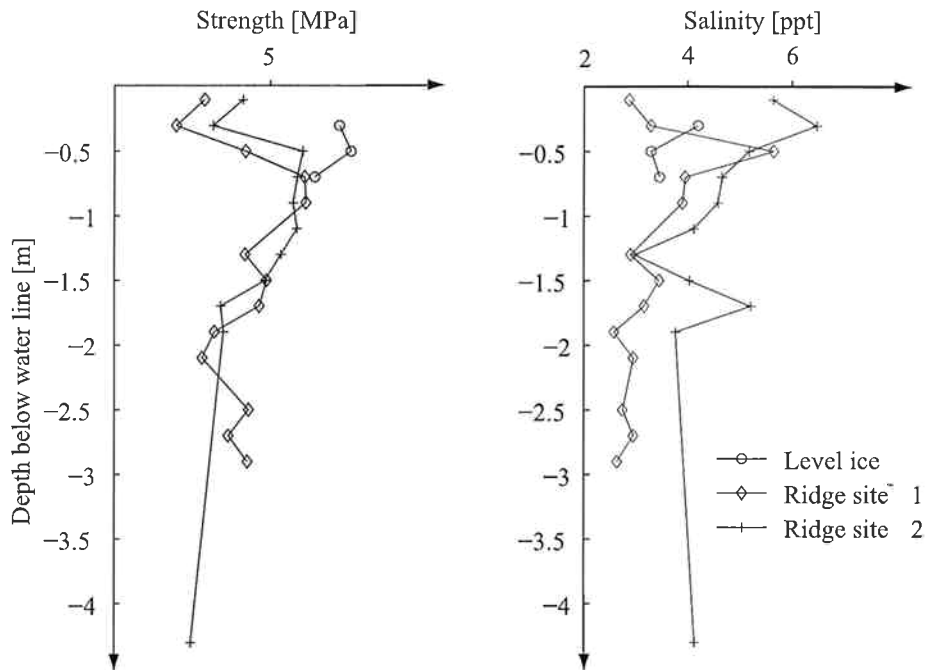

Figure 1: The average strength and the salinity of the level ice and the ridge in the Barents Sea

Fig 2a presents the strength plotted against the average stress-rate for 84 vertical samples from different depths in the level ice and 68 samples from the consolidated layer in the ice ridge. The stress-rate is defined as $\dot{\sigma} = \sigma_{max}/t$, where t is the time to failure and σ is the strength. The three failure mode explained by Kendall (1978) were all observed, but for samples loaded with $\dot{\sigma} > 0.4$ the failure was predominantly brittle (or premature in the terminology of Sinha (1981)). An increasing trend of strength with average stress-rate is seen, also for brittle samples.

We do not have the equipment to make a careful sample end preparation so that all the sample ends were not completely parallel. This means that end effects were probably present and this may have lowered the strength of our samples. The stiffness of the test machine is not yet measured but as the capacity is 100 kN it probably gives strain rates less than the desired 10^{-3} 1/s, and this could have affected both the failure mode and the

strength (Sinha and Frederking, 1979).

The results from the hardness tests in 2002 and 2003 are given in Fig 2b. The hardness tests gave a nice dependence on the ice temperature both in 2002 (Bonnemaire et al., 2003) and in 2003 (Vatne, 2003), but the obtained hardness values were not comparable. It seems as if more work have to be put down in specifying the procedures, especially we believe that the measurements of the footprint diameter may be person dependent. The surface preparation (manual or chain saw) was also of importance for the obtained hardness and the requirements for sample size are neither clear. The results are described more closely in Vatne (2003).
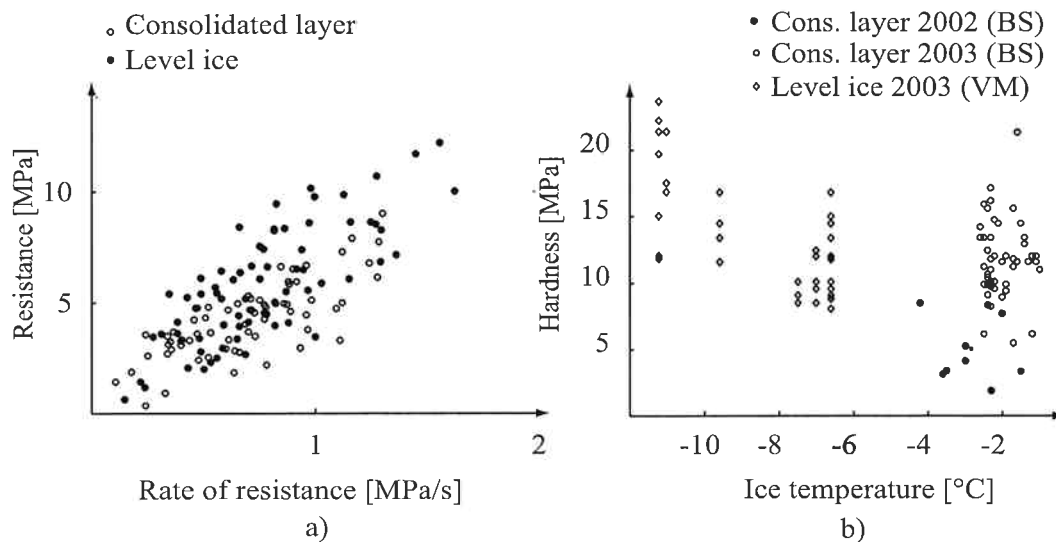

Figure 2: a) Resistance versus rate of resistance, b) Hardness versus the ice temperature.

CONCLUSIONS

Different types of ice has been sampled and tested in unconfined compressive tests in the UNIS laboratory and in-situ hardness tests have been performed. The main conclusions are:

- The average unconfined strength of vertical samples from the consolidated layer was 5.0 MPa and 6.0 MPa for vertical samples of level ice

- The level ice was stronger than the ridged ice

166

- The vertical samples were in general stronger than the horizontal samples. We do not know if this was due to our sampling technique or if the orientation of the brine channels makes the horizontal samples weaker

- The average strength of ice tested at T=-2°C was 3.4 MPa, and we believe this in upper range of what may be expected in the rubble in-situ

- The hardness of the consolidated layer was similar to that of the level ice, and stronger than the rubble. In general the the hardness had a clear dependency on the ice temperature, but the obtained value seems to depend on the person testing

References

Blanchet, D. (1998). Ice loads from first-year ice ridges and rubble fields. *Canadian Journal of Civil Eng.*, (25). 206-219.

Bonnemaire, B., Høyland, K. V., Liferov, P., and Moslet, P. (2003). An ice ridge in the Barents Sea, Part I: Morphology and physical parameters. In *Proc. of the 17th Int. Conf. on Port and Ocean Eng. under Arctic Conditions (POAC), NTNU, Trondheim, Norway*, 2: pp. 559-568.

Frederking, R. and Timco, G. (1989). Compressive behaviour of Beaufort sea ice under vertical and horizontal loading. In *3rd Symp. on Offshore Mechanics and Arctic Eng. (OMAE), New Orelans, USA*, 3: pp. 145-149.

Frederking, R. and Wright, B. (1982). Characteristics and stability of an ice rubble field Issugnak, February-March 1980. Technical Report 134, National Research Centre of Canada. p. 230-247.

Høyland, K. V., Kjestveit, G., Heinonen, J., and Määttänen, M. (2000). Loleif ridge experiments at Marjanimi; The size and strength of the consolidated layer. In *Proc. of the 15th Int. Symp. on Ice (IAHR), Gdansk, Poland*, 1: pp. 45-52.

Høyland, K. V., Liferov, P., Moslet, P. O., Løset, S., and Bonnemaire, B. (2002). Medium scale modelling of ice ridge scouring of the sea bed, Part II: Consolidation and physical properties. In *Proc. of the 16th Int. Symp. on Ice (IAHR), Dunedin, New Zealand*, 2: pp. 94-100.

Høyland, K. V., Valkonen, J., and Dettwiler, B. (2003). An ice ridge in the Barents Sea Part II: Laboratory investigations. In *Proc. of the 17th Int. Conf. on Port and Ocean Eng. under Arctic Conditions (POAC), NTNU, Trondheim, Norway*, 2: pp. 569-576.

Kendall, K. (1978). Complexity of compression failure. *Proc. of Roy Soc.*, (361). 245-263.

Liferov, P. and Høyland, K. V. (2004). Ice ridge scouring experiments, Part I: Experimental set up and basic results. *Submitted to Cold Regions Science and Technology*.

Sinha, N. K. (1981). Rate sensitivity of compressive strength of columnar-grained ice. *Experimental Mechannics*, (26,6). 209-218.

Sinha, N. K. and Frederking, R. M. (1979). Effect of test system stiffness on strength of ice. In *Proc. of the 5th Int. Conf. on Port and Ocean Eng. under Arctic Conditions (POAC), Trondheim, Norway*, volume Vol. 1, pp. 708-717.

Vatne, L. (2003). Interaction between a riser armour and ice rubble. Master's thesis, The University Courses in Svalbard, UNIS / Department of Marine Engineering, NTNU. 97 p.

Veitch, B., Lensu, M., Riska, K., Koslof, P., Keiley, P., and Kujala, P. (1991). Field observations of ridges in the northern Baltic Sea. In *Proc. of the 11th Int. Conf. on Port and Ocean Eng. under Arctic Conditions (POAC), St.Johns, Canada*, pp. 381-438.

10 Conclusions and recommendations for further work

10.1 Conclusions

10.1.1 Global design ice loads

Measured ice pressure on fixed structures varies significantly. A summary of measured data shows that categorization with respect to environmental conditions, structure type and geographical location may help to explain the scatter.

The highest reported ice pressures were in the range 2.7 MPa to 5.0 MPa and may be explained by at least two effects:

• Low aspect ratios between structural width and ice thickness causing a confined loading situation,

• Possible dynamic amplification of ice loads due to ice-induced vibrations.

Investigations were conducted on time series from ice crushing. The main findings were:

• Simultaneous ice crushing at low drift speeds

• Non-simultaneous failure during higher drift speeds

• A quasi-simultaneous failure mode was observed with several local load peaks that dropped simultaneously during initially non-simultaneous failure.

The present analyses showed that an assumption with ice crushing as a stochastic process might not be reasonable during the prediction of the highest ice loads on structures.

10.1.2 Applications of continuous wavelet transforms on signals from ice actions

Measured ice load signals were analysed with the continuous wavelet transform (CWT) for the detection of intervals with possible frequency locked-in ice crushing. A brief introduction to the theory of scaleable wavelet functions was presented with few applications of the Fast Fourier Transform (FFT) and CWT. It was found that FFT could provide information about dominant frequencies if the signal was properly cropped in time where CWT was found suitable to indicate dominant frequencies and their location

in time, simultaneously. The fundamental frequency of the structure was reported to be in the range 2.3-2.8 Hz. Hence, coefficients in the wavelet matrices were averaged within this range of frequencies to obtain a 2D signal that was comparable with measured responses. A further step in the analyses was to check whether the detected interval with dominant frequencies in the load signal was in the same range as intervals with significant responses at the same frequencies.

The principal findings from the application of CWT on five different events with ice actions on the Norströmsgrund lighthouse were:

• Intervals with intermittent crushing were found to have lengths between 6.8 s and 30.6 s detected by CWT

• High energy in ice load signals were on average 1.1 seconds shorter than those detected from measured acceleration responses during the same event.

Further applications of CWT were presented using wavelet cross-spectra on locally measured ice loads between ice loads and the correspondingly measured response. Key points from the application of wavelet cross-spectra were:

• Locally measured ice loads were found to be synchronized in intervals lasting from 1.8 s to 7.1 s

• Ice loads and the corresponding response was found to have high common energy in intervals from 2.0 s to 10.0 s.

Subsequently, analyses of 99 selected intervals of ice crushing were conducted using FFT and CWT. All events were categorized as either intermittent crushing with steady state vibrations or continuous crushing with small amplitude vibrations of stochastic character. From studies of the onset phases, intervals with intermittent crushing were found to be triggered by two different phenomena, namely;

• Circumferential cracking introducing a smooth ice edge subsequently causing simultaneous contact between the ice edge and the structure

• High loads on one or two panels simultaneously with subsequent internal cracking in the ice-structure contact zone.

Further, more attention was given to the corresponding parameters. These were drift speed, ice thickness and air temperature. Here the following trends were detected:

• Continuous crushing with drift speeds higher than 0.1 m/s

• Intermittent crushing for drift speeds between 0.02 m/s and 0.08 m/s with a trend where the upper transition speed seemed to increase slightly for both increasing ice thickness and increasing temperatures.

10.1.3 Ice ridges and actions on structures

The present work contains two separate studies on ice ridges. The first study is the analyses of 14 incidents with ice actions from ridged ice on the Norströmsgrund lighthouse with a focus on the geometry of ridges, failure modes and loads from the ridge keels. The findings about ridge geometry were:

• The keel-to-sail ratio was estimated as 8.2, which is higher than that reported in two other comparable surveys

• Average ridge keel depths seem to decrease by 0.04 m/day, which is slightly faster than that investigated on a single ridge in landfast ice.

The failure mode of ridges was categorized in four modes as:

• Ridges with keels deeper than 6.3 m that tend to fail either on a rubble wedge or by splitting

• Ridges with keels in the range 3.5 m to 6.1 m failed in either bending or crushing.

From the analyses of loads measured by 1.5 m high load panels recorded during interaction between a vertical structure and ridged ice, the following trends were detected:

• Keel depth of an ice ridge has a minor influence on the highest ridge loads

• Loads from deeper parts in the ridge keel were more significant during crushing failure than during failure on a rubble wedge

• The highest loads from ridges were found to increase with increasing thickness of the consolidated layer

- A load peak was detected during the transition between local crushing and the global splitting of a ridge.

Subsequently, a study on the mechanical properties of arctic ice ridges was offered. The work was conducted during the spring 2003. Ice was sampled from ridged ice and level ice, both in the Barents Sea near Hopen Island and in the Van Mijen fjord on Svalbard. The main conclusions were:

- The average unconfined strength of vertical samples from the consolidated layer and level ice were found to be 5.0 MPa and 6.0 MPa, respectively

- The average strength of ice tested at $T = -2°C$ was 3.4 MPa, a strength which was supposed to be in the upper range of what might be expected in ice rubble

- The hardness of the consolidated layer in a ridge was similar to that of level ice, and harder than ice rubble

- The hardness of sea ice was clearly dependent on both ice temperature and the people who investigated the hardness. However it was unclear which of these factors influenced most.

10.2 Recommendations for further work

The following topics seem promising when extensions of the present work are being considered:

10.2.1 Ice actions in general

Quantification of ice loads and physical description of scenarios that give the highest global ice loads with key questions:

- How do global ice loads vary with ice thickness, drift speed and ice temperature?

- How should the surface piercing width of the structure be treated in the prediction of global ice loads and is it conservative to reduce the full structural width during ice load prediction?

10.2.2 Wavelet transforms and dynamic ice actions

The present work shows the first application of wavelet transforms to ice load signals and further applications are needed to confirm the value of the method. Key tasks in such further work are:

• Application of other wavelet forms that might describe ice actions better than the Morlet wavelet

• Determination of an autocorrelation coefficient that could describe a more realistic synthetic background spectrum for ice crushing

• Applications of the discrete wavelet transform with new possibilities to reproduce ice load signals from wavelet coefficient maps.

The onset of intervals with ice loads of lock-in type should be studied further. A better understanding of the triggering phase might produce ideas for concepts that can mitigate the problem with ice loads of resonant character.

10.2.3 Ice actions caused by ridged ice

Topics that might be addressed in further studies of ice ridge actions:

• Investigations of the influence of increasing keel depths on loads from ice ridges measured with devices that cover the entire keel depth

• Further investigations of the geometry and mechanical properties of the consolidated layer in first-year ice ridges.